

COOPERATIVE ADAPTIVE CRUISE CONTROL WITH PREDICTED VEHICLE  
INFORMATION: DEVELOPMENT AND EVALUATION

A THESIS SUBMITTED TO  
THE GRADUATE SCHOOL OF NATURAL AND APPLIED SCIENCES  
OF  
MIDDLE EAST TECHNICAL UNIVERSITY

BY

FURKAN KILIÇ

IN PARTIAL FULFILLMENT OF THE REQUIREMENTS  
FOR  
THE DEGREE OF MASTER OF SCIENCE  
IN  
ELECTRICAL AND ELECTRONICS ENGINEERING

AUGUST 2022



Approval of the thesis:

**COOPERATIVE ADAPTIVE CRUISE CONTROL WITH PREDICTED  
VEHICLE INFORMATION: DEVELOPMENT AND EVALUATION**

submitted by **FURKAN KILIÇ** in partial fulfillment of the requirements for the degree of **Master of Science in Electrical and Electronics Engineering Department, Middle East Technical University** by,

Prof. Dr. Halil Kalıpçılar  
Dean, Graduate School of **Natural and Applied Sciences** \_\_\_\_\_

Prof. Dr. İlkey Ulusoy  
Head of Department, **Electrical and Electronics Engineering** \_\_\_\_\_

Prof. Dr. Klaus Werner Schmidt  
Supervisor, **Electrical and Electronics Engineering, METU** \_\_\_\_\_

**Examining Committee Members:**

Prof. Dr. Kemal Leblebicioğlu  
Electrical and Electronics Engineering, METU \_\_\_\_\_

Prof. Dr. Klaus Werner Schmidt  
Electrical and Electronics Engineering, METU \_\_\_\_\_

Prof. Dr. Umut Orguner  
Electrical and Electronics Engineering, METU \_\_\_\_\_

Prof. Dr. Selahattin Çağlar Başlamışlı  
Mechanical Engineering, Hacettepe University \_\_\_\_\_

Assist. Prof. Dr. Serkan Sarıtaş  
Electrical and Electronics Engineering, METU \_\_\_\_\_

Date: 24.08.2022

**I hereby declare that all information in this document has been obtained and presented in accordance with academic rules and ethical conduct. I also declare that, as required by these rules and conduct, I have fully cited and referenced all material and results that are not original to this work.**

Name, Surname: Furkan Kılıç

Signature :

## **ABSTRACT**

### **COOPERATIVE ADAPTIVE CRUISE CONTROL WITH PREDICTED VEHICLE INFORMATION: DEVELOPMENT AND EVALUATION**

Kılıç, Furkan

M.S., Department of Electrical and Electronics Engineering

Supervisor: Prof. Dr. Klaus Werner Schmidt

August 2022, 81 pages

Using cooperative adaptive cruise control (CACC), it is possible for a platoon of vehicles to travel safely while increasing the traffic throughput and reducing the fuel consumption. Specifically, the maximization of the traffic throughput and the minimization of the fuel consumption is best supported by a constant spacing policy (CSP). In addition, driving safety requires the attenuation of any disturbances through the vehicle platoon, which is captured by the notion of string stability. In order to realize a CSP while maintaining string stability, each follower vehicle in a platoon should obtain leader and predecessor information via vehicle-to-vehicle (V2V) communication. In this context, it has to be respected that CACC platoons under the leader predecessor following (LPF) topology with CSP are affected by different delays in terms of string stability, performance and applicability. These are the leader follower (LF) communication delay, predecessor follower (PF) sensor and communication delay.

The main aim of this thesis is to recover the ideal delay-free LPF CSP performance even in the presence of the aforementioned delays, hence confirming the applicability of the LPF topology with CSP in practice. To this end, the thesis presents a robust

controller synthesis procedure and then proposes several modifications of the state-of-the-art control architecture. Hereby, the main novelty is given by prediction of the future leader acceleration, which can be used to eliminate the LF communication delay. Moreover, to remove the PF communication delay, a novel and simple method of estimating the predecessor vehicle acceleration from the leader acceleration is introduced. In order to increase the performance under predecessor disturbances, a prediction observer is employed to combine the communicated and estimated predecessor information. The developed overall control architecture is then further adapted to include a Smith predictor that helps overcome the PF sensor delay. Simulation experiments confirm that the performance of the introduced topologies closely approximates the ideal delay-free LPF topology with CSP.

**Keywords:** Cooperative Adaptive Cruise Control, Leader Predecessor Following, Constant Spacing Policy, Prediction Observer, Predicted Acceleration, Robust Controller Synthesis

## ÖZ

### **ARAÇ BİLGİ TAHMİNİ İLE KOOPERATİF ADAPTİF SEYİR KONTROLÜ: GELİŞTİRME VE DEĞERLENDİRME**

Kılıç, Furkan

Yüksek Lisans, Elektrik ve Elektronik Mühendisliği Bölümü

Tez Yöneticisi: Prof. Dr. Klaus Werner Schmidt

Ağustos 2022 , 81 sayfa

Kooperatif Adaptif Seyir Kontrolü (KASK) sayesinde bir araç konvoyunun güvenli bir şekilde seyahat ederken, trafik akışını arttırması ve yakıt tüketimini azaltması mümkündür. Özellikle, trafik akışının en üst düzeye çıkarılması ve yakıt tüketiminin en aza indirilmesi sabit mesafe planı (SMP) ile sağlanır. Ek olarak, sürüş güvenliği konvoyda oluşan bozucu etkilerin sönmülmesini gerektirmektedir. Bu gereklilik dizi kararlılığı ile sağlanır. Araçlar arasında sabit bir mesafe sağlanırken, dizi kararlılığının da korunabilmesi için takipçi araçların hem lider hem de öncül araç bilgilerine ulaşması gereklidir. Bu kapsamda, lider öncül araç takibi (LÖAT) topolojisini SMP ile kullanan KASK araç konvoyları dizi kararlılığı, performans ve pratik uygulanabilirlik yönünden farklı zaman gecikmelerinden etkilenebilir. Bu zaman gecikmeleri lider takipçi (LT) haberleşme gecikmesi, öncül takipçi (ÖT) sensör ve haberleşme gecikmeleridir.

Bu tezin amacı, zaman gecikmeleri altında bile dizi kararlılığını korurken, teknolojinin geldiği son noktadaki SMP LÖAT topolojisini değiştirerek, ideal, gecikmesiz SMP LÖAT performansına ulaşmak ve uygulanabilirliğini doğrulamaktır. Bu sebeple,

SMP LÖAT için gürbüz bir kontrolör sentez prosedürü ve devamında teknolojinin bugünkü durumundaki kontrol mimarisine birçok değişiklik sunulmuştur. Bu noktada tanıtılan ana yenilik, LT haberleşme gecikmesini ortadan kaldırmak için kullanılabilir, gelecek lider ivme kestirimidir. Dahası, ÖT haberleşme gecikmesini ortadan kaldırabilmek için, lider araç ivmesinden, öncül araç ivmesini kestirecek özgün ve basit bir metod verilmiştir. Öncül araç bozucuları altındaki performansı arttırmak için, haberleşmeyle elde edilen ve kestirilen öncül araç ivmeleri, tahmin gözlemcisi ile birleştirilmiştir. Geliştirilen genel kontrol mimarisi, ÖT sensör gecikmesinin üstesinden gelmek için değiştirilmiş ve sonunda bir Smith predictor topolojisi ve birleştirilmiştir. Simulasyon sonuçları, tanıtılan topolojilerin performanslarının ideal, zaman gecikmesiz SMP LÖAT ile oldukça yakınsadığını doğrulamaktadır.

Anahtar Kelimeler: Kooperatif Adaptif Seyir Kontrolü, Lider Öncel Araç Takibi, Sabit Mesafe Prensibi, Tahmin Gözlemcisi, İvme Tahmini, Gürbüz Kontrolcü Sentezi

## **ACKNOWLEDGEMENTS**

I would like to thank my advisor Prof. Dr. Klaus Werner Schmidt for his invaluable guidance and support throughout this thesis. His insights and knowledge made this thesis, what it is.

I would like to show my appreciation for my close friends, who bolstered my spirit.

I would like to express my gratitude for my family who has been there for me all my life. All my accomplishments are thanks to their care, love and support.

Lastly, I would like to thank my love Misra, who has literally been with me the whole process side by side, through thick and thin. What made this thesis, is her endless and rigorous support.

*To my family and my love...*

## TABLE OF CONTENTS

ABSTRACT . . . . .	v
ÖZ . . . . .	vii
ACKNOWLEDGMENTS . . . . .	ix
TABLE OF CONTENTS . . . . .	xi
LIST OF FIGURES . . . . .	xiii
LIST OF TABLES . . . . .	xviii
LIST OF ABBREVIATIONS . . . . .	xix
CHAPTERS	
1 INTRODUCTION . . . . .	1
2 BACKGROUND INFORMATION . . . . .	5
2.1 Cooperative Adaptive Cruise Control . . . . .	5
2.2 Vehicle Model . . . . .	6
2.3 String Stability . . . . .	6
2.4 Leader Predecessor Following . . . . .	7
3 LEADER PREDECESSOR FOLLOWING CONTROLLER SYNTHESIS . . . . .	15
3.1 Iterative Transfer Functions . . . . .	16
3.2 $H_\infty$ Controller Synthesis . . . . .	17
3.3 Effects of Delays . . . . .	27

4	PREDICTED LEADER AND PREDECESSOR ACCELERATION FOLLOWING . . . . .	37
4.1	Predicted Leader Acceleration . . . . .	38
4.2	Modified Leader Predecessor Following . . . . .	41
4.3	Modified Leader Predecessor Following with Predicted Predecessor Acceleration . . . . .	47
4.3.1	Prediction Observer . . . . .	47
4.3.2	Modified Leader Predecessor Following with Prediction Observer . . . . .	52
4.4	MLPFO with Smith Predictor . . . . .	62
4.5	Comparison . . . . .	68
5	CONCLUSION . . . . .	73
	REFERENCES . . . . .	75
	APPENDICES	
A	CONTROLLERS . . . . .	81

## LIST OF FIGURES

### FIGURES

Figure 2.1	A CACC equipped vehicle platoon [1]. . . . .	6
Figure 2.2	Ideal LPF block diagram. . . . .	9
Figure 2.3	LPF Vehicles [2]. . . . .	10
Figure 2.4	LPF block diagram. . . . .	11
Figure 2.5	An ideal CSP LPF platoon accelerations, under constant acceleration input. . . . .	14
Figure 2.6	An ideal CSP LPF platoon distance errors, under constant acceleration input. . . . .	14
Figure 3.1	The block diagram for $H_\infty$ synthesis. . . . .	17
Figure 3.2	The LFT block diagram for $H_\infty$ synthesis. . . . .	18
Figure 3.3	The closed loop Bode plot and step response of the transfer function between the leader and first follower accelerations. . . . .	20
Figure 3.4	The Bode plot and step response of the transfer function between the distance error and acceleration input. . . . .	21
Figure 3.5	The Bode plot of the $T_p(s) = T_l(s)$ . . . . .	22
Figure 3.6	The Bode plot of the transfer functions between the leader and follower accelerations given in Equation (3.1). . . . .	23

Figure 3.7	The Bode plot of the transfer functions between the leader acceleration and distance errors the vehicles as in Equation (3.3).	23
Figure 3.8	The step response of the transfer functions between the leader acceleration and distance errors.	24
Figure 3.9	The distance error between the vehicles for an acceleration disturbance at the first vehicle.	25
Figure 3.10	The accelerations of the vehicles for an acceleration disturbance at the first vehicle.	26
Figure 3.11	The distance error between the vehicles for a velocity disturbance at the first vehicle.	26
Figure 3.12	The accelerations of the vehicles for an velocity disturbance at the first vehicle.	27
Figure 3.13	The illustration of information flow and related delays.	28
Figure 3.14	The effect of different delays on the transfer function between the $E_1(s)$ and $A_l(s)$ .	30
Figure 3.15	The effect of leader-follower communication delay on distance errors between the vehicles.	31
Figure 3.16	The effect of leader-follower communication delay on accelerations of each vehicle.	31
Figure 3.17	The effect of PF sensor delay on the transfer function between the distance errors.	32
Figure 3.18	The effect of PF communication delay on the transfer function between the distance errors.	33
Figure 3.19	The maximum distance comparison for the ideal and 0.1s PF communication delay case.	34

Figure 3.20	The effect of PF communication delay on distance errors between the vehicles. . . . .	34
Figure 3.21	The effect of combined delays on distance errors between the vehicles. . . . .	35
Figure 4.1	The block diagram of the LPF with predicted leader acceleration.	38
Figure 4.2	The distance errors of the vehicles for a step acceleration of the leader. . . . .	40
Figure 4.3	The accelerations of the vehicles for a step acceleration of the leader. . . . .	40
Figure 4.4	The block diagram of the modified leader predecessor following (MLPF). . . . .	41
Figure 4.5	The distance errors of the vehicles for a step acceleration of the leader. . . . .	43
Figure 4.6	The accelerations of the vehicles for a velocity disturbance at the first vehicle. . . . .	44
Figure 4.7	The accelerations of the vehicles for a step acceleration of the leader. . . . .	44
Figure 4.8	The accelerations of the vehicles for an acceleration disturbance at the first. . . . .	45
Figure 4.9	The distance errors of the vehicles for a velocity disturbance at the first vehicle. . . . .	45
Figure 4.10	The accelerations of the vehicles for a velocity disturbance at the first vehicle. . . . .	46
Figure 4.11	2-stage prediction observer block diagram. . . . .	48
Figure 4.12	2-stage FIP prediction observer block diagram. . . . .	50

Figure 4.13	The prediction observer step responses. . . . .	51
Figure 4.14	The bode plots of the $F(s)$ and $\tilde{F}(s)$ for $L = 360$ . . . . .	52
Figure 4.15	MLPFO block diagram. . . . .	53
Figure 4.16	The magnitude bode plot of the $\gamma_i(s), i > 1$ . . . . .	55
Figure 4.17	The magnitude bode plot of the $\Gamma_i(s)$ . . . . .	56
Figure 4.18	The magnitude plots of $\Gamma_i(s)$ and $\gamma_i(s)$ . . . . .	56
Figure 4.19	The string stable platoon length for different PF sensor and communication delays. . . . .	57
Figure 4.20	The distance errors of the vehicles for a step acceleration of the leader. . . . .	59
Figure 4.21	The accelerations of the vehicles for a step acceleration of the leader. . . . .	59
Figure 4.22	The distance errors of the vehicles for an acceleration disturbance at the first vehicle. . . . .	60
Figure 4.23	The accelerations of the vehicles for an acceleration disturbance at the first vehicle. . . . .	60
Figure 4.24	The distance errors of the vehicles for a velocity disturbance at the first vehicle. . . . .	61
Figure 4.25	The accelerations of the vehicles for a velocity disturbance at the first vehicle. . . . .	61
Figure 4.26	MLPFO with Smith predictor block diagram. . . . .	62
Figure 4.27	Smith predictor implemented loop block diagram. . . . .	63
Figure 4.28	The magnitude bode plot of the $\Gamma_i(s)$ . . . . .	64
Figure 4.29	The distance errors of the vehicles for a step acceleration of the leader. . . . .	65

Figure 4.30	The accelerations of the vehicles for a step acceleration of the leader. . . . .	65
Figure 4.31	The distance errors of the vehicles for a acceleration disturbance at the first vehicle. . . . .	66
Figure 4.32	The accelerations of the vehicles for an acceleration disturbance at the first vehicle. . . . .	66
Figure 4.33	The distance errors of the vehicles for a velocity disturbance at the first vehicle. . . . .	67
Figure 4.34	The accelerations of the vehicles for a velocity disturbance at the first vehicle. . . . .	67
Figure 4.35	The distance errors of the vehicles for a step acceleration of the leader vehicle. . . . .	69
Figure 4.36	The accelerations of the vehicles for a step acceleration of the leader vehicle. . . . .	70
Figure 4.37	The distance errors of the vehicles for an acceleration disturbance at the first vehicle. . . . .	70
Figure 4.38	The accelerations of the vehicles for an acceleration disturbance at the first vehicle. . . . .	71
Figure 4.39	The distance errors of the vehicles for an velocity disturbance at the first vehicle. . . . .	71
Figure 4.40	The accelerations of the vehicles for a velocity disturbance at the first vehicle. . . . .	72

## LIST OF TABLES

### TABLES

Table A.1 The controllers used in the thesis . . . . .	81
--	----

## LIST OF ABBREVIATIONS

CACC	Cooperative Adaptive Cruise Control
V2V	Vehicle-to-vehicle
CSP	Constant Spacing Policy
CTHP	Constant Time Headway Policy
LPF	Leader Predecessor Following
PF	Predecessor Follower
LF	Leader Follower
MLPF	Modified Leader Predecessor Following
MLPFO	Modified Leader Predecessor Following with Prediction Observer
$x$	Position
$v$	Velocity
$a$	Acceleration
$u$	Control input
$e$	Distance error
$d$	Desired distance
$L$	Constant distance between the vehicles
$\phi$	Communication and sensor delay
$\Gamma$	String stability transfer function
$T$	The transfer function between accelerations
$S$	The transfer function between the acceleration and acceleration error
$\tilde{S}$	The transfer function between the acceleration of the and distance error

$\tilde{T}$	Transfer function between the leader acceleration and estimated predecessor acceleration
$W$	Weighting transfer function
$Z$	Weighted output
$P$	Weighted transformation matrix
$d_v, d_a$	Disturbance input
$\hat{G}$	Prediction transfer function
$M$	Characteristic equation of the matrix
$F$	Prediction observer transfer function
$\tilde{a}$	Estimated acceleration
$\hat{a}$	Predicted acceleration from combined information
$\bar{T}_p$	The modified transfer function between the accelerations
$T_{l,i}$	The modified transfer function between the acceleration of the leader and other vehicles

## CHAPTER 1

### INTRODUCTION

With the ever-increasing population and economy, a more efficient use of the traffic in order to reduce congestion, pollution, emission, and fuel consumption; increasing the safety and comfort of the passengers became a necessity. Therefore, over the recent years, the autonomous driving technology has shown a tremendous progress. The advances came to a level, where a fully autonomous transportation can be expected in the not so far future. In principle, autonomous driving requires the longitudinal and lateral control of the vehicle. One component of the longitudinal control is vehicle following, whereby an efficient method of multiple vehicles to follow each other is constituting a vehicle platoon. Thus, the research on the best vehicle platoon control method has continued and the Cooperative Adaptive Cruise Control (CACC) is being developed and studied for years.

In brief, CACC is a method to control the longitudinal motion of the vehicle, satisfying the desired acceleration, velocity and inter-vehicle distances, using the on-board sensors of the vehicle and the received information from the wireless vehicle-to-vehicle (V2V) communication [1–4]. A very important property of the CACC is string stability [5]. String stability requires the attenuation of disturbances along the vehicle platoon, as they travel towards to last vehicle [6, 7]. Over time, many different control architectures for CACC have been developed using the information of the different vehicles in the platoon, such as predecessor following, leader predecessor following, bidirectional following [8–10]. Furthermore, multiple spacing policies are introduced in order to designate the characteristics of the distances between the vehicles during longitudinal motion. A variety of spacing policies is used in order to increase the traffic throughput, fuel consumption and safety [11, 12]. Among

these, the smallest inter-vehicle distances, hence the maximum traffic throughput can be achieved with constant spacing policy (CSP) leader predecessor following (LPF) topology [12–14], which is also the focus of this thesis.

Different research works have been carried out on the CSP LPF with or without including potential delays that are caused by sensors, actuators and V2V communication. Many works deal with the controller design and ways to handle the delays using different control designs and architectures. In [15], an  $H_\infty$  control synthesis method for CSP LPF, which satisfies string stability, is given without considering delays. In [16, 17], a virtual predecessor method for vehicles with the CSP LPF policy is presented for platoons with different topologies. In [18], a robust controller synthesis method is given for a heterogeneous CSP LPF vehicle platoon with uniform communication delay. In [19], a means to synchronize all the delayed information received by the vehicle in a CSP LPF platoon, with respect to the largest delayed variable, focusing on the LF communication delay is presented. In [20], the string stability of the CSP LPF under ideal, delay free case is analyzed extensively and a controller design based on the Routh-Hurwitz criterion is given. In [21], a string stabilizing controller design method, including the sensor delay is shown. Despite the high payoff, the CSP LPF suffers from predecessor follower (PF) sensor and communication delay, and leader follower (LF) communication delay [19, 22]. Due to its complex nature of receiving multiple pieces of information over the network at different times, synchronization of the received information and dealing with different delays and their effects, the applicability of the CSP LPF is still limited and experimental results are absent in the literature. In this context, the major problem of the so-called "boundless increment of the distances" between the vehicles, which is observed under leader acceleration and LF communication delay is shown in [16, 19, 23].

This thesis is originated from the idea of the possible prediction of the leader vehicle states for a short amount of time, and transferring the state information to the follower vehicles via V2V communication, in order to deliver them a delay-free information. Assuming a fully autonomous leader vehicle, using the combination of Kalman filters, GPS, navigation and path planning algorithms, it is possible to predict the future state of the vehicle. Under this assumption, the first contribution of the thesis is conducting an  $H_\infty$  controller synthesis similar to [15]. As an advancement, the logic

behind the selection of the weights is defined clearly, the string stability of the resulting controller with the commonly used string stability definitions is shown and the performance of the control loop under preceding and leader vehicle disturbances is examined. The second contribution is the comprehensive evaluation of the effect of different delays in the CSP LPF policy in the frequency domain and the development of a possible solution for practical use and performance increase of CSP LPF for each delay. The third contribution is that, for the handling of different delays, new controller architectures are introduced. In order to remove the LF communication delay, an imminent approach of predicted leader acceleration is introduced. A method to estimate the predecessor acceleration from a predicted leader acceleration is acquainted and the effect of PF communication delay is handled. Hereby, the prediction observer developed in [24] is utilized, examined in frequency domain and used for a further increase in performance under PF communication delay. Finally, a Smith predictor based topology is merged with the current control architecture to manage the PF sensor delay. The performance under worst case possible scenarios is simulated, the results of the newly introduced control architectures are compared in detail. All of the frequency domain calculations are done in MATLAB, while the simulation results are executed on Simulink. To sum up, an overall approach to remove the effect of the delays from the loop is executed. As the main result, a practical method that leads to a behavior that is close to the ideal, delay free CSP LPF is achieved.

The organization of the thesis is as follows. In Chapter 2, the required background information is given. In Chapter 3, a further elaboration on the CSP LPF equations, the robust controller synthesis and the effect of delays are shown. In Chapter 4, a new controller architecture for the different delays is presented and evaluated. Finally, Chapter 5 provides conclusions and directions for future work.



## CHAPTER 2

### BACKGROUND INFORMATION

In this chapter, general information about cooperative adaptive cruise control (CACC) will be given in Section 2.1. The main elements of the control loop and the system model are provided in Section 2.2 and 2.3. The selected information flow topology and the vehicle following policy will be defined in Section 2.4. The related equations to understand the theoretical background will be introduced.

#### 2.1 Cooperative Adaptive Cruise Control

The increasing demand in traffic, creates congestion and requires the capacity of the roads to be increased. With the increasing traffic density, the time spent on the traffic, fuel consumption, emission increases. It is possible to organize the traffic in automated vehicle platoons and reduce these effects. Using the on-board sensors such as lidar/radar and the information shared throughout the communication network, the vehicle platoons or so called vehicle strings, that follow each other with a predefined spacing policy can be formed. This autonomous and controlled formation topology is called cooperative adaptive cruise control (CACC). The primary purpose of CACC is reducing the fuel consumption and increasing the traffic throughput by decreasing the distance between the vehicles [3]. It is known that the road capacity [25] and traffic throughput can be increased [26] with CACC since it creates an aerodynamically efficient vehicle string [27] and reduces the fuel consumption and emission [28]. Furthermore, with CACC the passengers comfort [29] and safety is increased [30]. A general descriptive CACC equipped vehicle platoon can be seen in Figure 2.1.

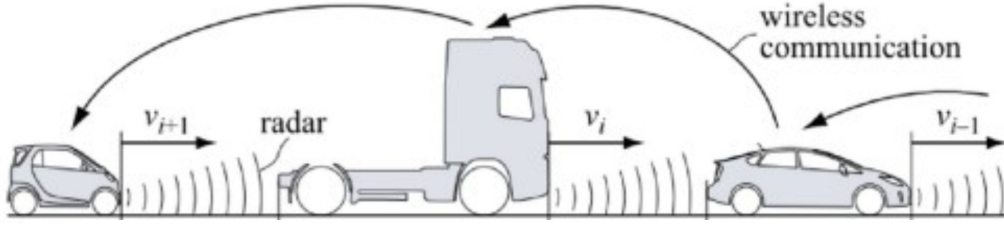


Figure 2.1: A CACC equipped vehicle platoon [1].

## 2.2 Vehicle Model

The linear vehicle model, that is being commonly used in the literature for CACC studies is employed [31]. Taking the position, velocity and acceleration of the vehicle as  $x_i$ ,  $v_i$  and  $a_i$  respectively and  $u_i$  as control input:

$$\begin{bmatrix} \dot{x}_i(t) \\ \dot{v}_i(t) \\ \dot{a}_i(t) \end{bmatrix} = \begin{bmatrix} 0 & 1 & 0 \\ 0 & 0 & 1 \\ 0 & 0 & -1/\tau \end{bmatrix} \begin{bmatrix} x_i(t) \\ v_i(t) \\ a_i(t) \end{bmatrix} + \begin{bmatrix} 0 \\ 0 \\ 1/\tau \end{bmatrix} u_i(t) \quad (2.1)$$

The resulting transfer function from  $u_i$  to  $x_i$ :

$$H(s) = \frac{X_i(s)}{U_i(s)} = \frac{1}{s^2(\tau s + 1)} = \frac{G(s)}{s^2} \quad (2.2)$$

Here a common description for  $\tau$  is driveline dynamics [1] or parasitic lag in the powertrain [32]. The given transfer function is the result of the low-level controllers. It is possible to equate different vehicles driveline dynamics and have a homogeneous vehicle string [33].

## 2.3 String Stability

During the platooning, the most important part is the safety of the people, thus any disturbances exposed throughout the vehicle platoon must be attenuated and the distances between the vehicles must stay bounded. The introduced property is called

string stability. In the literature many different definitions exist for the string stability property [33].

Assuming a transfer function

$$\Gamma_i(s) = \frac{E_{i+1}(s)}{E_i(s)} \quad (2.3)$$

between the given signals of interest of the consecutive vehicles, the definition of string stability that will be used in the thesis can be explained as follows. This signal of interest is commonly selected as acceleration, velocity or distance errors between the vehicles. The capital letter variables represent the Laplace transform of the signal. Since throughout this thesis, our main focus will be on the error signals, the transfer function is selected accordingly. As a result, the notion of string stability can be achieved if for each vehicle  $i$ ,

$$\|\Gamma_i\|_\infty \leq 1 \quad (2.4)$$

The Equation (2.4) shows the  $H_\infty$  norm of the transfer function. Satisfying the  $H_\infty$  norm of the related transfer function, results in  $L_2$  string stability of the vehicle platoon. It can be understood that, the controller to be designed should stabilize the vehicle, furthermore guarantee the string stability of the vehicle platoon in the sense that the  $L_2$ -norm of the error signals should decrease along the string.

## 2.4 Leader Predecessor Following

There are multiple information flow topologies for the implementation of CACC [11]. The leader predecessor following (LPF) topology is selected for detailed examination in order to exploit its multiple information receiving characteristic. Furthermore, there exist different policies in the literature for defining the desired distance between the vehicles [12]. These policies developed around the idea of either increasing the distance between the vehicles with increasing vehicle velocity, which is called constant time headway policy or aiming to keep the distance between the vehicles constant for all times, which is called constant spacing policy. In this research, the constant spacing policy (CSP) will be applied.

The policy we are using is a constant spacing one, hence the desired distances between the consecutive vehicles  $d_i(t)$ , and the desired distances between the leader and the

$i^{th}$  follower  $d_{l,i}(t)$  are of the form,

$$\begin{aligned} d_i(t) &= L_i \\ d_{l,i}(t) &= \sum_{j=1}^i L_j \end{aligned} \quad (2.5)$$

which generates the spacing errors between follower and predecessor as  $e(t)$  and follower and leader as  $e_{l,i}(t)$ .

$$\begin{aligned} e_i(t) &= x_i(t) - x_{i-1}(t) + L_i, i \geq 1 \\ e_{l,i}(t) &= x_i(t) - x_l(t) + \sum_{j=1}^i L_j \end{aligned} \quad (2.6)$$

And with the assumption of homogeneity (that is, identical vehicles),  $L_i$  can be replaced by  $L$  [20].

The control input for CSP LPF is generated by the combination of the leader and predecessor accelerations, velocities and distances. The notation will be as follows.  $a_l(t)$ ,  $v_l(t)$  and  $x_l(t)$  is used for the acceleration, velocity and position of the leader vehicle. Similarly, for the follower vehicle subscript  $i$  and for the predecessor subscript  $i - 1$  will be used. The commonly used time domain [20] equation in the literature for the control input of the  $i^{th}$  vehicle is given in Equation (2.7).

$$\begin{aligned} u_i(t) &= k_{ap} a_{i-1}(t) - k_{vp} (v_i(t) - v_{i-1}(t)) \\ &\quad - k_{pp} (x_i - x_{i-1}(t) + L) \\ &\quad + k_{al} a_l(t) - k_{vl} (v_i - v_l(t)) \\ &\quad - k_{pl} (x_i - x_l(t) + \sum_{j=1}^i L) \end{aligned} \quad (2.7)$$

The control loop block diagram regarding the CSP LPF is then as follows:

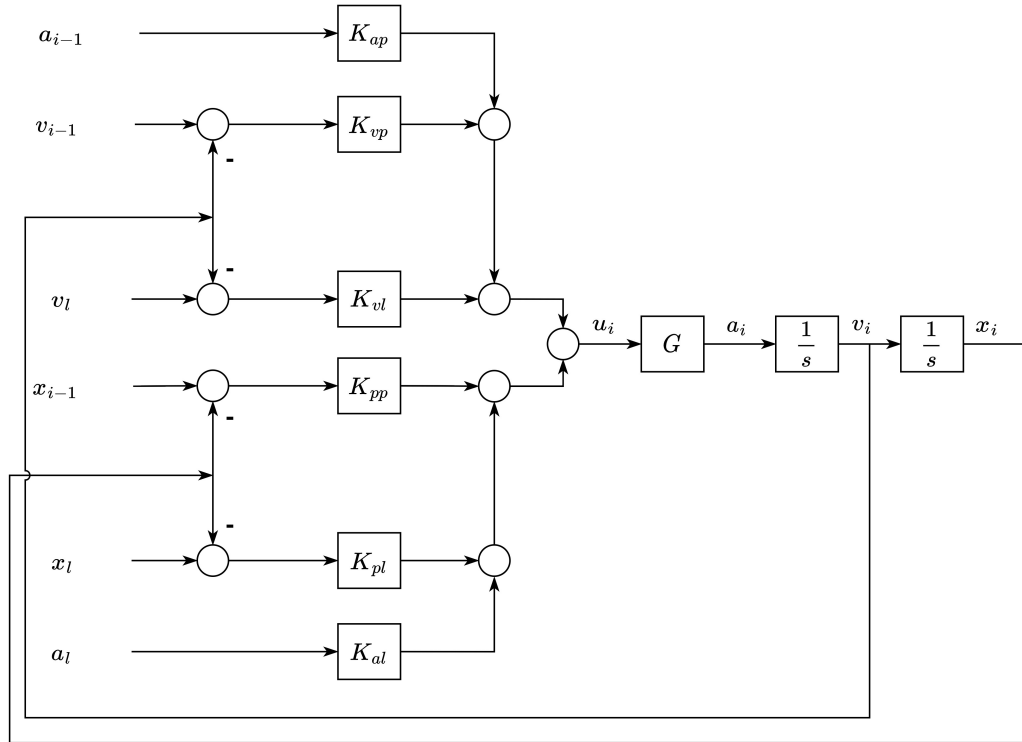


Figure 2.2: Ideal LPF block diagram.

For the CSP LPF, it is required that all the vehicles receive the acceleration information of their predecessors, and acceleration, velocity and position information of their leader via V2V communication. The sensor on the follower vehicle, such as lidar or radar, measures the velocity and position differences directly. Furthermore, for the leader loop, the vehicles exact location and velocity is assumed to be known without any delay. The communication delay between the leader  $l$  and each follower  $i$  is represented with  $\phi_l$ , whereas for the delay between every predecessor  $i - 1$  and follower  $i$ ,  $\phi_p$  is used. Lastly, for the sensor delay between the predecessor  $i - 1$  and follower  $i$ ,  $\phi_s$  is used. For the non delayed variables  $t$  is omitted for readability. Without a loss of generality the vehicle length  $L$  can be set to 0 for the analysis. Including the

delays, the time domain equation of the LPF takes the form in Equation (2.8).

$$\begin{aligned}
u_i(t) = & k_{ap} a_{i-1}(t - \phi_p) - k_{vp} (v_i(t - \phi_s) - v_{i-1}(t - \phi_s)) \\
& - k_{pp} (x_i(t - \phi_s) - x_{i-1}(t - \phi_s) + L) \\
& + k_{al} a_l(t - \phi_l) - k_{vl} (v_i - v_l(t - \phi_l)) \\
& - k_{pl} (x_i - x_l(t - \phi_l) + \sum_{j=1}^i L)
\end{aligned} \tag{2.8}$$

It will be assumed that, there exist  $N$  vehicles in a platoon. With the introduced V2V communication and vehicle indexes, the CSP LPF vehicle platoon can be seen in Figure 2.3.

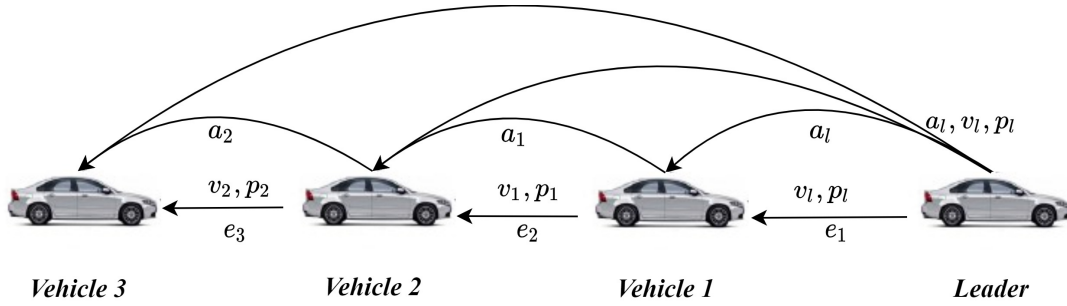


Figure 2.3: LPF Vehicles [2].

Since a frequency domain approach to the LPF, will be used throughout the thesis and the resulting controllers will be of higher order, the preferred notation for control input of the vehicle will be derived in frequency domain, which can be seen in Equation (2.9).

$$\begin{aligned}
U_i(s) = & (K_{ap}(s) e^{-s\phi_p} + (\frac{K_{vp}(s)}{s} + \frac{K_{pp}(s)}{s^2}) e^{-s\phi_s}) A_{i-1}(s) \\
& - ((\frac{K_{vp}(s)}{s} + \frac{K_{pp}(s)}{s^2}) e^{-s\phi_s} + (\frac{K_{vl}(s)}{s} + \frac{K_{pl}(s)}{s^2})) A_i(s) \\
& + (K_{al}(s) + \frac{K_{vl}(s)}{s} + \frac{K_{pl}(s)}{s^2}) e^{-s\phi_l} A_l(s)
\end{aligned} \tag{2.9}$$

Including the delays and moving the integrator terms inside the controller, the related block diagram of the LPF can be seen in Figure 2.4.

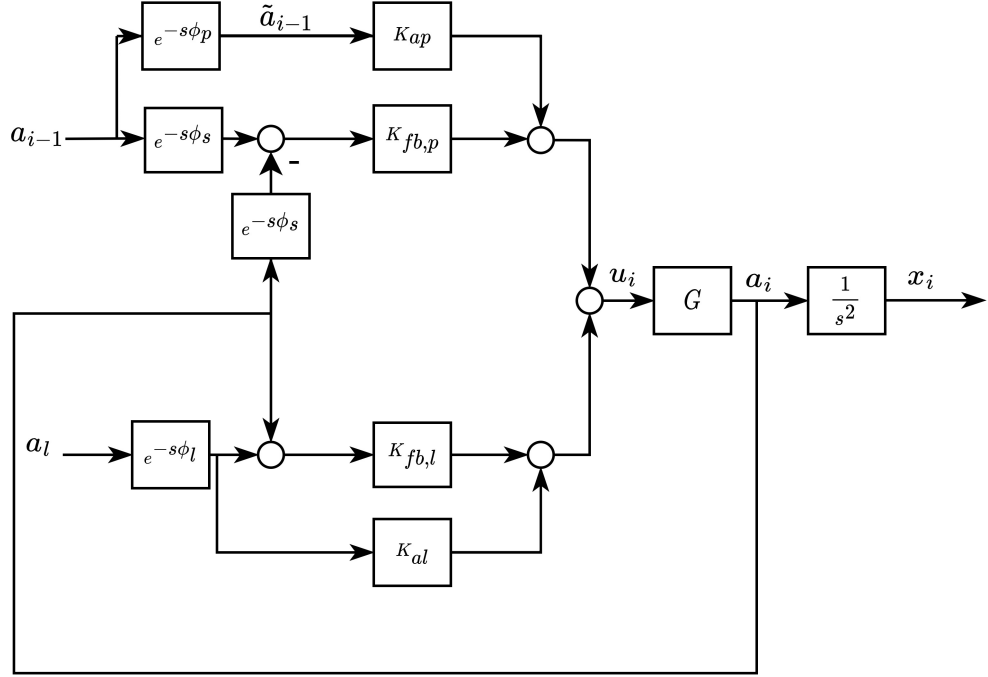


Figure 2.4: LPF block diagram.

In principle, the controller input also comprises velocity and position as can be seen in Figure 2.2. For the simplification of the equations and notation, the integrator terms are moved inside controller and the input of the upper loop is named as acceleration. For CSP LPF, there exist two control loops, which we will name as predecessor and leader loop. Formally, replacing the feedback controllers as stated below, we get the simplified representation

$$\begin{aligned}
 K_{fb,p}(s) &= \frac{K_{vp}(s)}{s} + \frac{K_{pp}(s)}{s^2} \\
 K_{fb,l}(s) &= \frac{K_{vl}(s)}{s} + \frac{K_{pl}(s)}{s^2} \\
 U_i(s) &= (K_{ap}(s)e^{-s\phi_p} + K_{fb,p}(s)e^{-s\phi_s})A_{i-1}(s) \\
 &\quad - (K_{fb,p}(s)e^{-s\phi_s} + K_{fb,l}(s))A_i(s) \\
 &\quad + (K_{al}(s) + K_{fb,l}(s))e^{-s\phi_l}A_l(s) \\
 &= K_p(s)A_{i-1}(s) - K_i(s)A_i(s) + K_l(s)A_l(s)
 \end{aligned} \tag{2.10}$$

For the rest of the equations the Laplace variable  $s$  is omitted for readability. Using (2.2) and (2.10) together, the resulting transfer function between the accelerations is

derived as follows:

$$\begin{aligned}
A_i &= T_p A_{i-1} + T_l A_l \\
T_p(s) &= \frac{K_p G}{1 + K_i G} = \frac{G(K_{ap} e^{-s\phi_p} + K_{fb,p} e^{-s\phi_s})}{1 + GK_i} \\
&= \frac{K_{ap} s^2 e^{-s\phi_p} + (K_{vp} s + K_{pp}) e^{-s\phi_s}}{\tau s^3 + s^2 + s(K_{vp} e^{-s\phi_s} + K_{vl}) + K_{pp} e^{-s\phi_s} + K_{pl}} \quad (2.11) \\
T_l(s) &= \frac{K_l G}{1 + K_i G} = \frac{G(K_{al} + K_{fb,l}) e^{-s\phi_l}}{1 + GK_i} \\
&= \frac{(K_{al} s^2 + K_{vl} s + K_{pl}) e^{-s\phi_l}}{\tau s^3 + s^2 + s(K_{vp} e^{-s\phi_s} + K_{vl}) + K_{pp} e^{-s\phi_s} + K_{pl}}
\end{aligned}$$

Without the delays, for the ideal CSP LPF equation, the transfer functions reduce to following equations.

$$\begin{aligned}
T_p(s) &= \frac{K_{ap} s^2 + K_{vp} s + K_{pp}}{\tau s^3 + s^2 + K_v s + K_p} \\
T_l(s) &= \frac{K_{al} s^2 + K_{vl} s + K_{pl}}{\tau s^3 + s^2 + K_v s + K_p} \quad (2.12)
\end{aligned}$$

where  $K_v(s) = K_{vp}(s) + K_{vl}(s)$  and  $K_p(s) = K_{pp}(s) + K_{pl}(s)$ . Then, the transfer function between the distance error of the consecutive vehicles and the positions can be calculated as,

$$\begin{aligned}
A_{i-1} - A_i &= (1 - T_p) A_{i-1} - T_l A_l \\
E_i(s) &= X_{i-1} - X_i = \frac{A_{i-1} - A_i}{s^2} = S_p X_{i-1} - T_l X_l. \quad (2.13)
\end{aligned}$$

Here,  $S_p(s) = 1 - T_p(s)$  represents transfer function between the position of vehicle  $i - 1$  and the distance error between the vehicles  $i - 1$  and  $i$ . It can be interpreted as sensitivity transfer function between the acceleration input and the position error of the  $i^{th}$  vehicle. Usually the responses are compared with respect to acceleration inputs of the leader vehicle, in that case the given transfer function can be manipulated accordingly. Moreover, the transfer function between the distance errors and the acceleration of the leader vehicle can be shown iteratively.

$$\frac{E_i}{E_{i-1}} \frac{E_{i-1}}{E_{i-2}} \cdots \frac{E_1}{X_l} = \frac{S_p X_{i-1} - T_l X_l}{X_l} \quad (2.14)$$

Finally, the transfer function between the errors can be calculated as follows.

$$\begin{aligned}
\frac{E_{i+1}(s)}{E_i(s)} &= \Gamma_i(s) = \frac{A_i - A_{i+1}}{A_{i-1} - A_i} \\
&= \frac{(1 - T_p)A_i - T_l A_l}{(1 - T_p)A_{i-1} - T_l A_l} = \frac{(1 - T_p)(T_p A_{i-1} + T_l A_l) - T_l A_l}{(1 - T_p)A_{i-1} - T_l A_l} \\
&= \frac{T_p((1 - T_p)A_{i-1} - T_l A_l)}{(1 - T_p)A_{i-1} - T_l A_l} \\
\Gamma_i(s) &= \Gamma(s) = T_p(s)
\end{aligned} \tag{2.15}$$

As calculated the transfer function between the distance errors of the consecutive vehicles is equal to the closed loop transfer function of the predecessor loop of LPF.

Before presenting any simulation results, the general simulation parameters must be introduced. From the beginning to the end, the simulation parameters used are as following.

- Communication frequency is set to  $20Hz$
- Control loop frequency is set to  $1000Hz$
- Controllers are given in Appendix A
- All the controllers are discretized according to loop frequency

For a better understanding, a string stable vehicle platoon in terms of distance errors, under constant acceleration of the leader vehicle for a long period of 40 seconds is given in Figures 2.5 and 2.6. In the given example, all of the delays introduced are selected as zero to show the ideal LPF CSP case. Observing that the distance errors are bounded and decreasing along the platoon confirms that string stability is fulfilled. Furthermore, it can be seen that the string stability property is not satisfied for the acceleration signals.

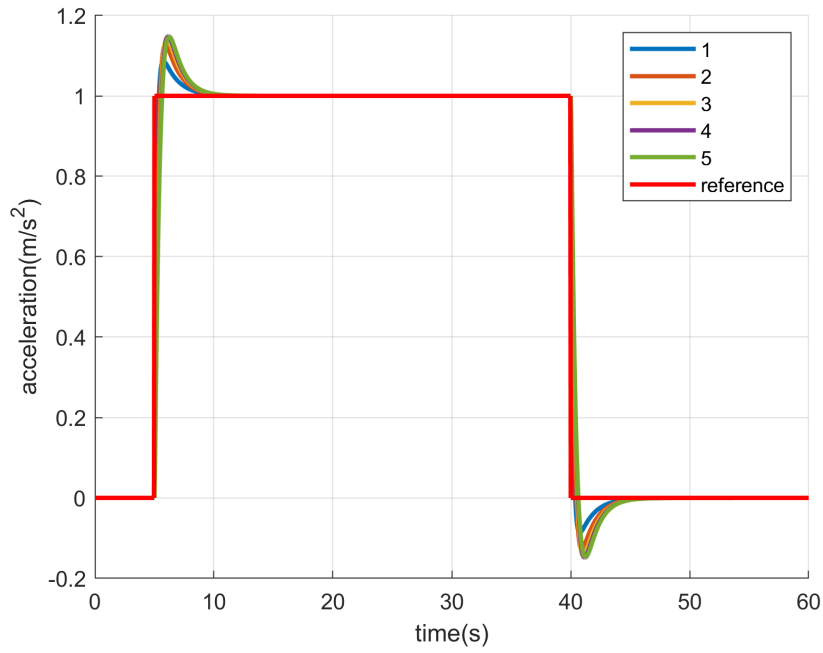


Figure 2.5: An ideal CSP LPF platoon accelerations, under constant acceleration input.

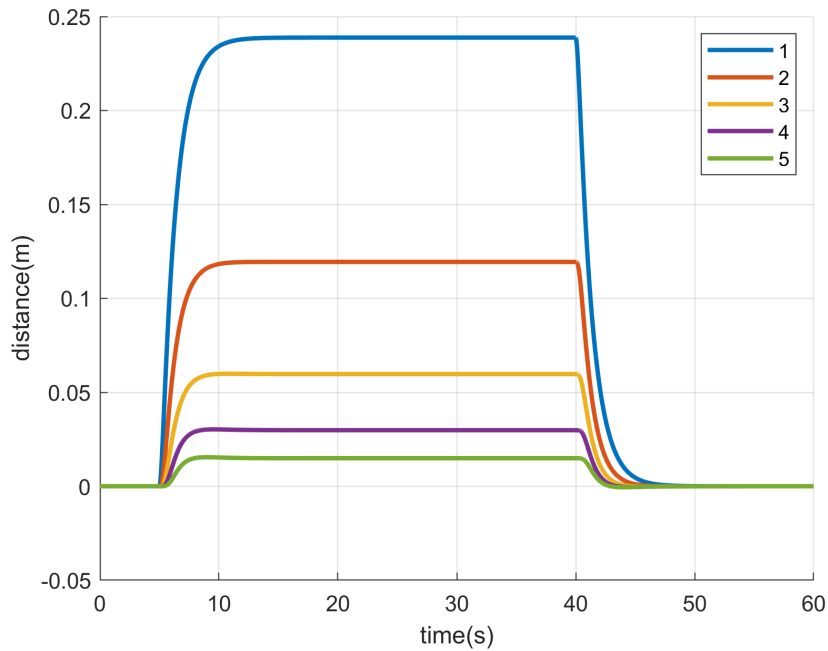


Figure 2.6: An ideal CSP LPF platoon distance errors, under constant acceleration input.

## CHAPTER 3

### LEADER PREDECESSOR FOLLOWING CONTROLLER SYNTHESIS

In this chapter, the work conducted will be explained in detail. Exercising leader predecessor following, a small maximum gap between the vehicles can be achieved. A shortcoming of the CSP LPF is that, it is sensitive to communication delays. The leader follower (LF) communication delay causes followers to track the delayed state of the leader vehicle, which creates an effect of distance increase under leader acceleration [16, 19, 22, 23]. The PF communication and sensor delays, increase the maximum distances between the vehicles. If they are increased too much, they can create string instability. To annihilate these undesirable behaviours in the vehicle platoon, the aforementioned delays must be handled accordingly.

As it was discussed in Section 2.2 and 2.3, the vehicle string will be considered homogeneous and all the vehicles are assumed to have the same controller implemented on them. The clocks of the vehicles are synchronized. The information received by each vehicle, can be used at the same time, thus all the vehicles are exposed to the same communication and sensor delays.

Throughout this section, the iterative transfer function between the vehicles will be calculated in Section 3.1, a robust controller design method with simple weights for the perfect, delay free case will be studied in Section 3.2. The string stability will be checked and the performance of the controller will be evaluated. Furthermore, the iterative transfer functions required for simulation and analysis of the different control architectures will be calculated. The effects of each delay will be examined in detail in Section 3.3.

### 3.1 Iterative Transfer Functions

The acceleration relation between the leader, predecessor and followers for the CSP LPF topology is given in (2.11). Using (2.11), we can write an iterative transfer function between the acceleration of the leader and the followers.

$$\begin{aligned}
A_i(s) &= T_p A_{i-1} + T_l A_l \\
A_1(s) &= (T_p + T_l) A_l = \tilde{T}_1 A_l \\
A_2(s) &= T_p A_1 + T_l A_l \\
&= (T_p \tilde{T}_1 + T_l) A_l = \tilde{T}_2 A_l \\
&\dots \\
A_i(s) &= \tilde{T}_i A_l
\end{aligned} \tag{3.1}$$

As can be seen, the acceleration of the  $i^{th}$  vehicle can be calculated directly from the leader acceleration, under ideal circumstances. For the given calculation to be perfectly true, the platoon should be considered homogeneous and there should not be any disturbances between any of the vehicles. Then the consecutive transfer functions between leader acceleration and the accelerations of the vehicle  $i$  and  $i + 1$ , can be attained recursively.

$$\begin{aligned}
\tilde{T}_{i+1}(s) &= T_p \tilde{T}_i + T_l, \forall i \geq 1 \\
\tilde{T}_1(s) &= T_p + T_l
\end{aligned} \tag{3.2}$$

Under the initial assumptions of homogeneity and the absence of disturbances, the acceleration of the predecessor can be estimated directly from the leader acceleration. This approach will be the basis of the predecessor acceleration estimation in the following sections. Using the iterative acceleration transfer functions together with (2.13), the transfer function between the consecutive distance errors of the vehicles and leader acceleration can be calculated.

$$\begin{aligned}
E_i(s) &= \frac{1 - T_p}{s^2} A_{i-1} - \frac{T_l}{s^2} A_l \\
E_1(s) &= \frac{S_p - T_l}{s^2} A_l = \tilde{S}_1 A_l \\
E_2(s) &= \frac{S_p \tilde{T}_1 - T_l}{s^2} A_l = \tilde{S}_2 A_l \\
&\dots \\
E_{i+1}(s) &= \frac{S_p \tilde{T}_i - T_l}{s^2} A_l = \tilde{S}_i A_l
\end{aligned} \tag{3.3}$$

Assuming a homogeneous platoon, another possible way of reaching the iterative transfer functions between the leader acceleration and distance errors is using the  $\Gamma_i = \Gamma, \forall i > 1$ .

$$\begin{aligned}
 E_1(s) &= \tilde{S}_1 A_l \\
 E_2(s) &= \Gamma \tilde{S}_1 A_l \\
 E_3(s) &= \Gamma^2 \tilde{S}_1 A_l \\
 &\dots \\
 E_i(s) &= \Gamma^{i-1} \tilde{S}_1 A_l
 \end{aligned} \tag{3.4}$$

### 3.2 $H_\infty$ Controller Synthesis

In the previous section, the ability to have string stable platoon with the CSP LPF topology is shown. Before studying the effects of different delays, first a controller that creates a string stable platoon should be designed. In this thesis, a robust controller synthesis method is used for the controllers. For the controller synthesis, the block diagram of the control loop is as follows.

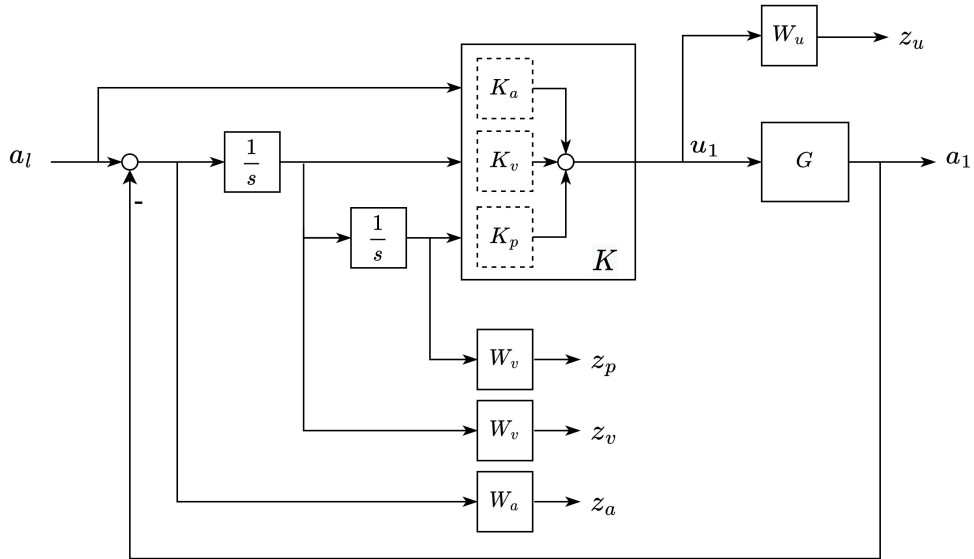


Figure 3.1: The block diagram for  $H_\infty$  synthesis.

The controller synthesis is done for the ideal LPF CSP case, which does not include the communication and sensor delays. Furthermore, the controller synthesis is done

over the block diagram given in Figure 3.1 which is applicable only to the vehicle 1, since the block diagram in Figure 3.1 is satisfied only for the case where the leader and predecessor is the same vehicle. Later, these controllers will be mapped to every other vehicle in the platoon. For the synthesis process the controllers are named as  $K_a(s)$  for the feedforward,  $K_v(s)$  and  $K_p(s)$  for the feedback controllers. The transfer function weights are also given on the diagram as  $W_u(s), W_v(s), W_p(s)$  and  $W_a(s)$ . The given block diagram in Figure 3.1 corresponds to the following LFT block diagram.

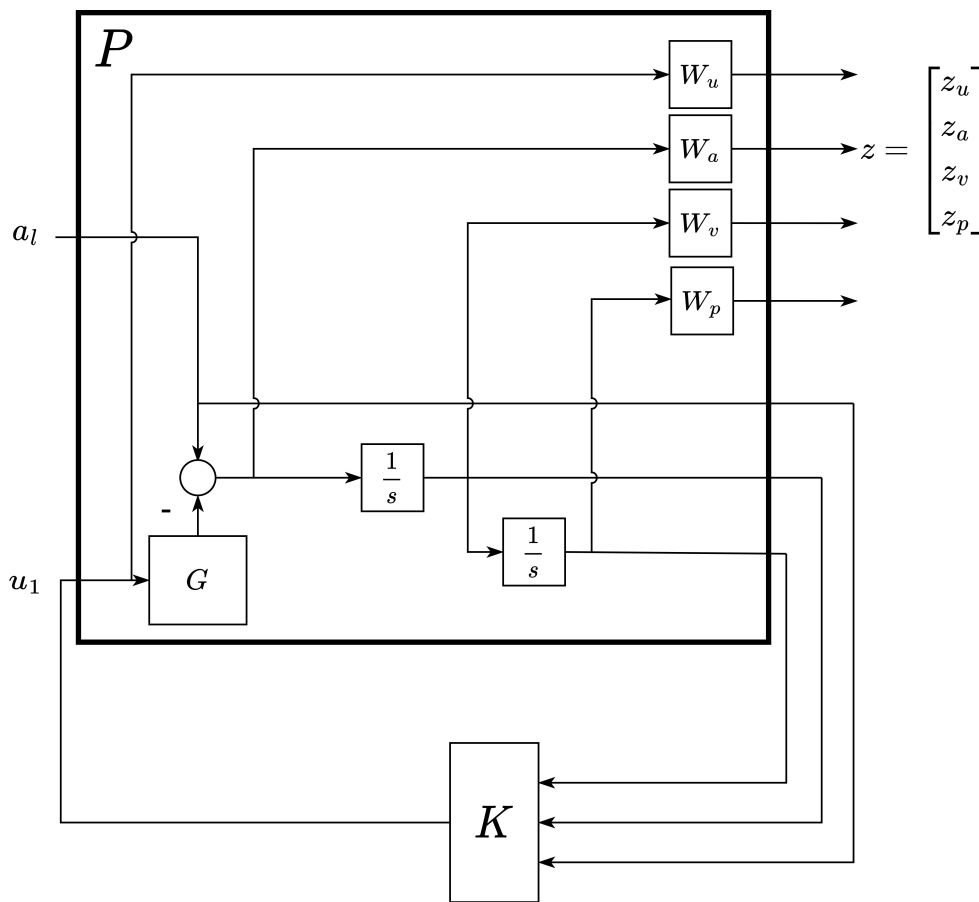


Figure 3.2: The LFT block diagram for  $H_\infty$  synthesis.

The following relations between the inputs and outputs of the  $H_\infty$  synthesis can be formulated. Again for the readability the Laplace transform variable  $s$  is omitted,

instead the Laplace domain signals are shown with capital letters.

$$\begin{aligned}
Z_u &= W_u U_1 \\
Z_a &= W_a(A_l - A_1) = W_a A_l - W_a G u_1 \\
Z_v &= W_v(V_l - V_1) = \frac{W_v A_l - W_v G u_1}{s} \\
Z_p &= W_p(X_l - X_1) = \frac{W_p A_l - W_p G u_1}{s^2}
\end{aligned} \tag{3.5}$$

$$\begin{bmatrix} Z_u \\ Z_a \\ Z_v \\ Z_p \\ \hline A_l \\ V_l - V_1 \\ X_l - X_1 \end{bmatrix} = \begin{bmatrix} 0 & W_u \\ W_a & -W_a G \\ W_v/s & -W_v G/s \\ W_p/s^2 & -W_p G/s^2 \\ \hline 1 & 0 \\ 1/s & -G/s \\ 1/s^2 & -G/s^2 \end{bmatrix} \begin{bmatrix} A_l \\ U_1 \end{bmatrix} = P \begin{bmatrix} A_l \\ U_1 \end{bmatrix} \tag{3.6}$$

The matrix  $P$  can be represented as follows.

$$P = \begin{bmatrix} P_{11} & P_{12} \\ P_{21} & P_{22} \end{bmatrix} \tag{3.7}$$

The  $K$  in Equation (3.1) is written in matrix form as  $K(s) = [K_a(s), K_v(s), K_p(s)]$ . Then with the lower linear fractional transformation  $F_l(K, P)$  [34],

$$F_l(K, P) = P_{11} + P_{12}K(I - P_{22}K)^{-1}P_{21} \tag{3.8}$$

the resulting lower linear fractional transformation (LLFT) matrix is as achieved.

$$F_l(K, P) = \begin{bmatrix} \frac{W_u(K_a s^2 + K_v s + K_p)}{s^2 + GK_v s + GK_p} \\ \frac{W_a s^2 (1 - GK_a)}{s^2 + GK_v s + GK_p} \\ \frac{W_v s (1 - GK_a)}{s^2 + GK_v s + GK_p} \\ \frac{W_p (1 - GK_a)}{s^2 + GK_v s + GK_p} \end{bmatrix} = \begin{bmatrix} W_u G_u \\ W_a S \\ W_v S/s \\ W_p S/s^2 \end{bmatrix} \tag{3.9}$$

The resulting LLFT will be used for  $H_\infty$  synthesis. The  $H_\infty$  norm of the given LLFT will be minimized. MATLAB's *hinfsyn* function is used for the synthesis. The objective of the optimization is given as  $\min_{\text{stabilizing}} \|F_l(K, P)\|_\infty$  [34].

The weights  $W_a(s)$ ,  $W_v(s)$  and  $W_p(s)$  are used to shape the sensitivity transfer function of the loop, which will result in a string stable distance error between vehicles. Not only the acceleration errors, but the velocity and position error's  $H_\infty$  norm are also bounded by a transfer function. With the selection of these weights, as long as a bounded closed loop transfer function can be achieved, the controllers can be mapped to obtain a  $\|\Gamma(s)\|_\infty \leq 1$  since  $\Gamma(s) = T_p(s)$ . Thus, the selection of the weights are not critical in terms of satisfying the string stability. Hence, the weights are selected in order to minimized the distance between the leader and first follower vehicle by an iterative, trial and error approach.  $W_u(s)$  is used to limit the control input. The  $W_u(s)$  is selected loosely, since the limitation of the control input is not in the scope of this thesis. For the synthesis the following weights are used.

$$\begin{aligned}
 W_u &= 0.01 \\
 W_a &= \frac{s/M_s + w}{s + w\epsilon}, w = 0.01, M_s = 5, \epsilon = 10^{-10} \\
 W_v &= 1 \\
 W_p &= 1
 \end{aligned} \tag{3.10}$$

The resulting controllers can be found in the Appendix A. The closed loop and sensitivity transfer functions, resulting from the controller synthesis can be seen in Figure 3.3 and 3.4.

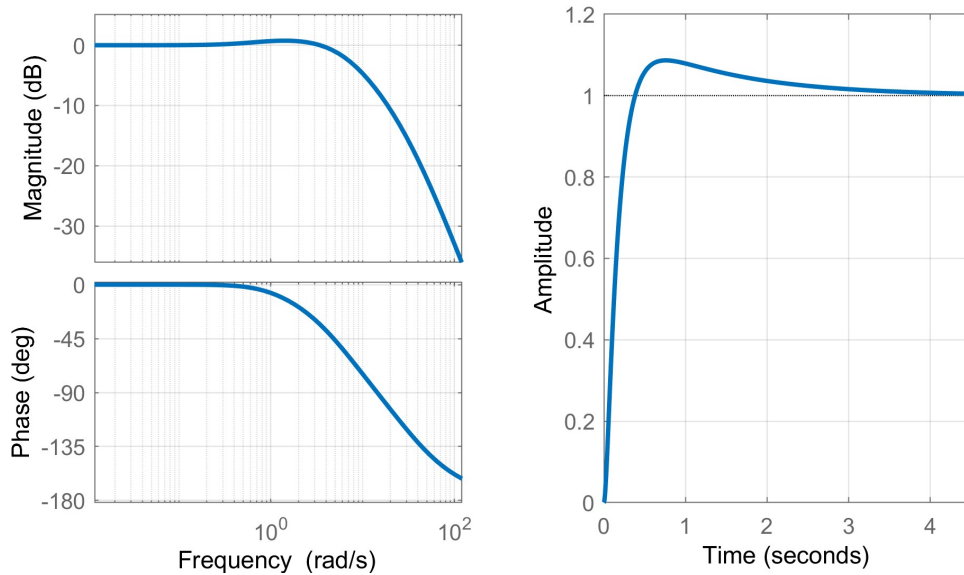


Figure 3.3: The closed loop Bode plot and step response of the transfer function between the leader and first follower accelerations.

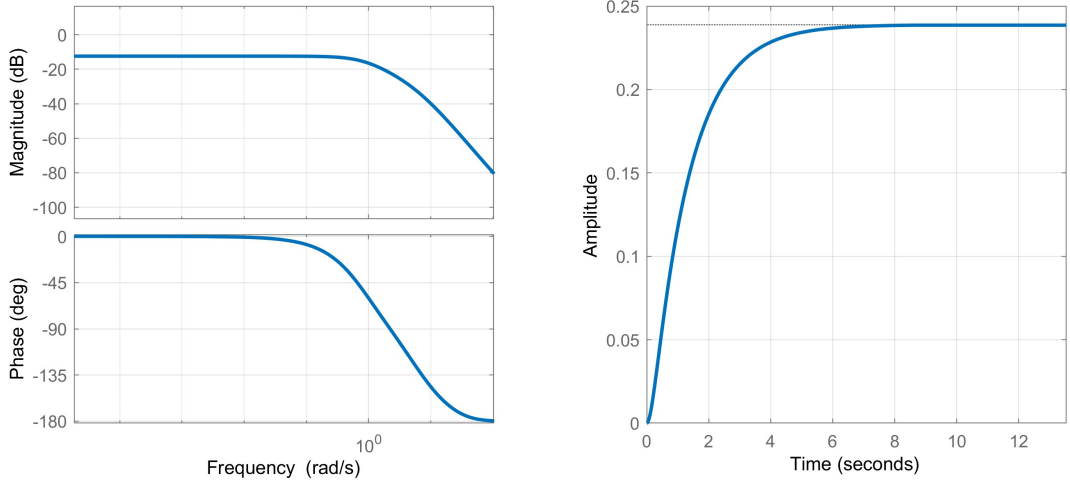


Figure 3.4: The Bode plot and step response of the transfer function between the distance error and acceleration input.

Naming the closed loop transfer function as  $T(s)$  and sensitivity as  $S(s)$ , the resulting transfer functions are as follows.

$$\begin{aligned} \frac{A_1(s)}{A_l(s)} = T(s) &= \frac{s^2 K_a + s K_v + K_p}{\tau s^3 + s^2 + s K_v + K_p} \\ \frac{E_1(s)}{A_l(s)} = \frac{S(s)}{s^2} &= \frac{\tau s + 1 - K_a}{\tau s^3 + s^2 + s K_v + K_p} \end{aligned} \quad (3.11)$$

According to the [35] and [15], the LPF CSP controller can be attained by the linear combination of the leader and predecessor inputs. This can be handled simply by multiplying the controller of the predecessor loop by  $\alpha$  and the leader loop by  $1 - \alpha$ , for  $\alpha < 1$ . Hence, the resulting controllers can be mapped to the controllers in the Equation (2.10) and Figure 2.4. With the mapping the LPF robust controller design would be complete. The controllers mapping are as follows.

$$\begin{aligned} [K_{ap}(s), K_{vp}(s), K_{pp}(s)] &= \alpha [K_a(s), K_v(s), K_p(s)] \\ [K_{al}(s), K_{vl}(s), K_{pl}(s)] &= (1 - \alpha) [K_a(s), K_v(s), K_p(s)] \\ T_p(s) &= \alpha T(s) \\ T_l(s) &= (1 - \alpha) T(s) \end{aligned} \quad (3.12)$$

Selecting  $\alpha = 0.5$  the following transfer functions for  $T_p(s) = T_l(s)$  is obtained for each vehicle. The bode plot of the  $T_p(s)$  is as follows.

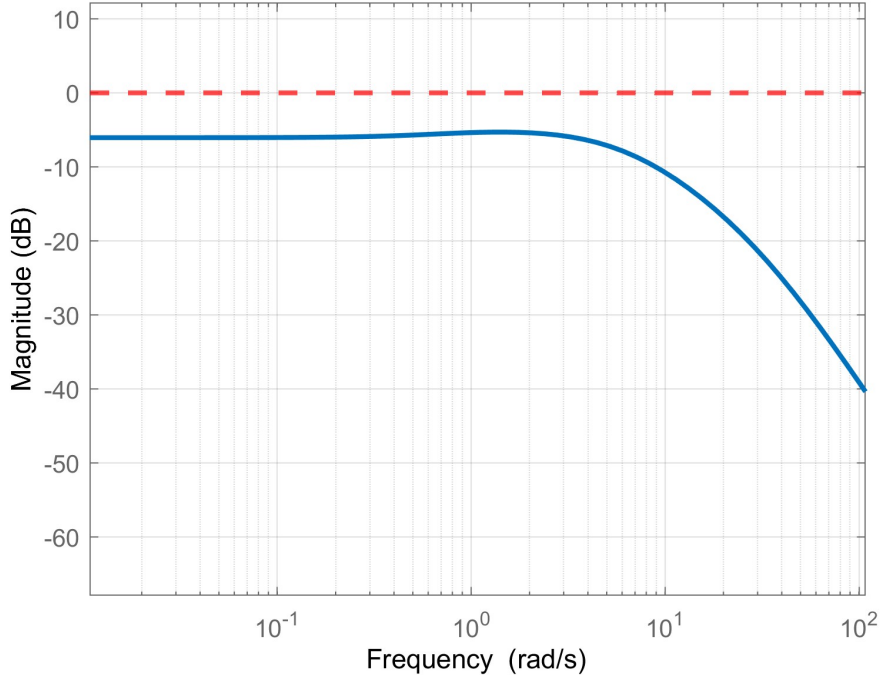


Figure 3.5: The Bode plot of the  $T_p(s) = T_l(s)$ .

The condition that the supremum of the  $T_p(s)$  transfer function should be bounded by 1 is confirmed in Figure 3.5 together with the Bode plot of  $T_p(s)$ . As it was given in Equation (2.15),  $T_p(s) = \Gamma(s)$ . As a result, with  $H_\infty$  synthesis, a string stable vehicle platoon in terms of the distance error between vehicles is achieved. For a platoon of nine vehicles, using the synthesized controller and the iterative equations given in (3.1) and (3.3), the bode plots of the transfer functions between the leader acceleration and the acceleration of the each vehicle is given in Figure 3.6. Also the bode plot of the transfer function between the leader acceleration and the distance errors between the vehicles  $\tilde{S}_i$ , are given in Figure 3.7. It can be shown that  $\tilde{S}_i$  are bounded by the  $\tilde{S}_1$ , moreover the ratio between the transfer functions corresponds to the  $\Gamma(s) = T_p(s)$  in Figure 3.5.

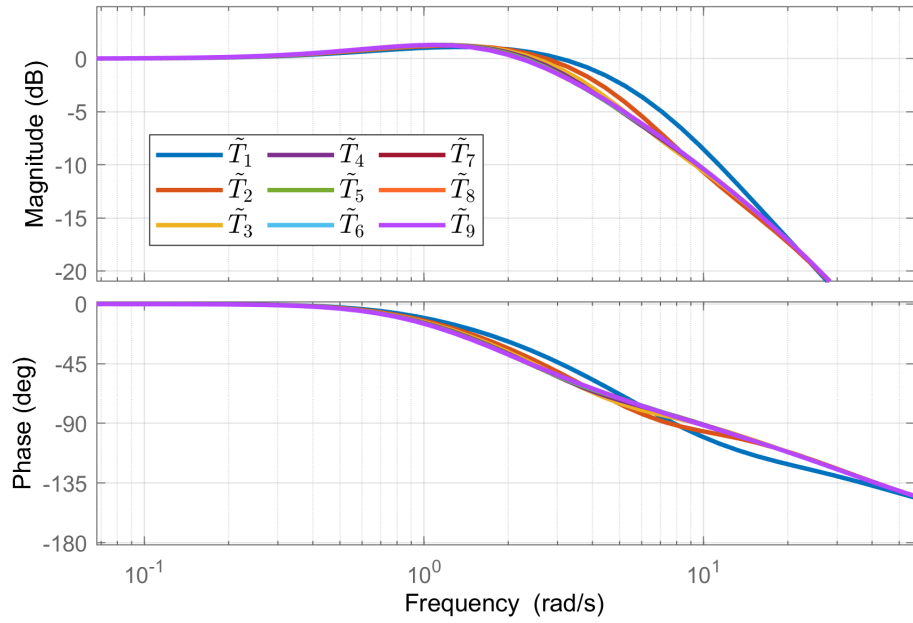


Figure 3.6: The Bode plot of the transfer functions between the leader and follower accelerations given in Equation (3.1).

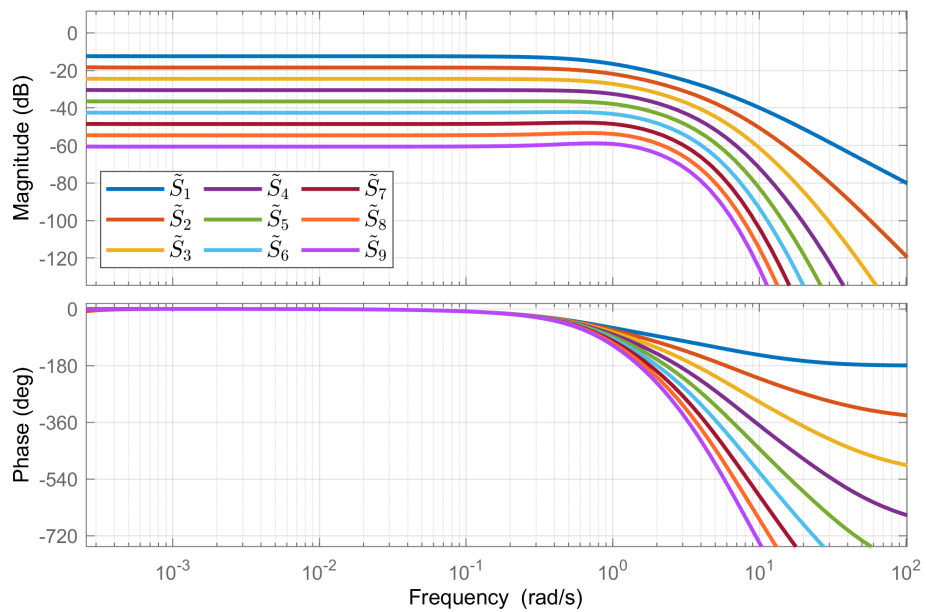


Figure 3.7: The Bode plot of the transfer functions between the leader acceleration and distance errors the vehicles as in Equation (3.3).

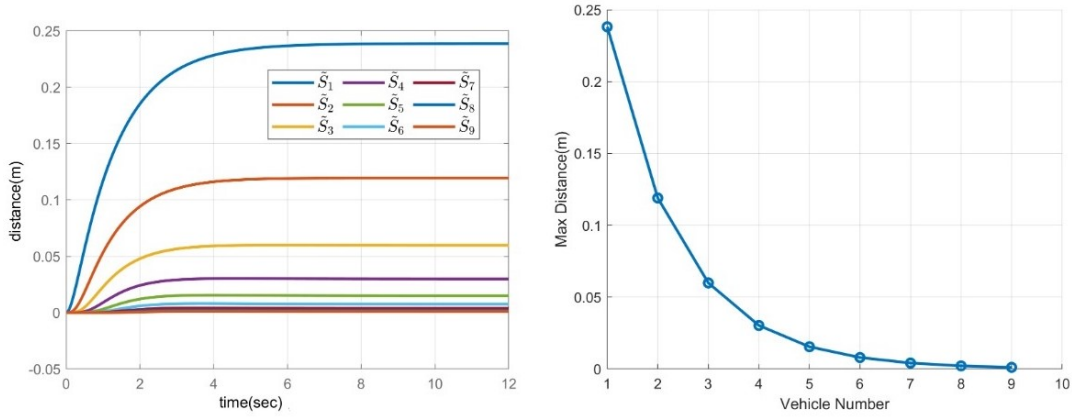


Figure 3.8: The step response of the transfer functions between the leader acceleration and distance errors.

For a step acceleration input at the leader acceleration, the distances between the vehicles can be seen in the following Figure 3.8. Moreover, the maximum distances between each vehicles is shown. This is also an example to the string stability of the synthesized controller. It is shown that, for a step acceleration input of the leader vehicle, the distances between the vehicles are attenuated as we travel along the platoon.

Another important property of the control loop is the disturbance rejection characteristics. Under a communication loss or preceding vehicles sensor error, a sudden jump on the acceleration input received by the followers can be encountered. Another possibility is that, each vehicles radar or lidar sensor might have internal software or hardware problems which can cause a leap at the output of the sensor, hence in the velocity and position of the predecessor vehicle measured by follower. In order to observe the designed controllers' worst case performance, the following extreme acceleration and velocity disturbance inputs are applied. These disturbances are applied to the first vehicle in order to see the effect as it travels through the platoon. The leader acceleration is set to zero for the disturbance cases. The acceleration disturbance is named as  $d_a(t)$  and the velocity disturbance is named as  $d_v(t)$ . For the acceleration disturbance:

$$d_a(t) = \begin{cases} 0 & t \leq 5 \\ 1 & 5 < t \leq 45 \\ 0 & 45 < t \end{cases} \quad (3.13)$$

For the velocity disturbance

$$d_v(t) = \begin{cases} 0 & t \leq 10 \\ 1 & 10 < t \leq 11 \\ 0 & 11 < t \end{cases} \quad (3.14)$$

The responses for the acceleration disturbance cases are given in the Figures 3.9 and 3.10. The velocity disturbance responses are given in Figure 3.11 and 3.12. Since the disturbances effect dominates the first and second vehicle, the third, fourth and fifth errors are plotted also separately for better visualization. Here it must be noted that, the robust controller synthesis method is the design selection in this thesis. Similar performances can be achieved with a properly tuned PID controller.

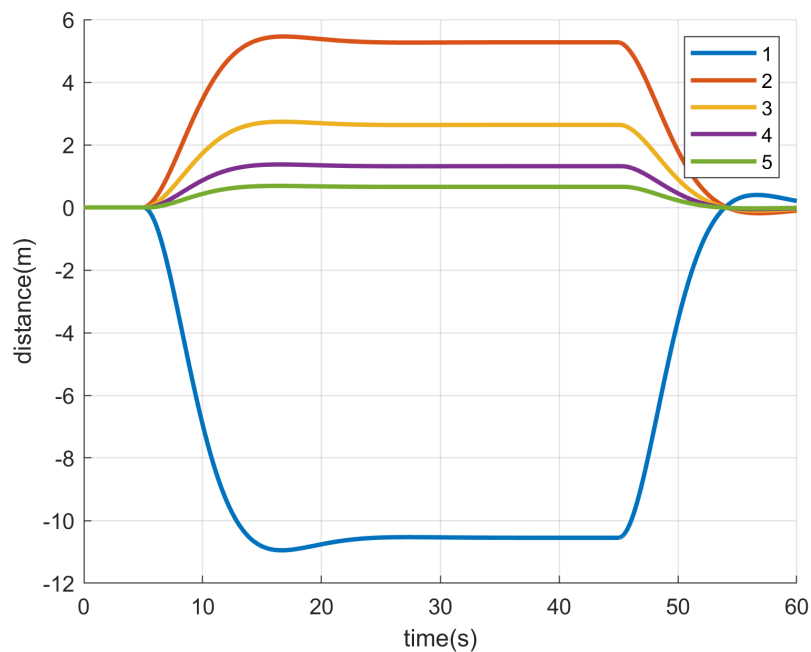


Figure 3.9: The distance error between the vehicles for an acceleration disturbance at the first vehicle.

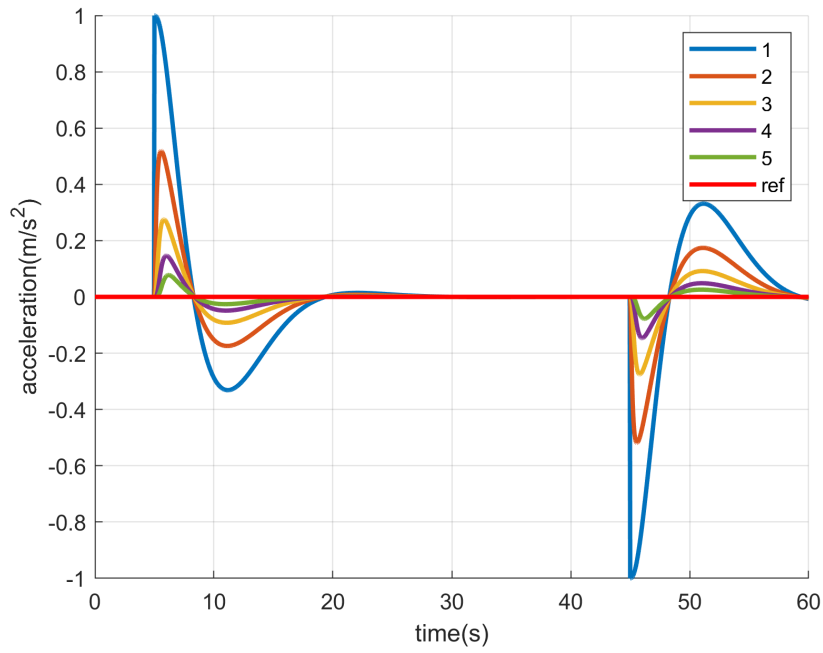


Figure 3.10: The accelerations of the vehicles for an acceleration disturbance at the first vehicle.

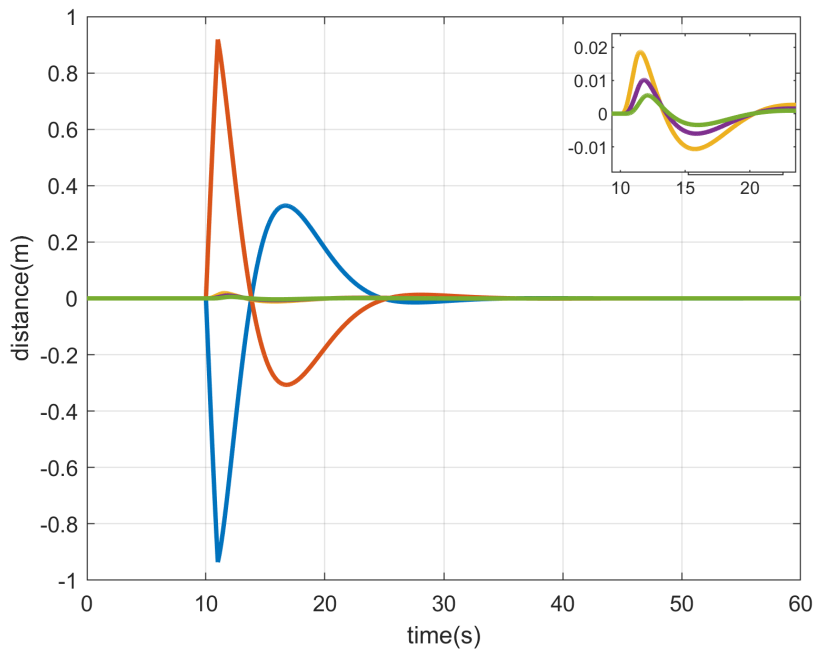


Figure 3.11: The distance error between the vehicles for a velocity disturbance at the first vehicle.

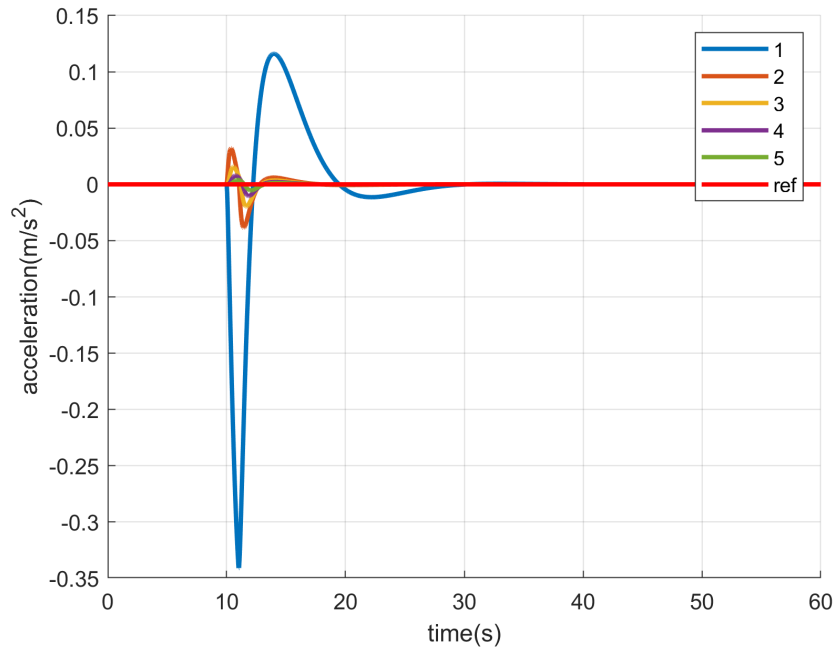


Figure 3.12: The accelerations of the vehicles for an velocity disturbance at the first vehicle.

### 3.3 Effects of Delays

Subsequently to the completion of the controller design, the effect of delays will be studied. There are mainly three delays to be considered. The PF communication delay, LF communication delay and PF sensor delay. The PF and LF communication delay occur due to the characteristics of the network. As every sensor, the PF sensor delays occur due to the electrical and mechanical characteristics of the sensor. These delays are assumed to be the same for each vehicle due to the clock synchronization of the vehicles. Hence each vehicles PF sensor and PF, LF communication delay is individually equal. For a clear understanding, each of delays will be examined one by one, while others are set to zero. And the effect of each delay is compared with the ideal, delay-less LPF CSP case. In Figure 3.13 an illustration of the information flow and the related delays can be seen.

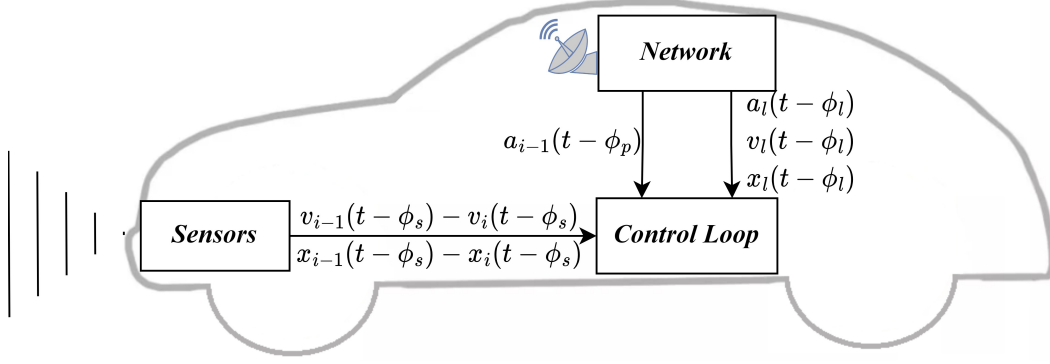


Figure 3.13: The illustration of information flow and related delays.

Under the LF communication, an increment in the distance errors occurs due to the delayed information tracking. Under PF sensor delay, we observe an increase in the  $H_\infty$  norm of the  $\Gamma(s)$ . Hence maximum distances between the vehicles, increase with increasing delay, and string instability occurs if the delays is increased beyond the boundaries. Under PF communication delay, we observe performance loss in the control loop resulting in a maximum distance increase.

First problem to be described is the LF communication delay. This is the overall network delay between the leader and the follower vehicles. Under the step acceleration input of the leader vehicle, the velocity of the vehicles will be ramp functions, and the positions will be parabolic functions. Since the vehicles are following the leader with communication delay, the distances between them will continue to increase. This problem can be seen in Equation (3.15).

$$\begin{aligned}
 e_{l,i,desired}(t) &= \sum_{j=1}^i L_j \\
 e_{l,i}(t) &= x_i(t) - x_i(t - \phi_l) + \sum_{j=1}^i L_j \\
 &= \sum_{j=1}^i L_j + \int_{t-\phi_l}^t v_l(\hat{t}) d\hat{t}
 \end{aligned} \tag{3.15}$$

This equation can be interpreted as follows. The desired distance is want to be kept as constant  $L_i$ , which we can select as zero as in 2.4. On the contrary, due to the communication delay, the delayed leader acceleration signal is used as an input to the follower control loop. Thus, the delayed information is being tracked. Furthermore, this problem can also be analyzed under frequency domain. To simplify the equations, only the first vehicle will be considered. From the Equations (2.11) and (2.12), it can be seen that the stable transfer function between the position of the leader and the distance error between leader and follower should be as follows for the delay-free case.

$$\begin{aligned} E_1(s) &= (1 - T_p - T_l)X_l(s) \\ \frac{E_1(s)}{A_l(s)} &= \frac{\tau s + 1 - K_{al} - K_{ap}}{\tau s^3 + s^2 + K_v s + K_p} \end{aligned} \quad (3.16)$$

Under only LF communication delay,  $E_i(s)$  changes as below.

$$\frac{E_1(s)}{A_l(s)} = \frac{s^2(\tau s + 1 - K_{al}e^{-s\phi_l} - K_{ap}) + sK_{vl}(1 - e^{-s\phi_l}) + K_{pl}(1 - e^{-s\phi_l})}{(\tau s^3 + s^2 + K_v s + K_p)s^2} \quad (3.17)$$

As can be seen, in Equation (3.16), the pole-zero cancellation at origin, creates a stable transfer function. For the case with LF communication delay, the required cancellation does not occur, which leads to an unstable transfer function and constant distance increase between vehicles under leader acceleration. The previously mentioned pole zero cancellation can still occur under PF sensor or PF communication delays. The same case can be shown for the other vehicles in the platoon. The elaborated effects can be seen through the Figure 3.14 with the Bode diagram of the transfer function between  $E_1(s)$  and  $A_l(s)$ . The extra integrator terms change the slope of the bode diagram at small frequencies. For the plot, all individual delays are selected as  $0.1s$ .

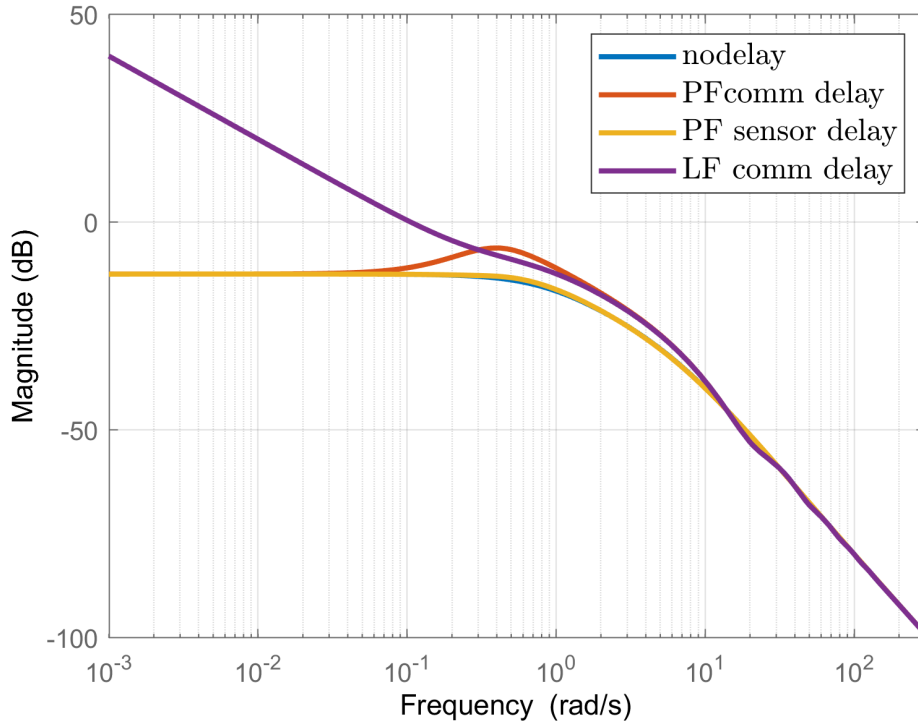


Figure 3.14: The effect of different delays on the transfer function between the  $E_1(s)$  and  $A_l(s)$ .

Assuming the leader vehicle is accelerating/decelerating, the distance between the vehicles can increase without a bound, which is not desired. The simulation results for step leader acceleration can be seen in Figure 3.15 and 3.16. In these figures, red corresponds to the ideal delay-less LPF CSP case, whereas the blue corresponds to the LPF CSP with LF communication delay. In the simulation, the communication delay between the leader and the follower is selected as 0.1 seconds.

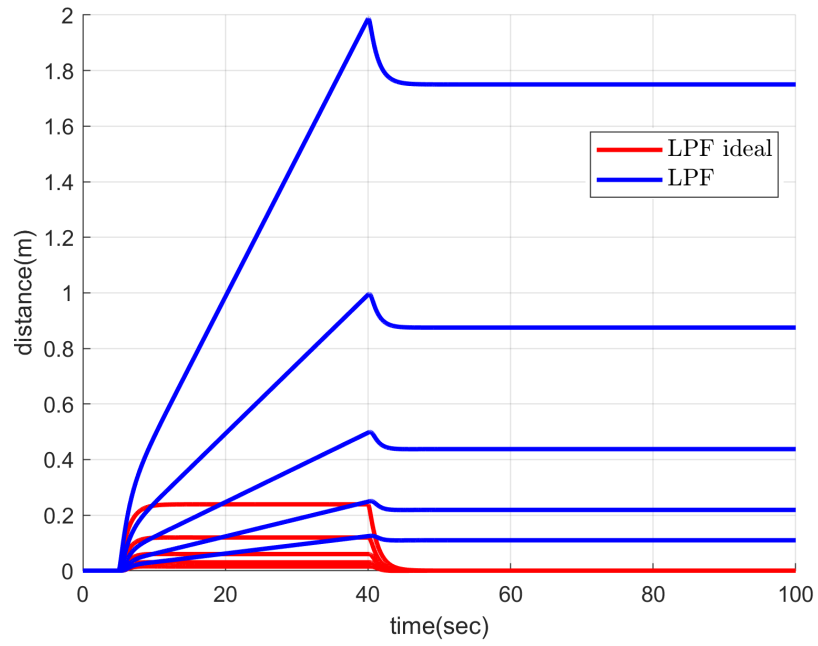


Figure 3.15: The effect of leader-follower communication delay on distance errors between the vehicles.

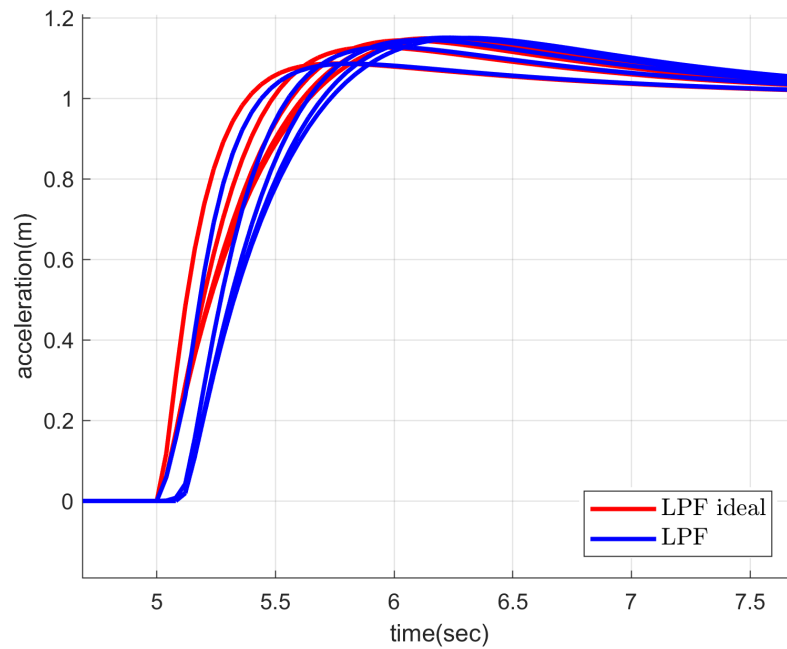


Figure 3.16: The effect of leader-follower communication delay on accelerations of each vehicle.

The second problem is the PF sensor delay. This delay corresponds to the velocity and distance error measurement, and it is on the feedback predecessor loop. This delay is much smaller than the communication delays and it is constant and deterministic, thus it is neglected commonly. Different from the LF communication delay, the PF sensor delay is inside the loop. Hence, as it is increased it creates instability. More importantly, it can cause string instability between vehicles. As the PF sensor delay increases, the maximum distance between the vehicles will increase, and eventually become string instable for large delay values. To see its effect clearly, for different PF sensor delays the  $\|\Gamma(s)\|_\infty$  is given in Figure 3.17.

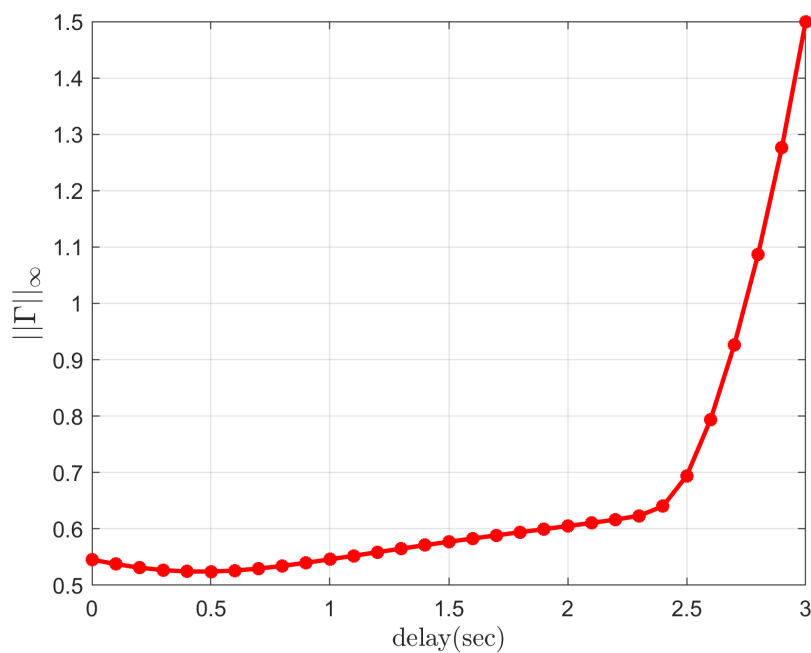


Figure 3.17: The effect of PF sensor delay on the transfer function between the distance errors.

The last delay to be analyzed is the PF communication delay. This is the overall network delay between the predecessor and the follower vehicle, which is on the feedforward predecessor loop. The effect of the PF communication is seen as a rise in the maximum distance between the vehicles under leader acceleration. This occurrence is due to the increase in  $\|\Gamma(s)\|_\infty$ . Again increasing the PF communication delay too much, causes string instability. For different delays, the  $\|\Gamma(s)\|_\infty$  can be

seen in Figure 3.18. For a nine vehicle platoon, under 0.1 s PF communication delay, we can see the change in maximum distance for each vehicle in Figure 3.19 with respect to ideal LPF CSP case. The resulting effect can be seen in time domain with the simulation results in the Figure 3.20. The red represents the ideal LPF CSP case. The PF communication delay increases the maximum distance even for a small amount of communication delay, unlike PF sensor delay.

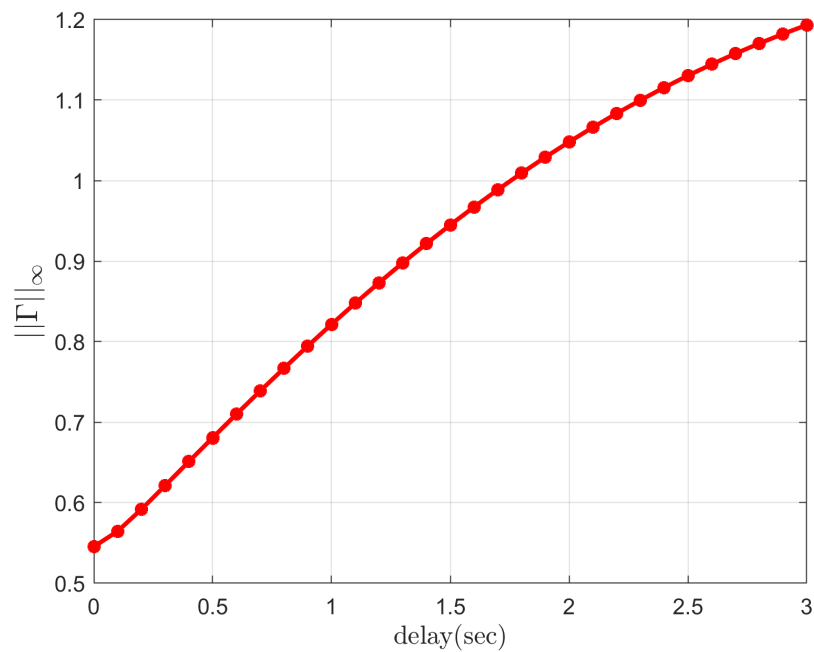


Figure 3.18: The effect of PF communication delay on the transfer function between the distance errors.

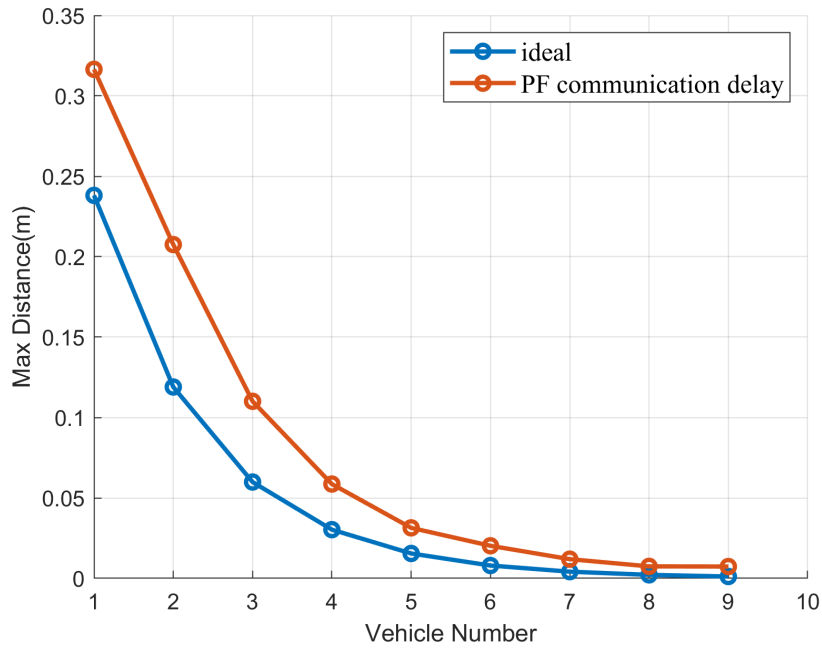


Figure 3.19: The maximum distance comparison for the ideal and 0.1s PF communication delay case.

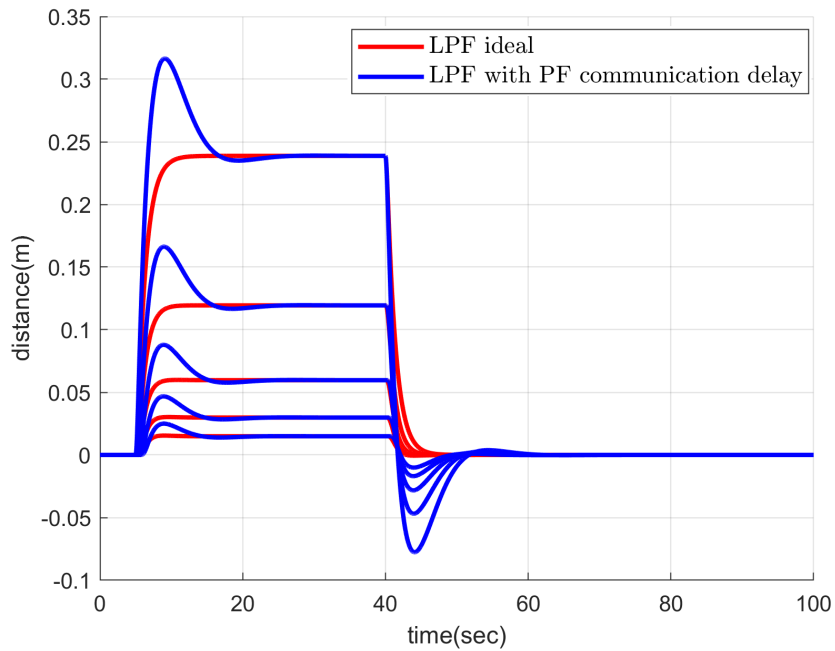


Figure 3.20: The effect of PF communication delay on distance errors between the vehicles.

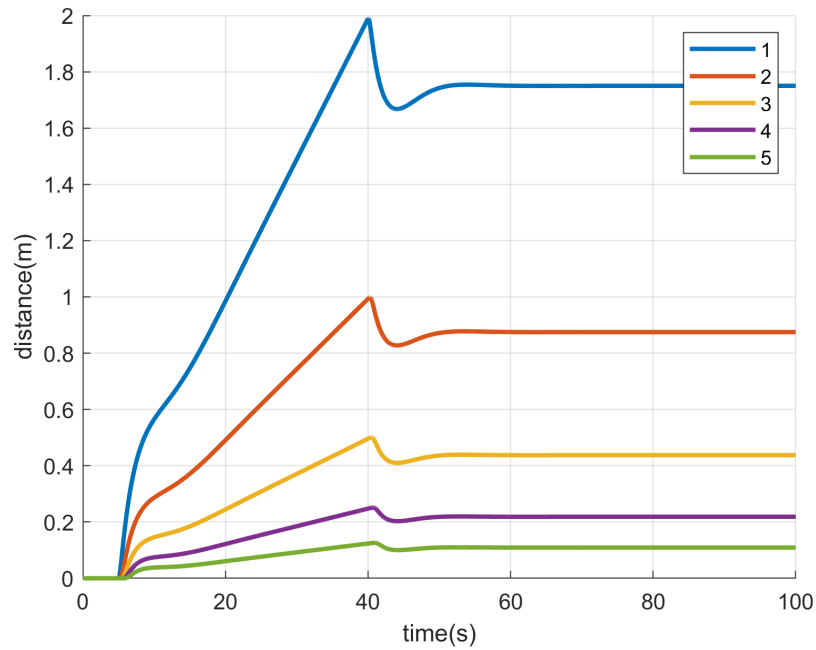


Figure 3.21: The effect of combined delays on distance errors between the vehicles.

When multiple delays are included, the combined effect is dominated by the LF communication delay in terms of maximum distance. In Figure 3.21, simulation results under the occurrence of all the included delays are given. All of the delays are set to 0.1 seconds.

To sum up, the LF communication delay results in an undesirable effect of increase of distance errors due to the control loops inability to handle step acceleration inputs. The PF communication and PF sensor delay decreases the performance of the controller in terms of preceding vehicle pursuit and increases the maximum possible distance between the vehicles, can even lead to string instability. These effects must be overcome for the CSP LPF to be employable. In addition, to reach the minimum possible distance between the vehicles, the PF communication delay must be handled. In the next sections, a possible solution to mitigating the effect of communication delays is introduced. A new modified topology, accommodating the solution is established.



## CHAPTER 4

### PREDICTED LEADER AND PREDECESSOR ACCELERATION FOLLOWING

In this chapter, a prospective future leader information estimation will be introduced in Section 4.1. A method to estimate the acceleration of the predecessor using the leader acceleration will be shown in Section 4.2. A new method utilizing a prediction observer for LPF CSP will be proposed in Section 4.3.1. Finally, a method to accommodate the PF sensor delay effect will be given in Section 4.4. The delays which are introduced in Chapter 3, will be handled one by one as we progress through the chapter. In each section, a comparison with respect to the previously introduced method will be given. At the end of the chapter, a comprehensive comparison of all the presented methods will be provided.

For the evaluation of the different control architectures, the results for the following cases will be compared. These cases are exaggerated inputs and disturbances, selected in order to observe the worst case performances of the given topologies. For each of the cases, the other inputs will be set to zero. The cases will be named as the standard cases.

- Accelerating leader vehicle with a step acceleration for 40 seconds
- Acceleration disturbance defined in Equation (3.13), applied to the first vehicle
- Velocity disturbance defined in Equation (3.14), applied to the first vehicle

#### 4.1 Predicted Leader Acceleration

The LF communication delay is the main problem behind the impracticality of CSP LPF. As it was explained in the Section 3.3, under the long time usage of CACC, the vehicles can drift from each other limitlessly. Nowadays, using path planing algorithms and navigation algorithms with Kalman filter for autonomous vehicles, it is possible to estimate the future state of the leader vehicle at least for short time periods. If the estimation can be done for a time window, larger than the maximum overall LF communication delay, it is possible to remove the effects of it. Leader vehicle being fully autonomous and the clocks of vehicles being synchronized, the broadcasted information can be received and used at the same time on every vehicle. Since the information will be reliable it can be buffered and used exactly at the correct time instant. Thus, the information used will be delay-free. For the maximum LF communication delay and the estimation horizon for the leader vehicle 0.33 s can be set as a practical boundary [36]. As a result, the block diagram of LPF will be as in Figure 4.1.

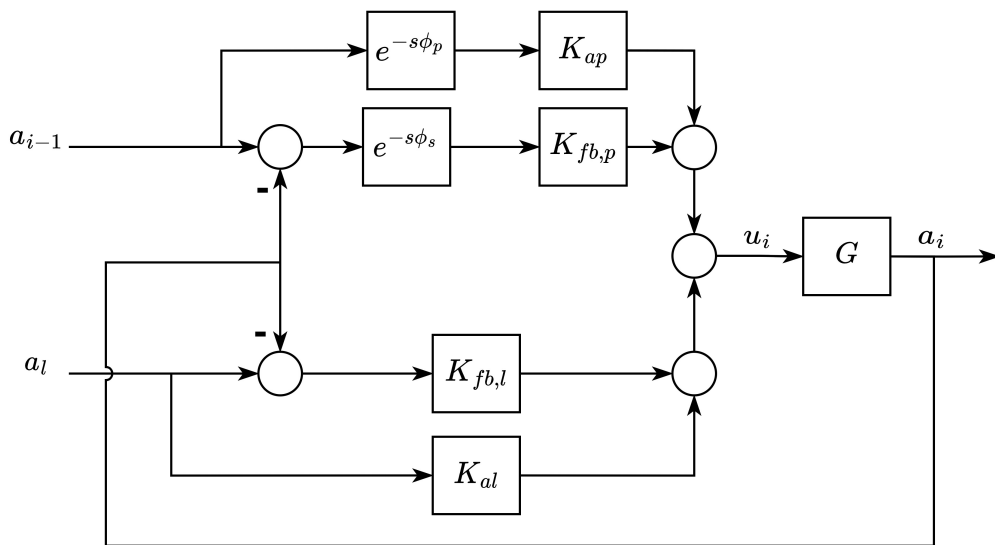


Figure 4.1: The block diagram of the LPF with predicted leader acceleration.

With the introduced predicted leader acceleration method, the effects caused by the LF communication delay is eradicated. This removal of the LF communication delay, will change the leader loop transfer function of LPF CSP, calculated in Equation

(2.11), as follows.

$$\begin{aligned}
 T_i(s) &= \frac{G(K_{al} + K_{fb,l})}{1 + GK_i} \\
 K_i(s) &= 1 + G(K_{fb,p}e^{-s\phi_s} + K_{fb,l})
 \end{aligned} \tag{4.1}$$

From this point on,  $T_i(s)$  will be regarded as in the LF communication delay free form in Equation (4.1). With the introduction of the predicted leader acceleration, the LPF with predicted leader acceleration and the standard LPF with all the introduced delays will be compared to show the benefits of the leader prediction acceleration. The comparison will be done over only the step leader acceleration case. Since for the disturbance cases, the leader acceleration is set to zero, a difference for those cases will not be observed. The main problem to be observed here, is the increasing distance under leader acceleration, hence the other cases are uninformative here. For both cases the PF communication delay is set to 0.1 seconds. For the standard LPF the LF communication delay is also set to 0.1 seconds. The controllers used can be found in Appendix A. The standard LPF will be represented with red, whereas the LPF with predicted leader acceleration will be blue.

From Figure 4.2, it can be seen that the distance increasing effect caused by the LF communication delay is eliminated. For the same leader acceleration, the distance errors between the vehicles changed dramatically. The accelerations that can be seen in Figure 4.3, with the response starting priorly, the blue graphs reflect the characteristic of a transfer function with less delay perfectly.

By employing the leader acceleration prediction, a major improvement in the distance between the vehicles is achieved. Assuming the usage of CSP LPF for CACC vehicle platoon for a very long time on a highway, if the average acceleration is not exactly zero under the LF communication delay the vehicles will drift further from each other as the time passes. With this application, the observed problem is avoided. In the next section the handling of the PF communication delay will be explained.

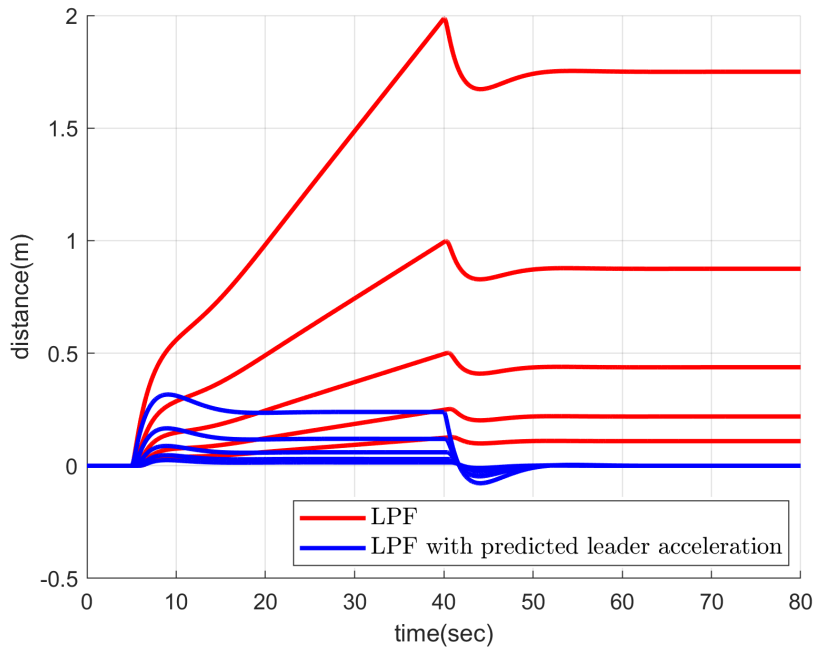


Figure 4.2: The distance errors of the vehicles for a step acceleration of the leader.

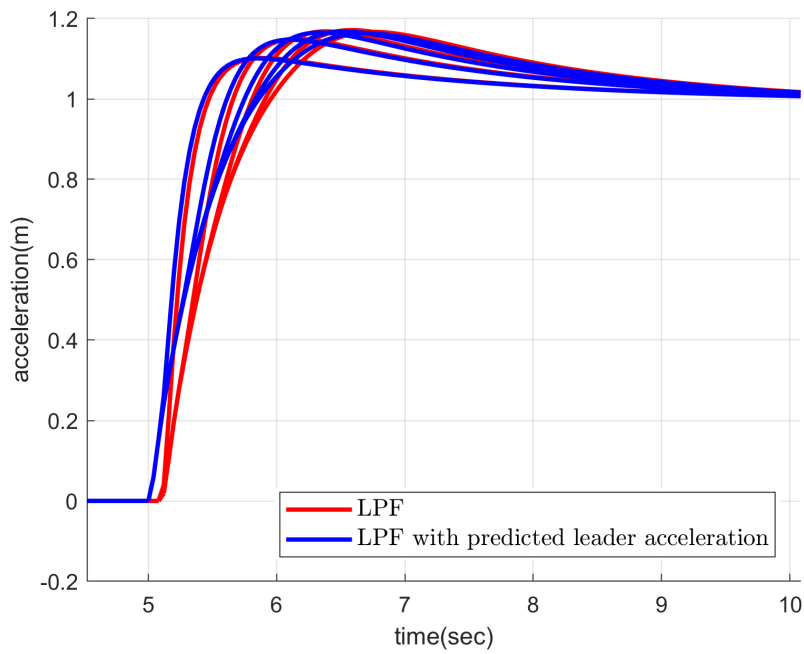


Figure 4.3: The accelerations of the vehicles for a step acceleration of the leader.

## 4.2 Modified Leader Predecessor Following

Introducing the predicted leader acceleration, now the leader acceleration can be received by the followers without delay. Thus, it is possible to estimate the predecessor acceleration from the leader acceleration using the Equations (3.1) and (3.2). The following relations can be used to estimate the acceleration of the preceding vehicle.

$$\begin{aligned}
 A_i(s) &= \tilde{T}_i A_l \\
 \tilde{T}_0(s) &= 1 \\
 \tilde{T}_1(s) &= T_p + T_l \\
 &\dots \\
 \tilde{T}_{i+1}(s) &= T_p \tilde{T}_i + T_l
 \end{aligned} \tag{4.2}$$

Then, the CSP LPF block diagram given in Figure 2.4 is modified incorporating the predecessor acceleration estimation, which will be called modified leader predecessor following (MLPF).

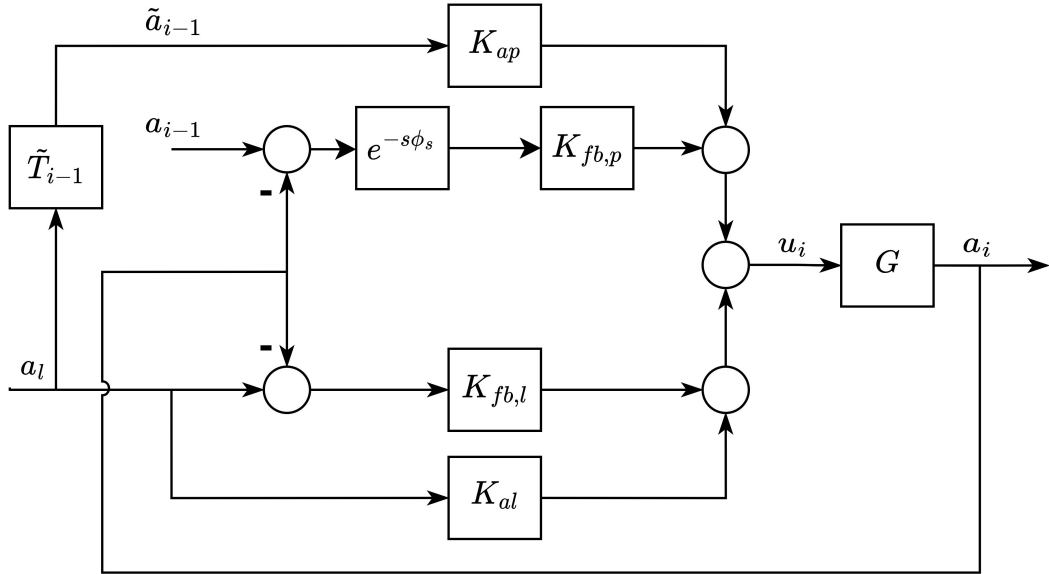


Figure 4.4: The block diagram of the modified leader predecessor following (MLPF).

For the first vehicle, the predecessor and leader is the same vehicle, thus an acceleration estimation is unnecessary. For the other vehicles, the predecessor acceleration estimation transfer function  $\tilde{T}_i(s)$  can be used. The resulting MLPF equations for the

first two vehicles after the leader is given. For the sum of transfer functions  $K_{fb,l}(s)$  and  $K_{fb,p}(s)e^{-s\phi_s}$ ,  $K_i(s)$  will be used. For the first vehicle  $\tilde{a}_0(t) = a_l(t)$  must be noted. The equations of the vehicle 1 are as follows.

$$\begin{aligned}
U_1(s) &= A_l(K_{al} + K_{ap} + K_i) - A_1K_i \\
A_1(s) &= \frac{(K_{al} + K_{ap} + K_i)G}{1 + GK_{fb}}A_l = (T_p + T_l)A_l \\
\frac{A_1(s)}{A_l(s)} &= T_1(s) = \tilde{T}_1(s)
\end{aligned} \tag{4.3}$$

For the rest of the vehicles the MLPF equations are as follows.

$$\begin{aligned}
U_i(s) &= A_l(K_{al} + K_{fb,l}) + \tilde{A}_{i-1}K_{ap} - A_iK_i \\
A_i(s) &= \frac{A_l(K_{al} + K_{fb,l})G + \tilde{A}_{i-1}K_{ap}G + A_iK_iG}{1 + GK_i} \\
\tilde{A}_{i-1}(s) &= \tilde{T}_{i-1}A_l = T_{i-1}A_l = A_{i-1}(s) \\
A_i(s) &= \frac{(K_{al} + K_{fb,l}) + \tilde{T}_{i-1}(K_{ap} + K_{fb,p}e^{-s\phi_s})}{1 + GK_i}A_l \\
&= T_pA_{i-1} + T_lA_l \\
\frac{A_i(s)}{A_l(s)} &= T_p\tilde{T}_{i-1} + T_l = \tilde{T}_i(s) = T_i(s)
\end{aligned} \tag{4.4}$$

Then the transfer function between errors is as follows

$$\begin{aligned}
E_i(s) &= X_{i-1} - X_i, \forall i \geq 1, X_0(s) = X_l(s) \\
\Gamma_i(s) &= \frac{E_{i+1}(s)}{E_i(s)} = T_p(s)
\end{aligned} \tag{4.5}$$

With the introduction of the MLPF, it can be seen that, the delay terms in the LPF which can be seen in Equation (2.9) are removed. Thus, the control loop's inability to handle step acceleration in leader acceleration and the maximum distance increase effect due to PF communication delay is overcome. The transfer functions between the accelerations of the vehicles did not change, as a result the transfer function between the distance errors  $\Gamma_i(s)$  did not change. Thus, an additional calculation to ensure the string stability is redundant. With the use of MLPF, the communication with the preceding vehicle became nonessential. Any effect caused by the PF communication delay is erased.

By removing the direct feedforward acceleration information received from the predecessor vehicle, it is expected that the performance, related to the disturbance

occurring in the acceleration or velocity of the preceding vehicle would change. For the follower vehicles, the disturbance effect would only be measured by the feedback input of the predecessor loop, instead of both feedback and feedforward loop inputs. Thus, under the given case, the acceleration and distance errors of the platoon should be analyzed. For that, the standard cases are used to evaluate the performance. The PF sensor delay is selected as 0.1 s. The controllers used in the simulation can be found in Appendix A.

At this point, the MLPF topology should be compared with LPF CSP with predicted leader acceleration. Both topologies do not contain LF communication delay. The only difference is the PF communication delay between them, whereas the LPF CPS topology has it, MLPF does not have the communication delay. In the following comparison figures the red color will represent LPF CSP and blue will represent MLPF. The distance errors and accelerations of the vehicles for each case will be given. The same generic inputs used for previous simulations will be used. In order to observe the difference better, the first 10 seconds of the accelerations are focused.

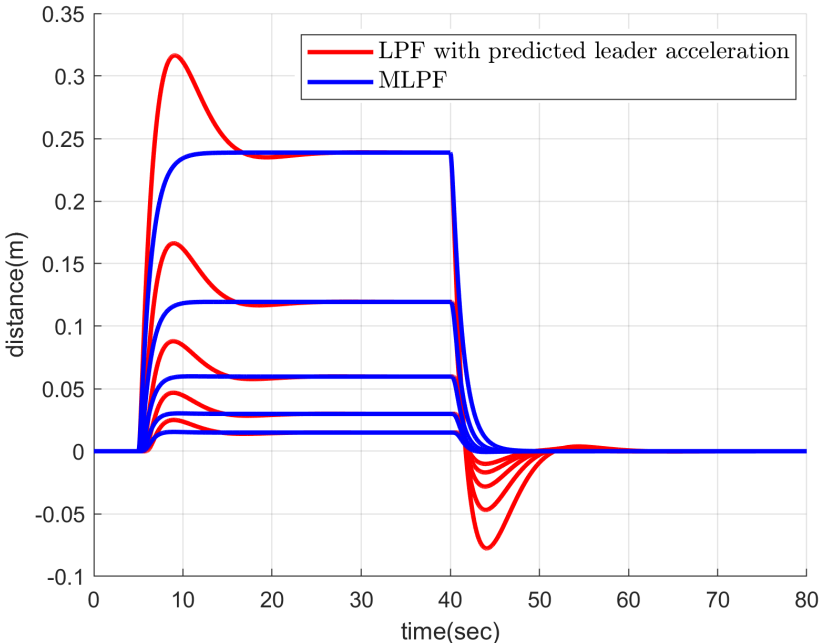


Figure 4.5: The distance errors of the vehicles for a step acceleration of the leader.

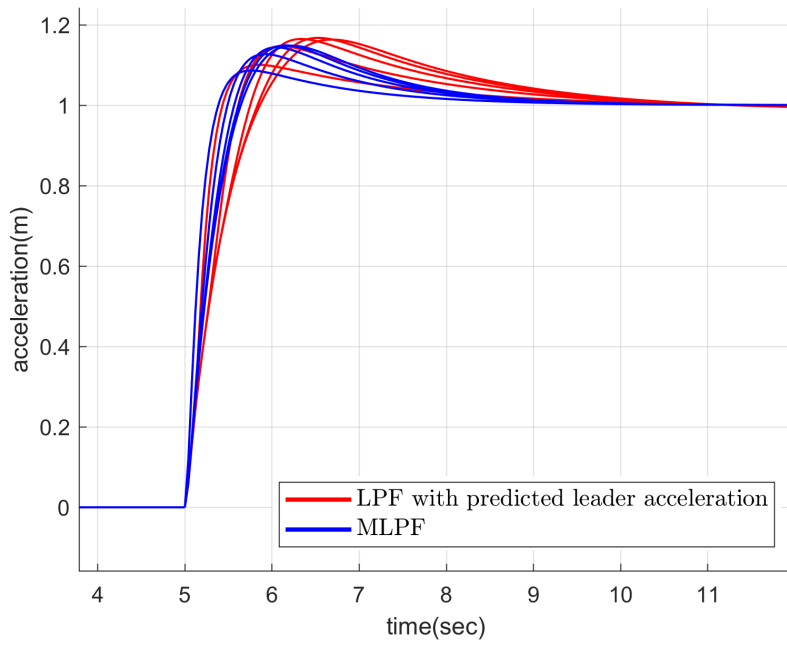


Figure 4.6: The accelerations of the vehicles for a velocity disturbance at the first vehicle.

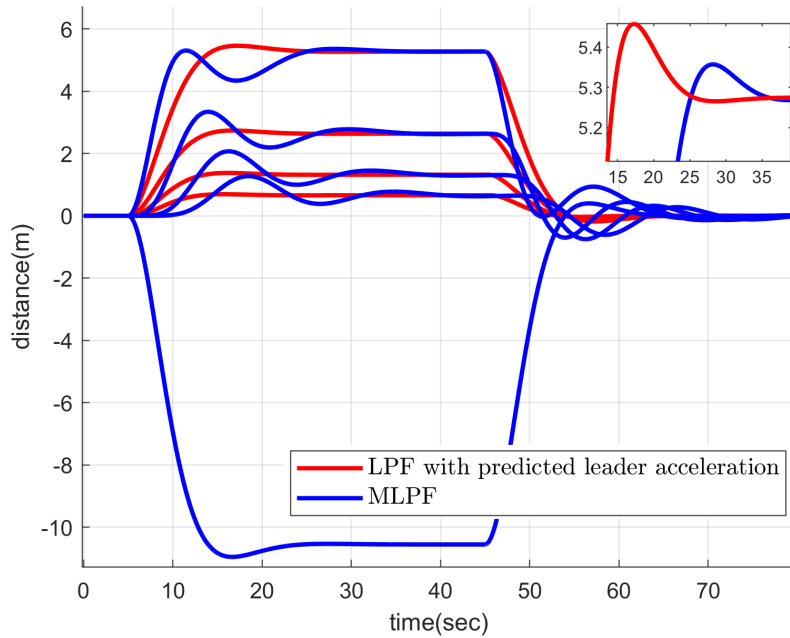


Figure 4.7: The accelerations of the vehicles for a step acceleration of the leader.

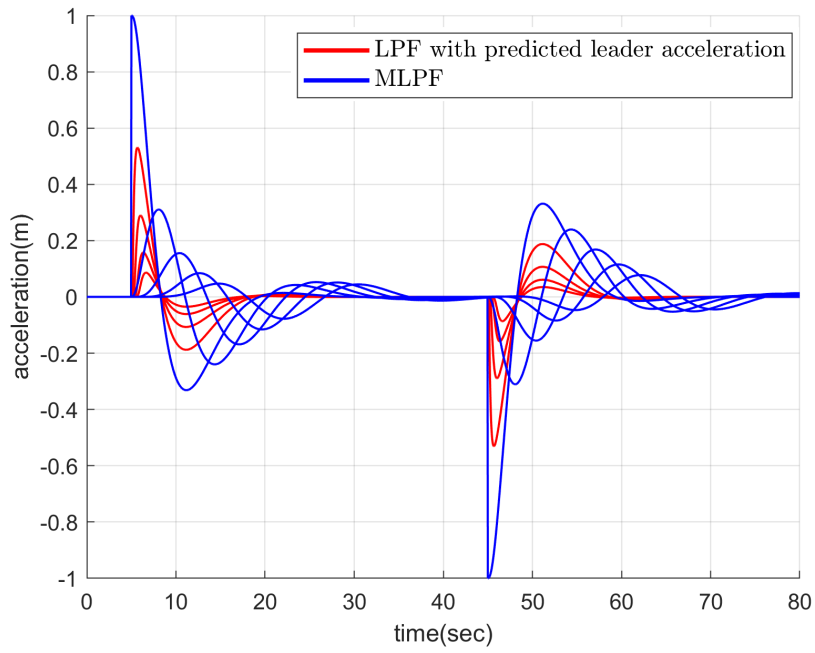


Figure 4.8: The accelerations of the vehicles for an acceleration disturbance at the first.

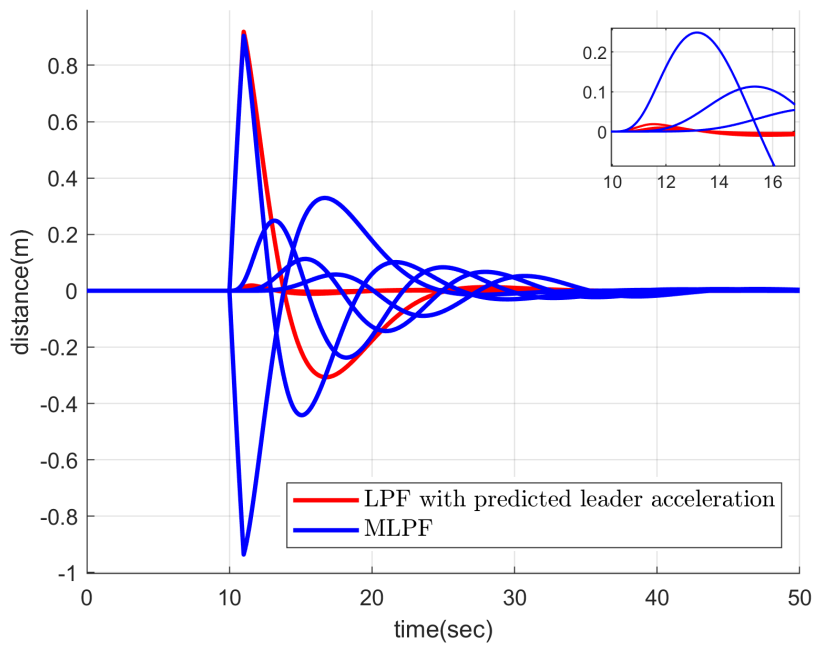


Figure 4.9: The distance errors of the vehicles for a velocity disturbance at the first vehicle.

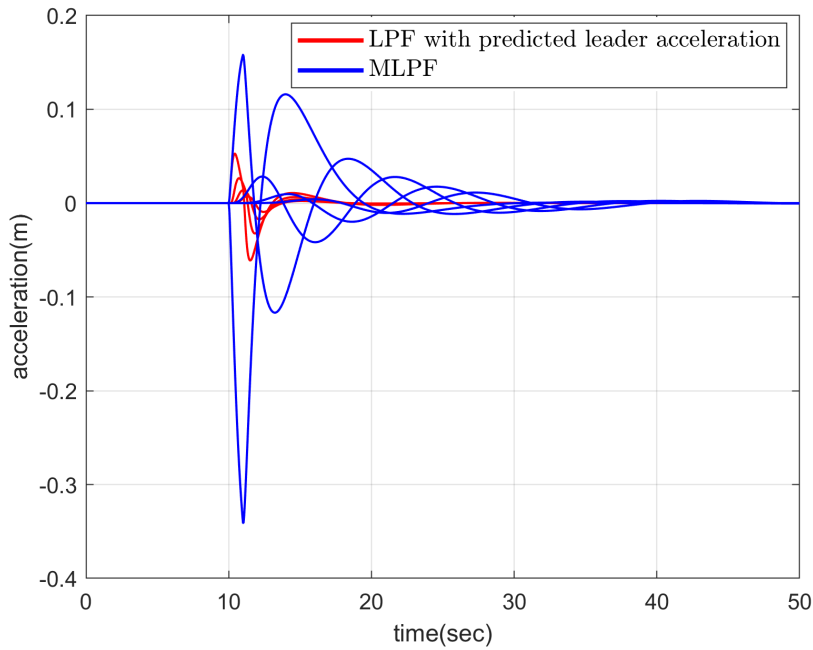


Figure 4.10: The accelerations of the vehicles for a velocity disturbance at the first vehicle.

The main property of the MLPF topology is that the communicated acceleration information from the predecessor is not used at all. Instead, the predecessor acceleration is directly estimated from the predicted leader acceleration. Together with the improvements achieved by the inclusion of the leader acceleration prediction, the vehicles' ability to continue platooning with minimal distance under leader acceleration is improved. This improvement can be seen in Figure 4.5. With the removal of the phase lag causing delay term, the accelerations converge faster as can be seen in Figure 4.6.

For the case, under acceleration disturbance of the first vehicle, a disturbance taking place in the acceleration of the first vehicle is reflected on the velocity and position of the vehicle. Even though the PF communication is removed, the resulting disturbance effect can be sensed by the follower through the velocity and position measurements. Thus, as can be seen in Figure 4.7, the response of the platoon to acceleration disturbance in the first vehicle for MLPF is similar to LPF with predicted leader acceleration. Moreover, the maximum distance between the vehicles show a slight progress. On the contrary, the response speed to an acceleration disturbance in the first vehicle

is reduced.

For the case with velocity disturbance, removing the PF communication received acceleration affected the worst. Skipping the first two vehicles dominated by the disturbance input at first vehicle, thus resulting in the same response; for the third vehicle and afterwards the maximum distance error increased by 12.5 times, from 0.02 to 0.25. The effect caused by the velocity disturbance could not be compensated as much without the feedforward predecessor loop.

With the use of MLPF, our main aim to reduce the maximum distance under leader acceleration and removing the PF communication delay effect is achieved. The maximum distance is reduced almost to the ideal LPF case, the LPF without any delay inclusion. While achieving our goal, some discrepancies under disturbance of the preceding vehicles are observed. In order to overcome them, an approach regarding the merging of the estimated and communicated predecessor acceleration should be followed.

### **4.3 Modified Leader Predecessor Following with Predicted Predecessor Acceleration**

The leader prediction is introduced in Section 4.1. Using the benefits of leader prediction, a method to estimate the predecessor acceleration is presented in Section 4.2. In the current circumstances, the delay-free acceleration of the predecessor estimated from the leader acceleration and the communicated predecessor acceleration exist. In order to combine these two accelerations, a prediction observer introduced by [37] and developed further by [24] is used. Before combining the predictor with MLPF topology, the details of the prediction observer will be explained.

#### **4.3.1 Prediction Observer**

The aim of the prediction observer is using an estimated plant output and delayed output measured from the system, predicting the future value of the linear system, in multiple stages. It is required that the delay is found in the input-output path. In [24],

the predictor is designed with  $n$  stages, whereby the number  $n$  corresponds to the prediction time steps. For example, for a delay of 100 ms, the prediction can be done with steps of 25 ms, which would result in  $n = 4$ .

For the prediction observer,  $n = 2$  is selected for our purposes and will be called as 2-stage prediction observer. The 2-stage prediction observer topology is modified for our usage as in the following figure.

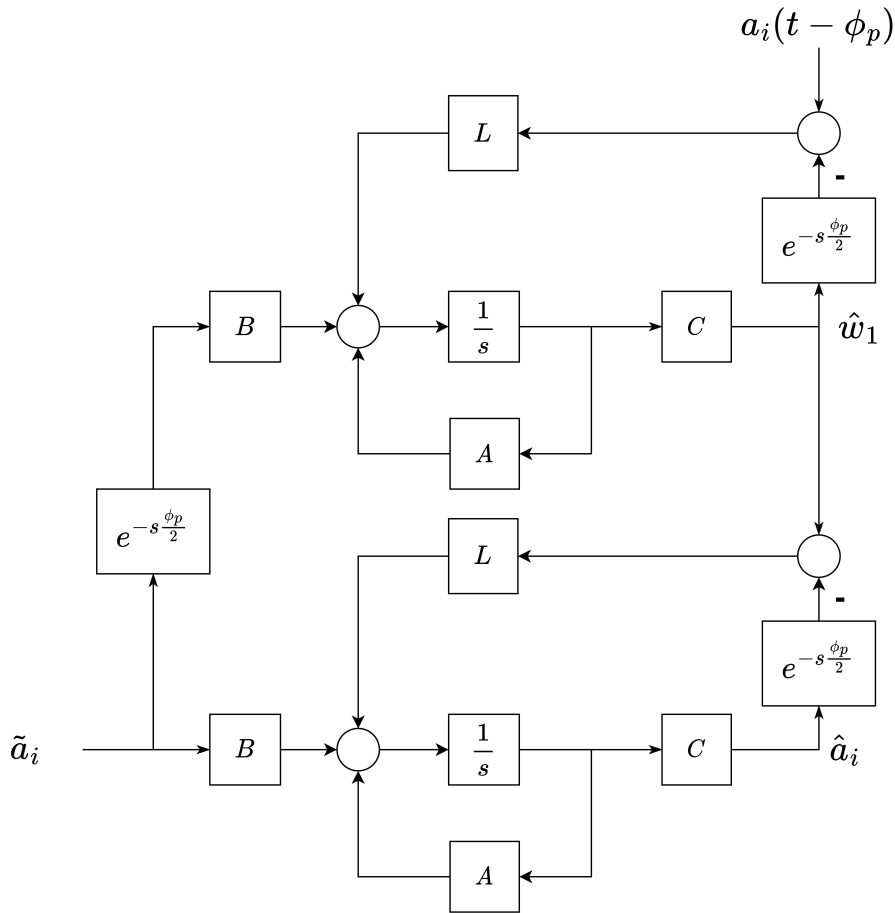


Figure 4.11: 2-stage prediction observer block diagram.

In Figure 4.11,  $\tilde{a}_i(t)$  corresponds to the estimated predecessor acceleration from the leader acceleration,  $a_i(t)$  is the communicated, delayed acceleration of the predecessor and  $\hat{a}_i(t)$  is the predicted predecessor acceleration acquired by the combination of  $\tilde{a}_i(t)$  and  $a_i(t)$ . In order to employ the prediction observer, a high bandwidth, virtual transfer function is placed between the  $\tilde{a}_i(t)$  and delayed  $a_i(t)$ . This transfer function

will be named  $\hat{G}(s)$ .

$$\hat{G}(s) = \frac{w}{s + w} \quad (4.6)$$

This transfer function is selected as a simple first order lowpass transfer function with  $w = 100$  rad/s, in order not to create any extra lag and reduce the success of the prediction. The bandwidth of the virtual transfer function is selected larger than ten times the bandwidth of the closed loop transfer function of the vehicles. Upper loop being the first stage and lower being the second, a middle variable  $\hat{w}_1(t)$  is defined. The state space form of the transfer function  $\hat{G}(s)$  is parameterized with  $A, B$  and  $C$  matrices. Finally,  $L$  corresponds to the observer gain. The relation between the  $\tilde{a}_i(t), a_i(t)$  and  $\hat{a}_i(t)$  is given as follows.

$$\begin{aligned} \dot{\hat{w}}_1(t) &= A\hat{w}_1(t) + B\tilde{a}_i(t - \phi_p/2) + L(a_i(t - \phi_p) - \hat{w}_1(t - \phi_p/2)) \\ \dot{\hat{a}}_i(t) &= A\hat{a}_i(t) + B\tilde{a}_i(t) + L(\hat{w}_1(t) - \hat{a}_i(t - \phi_p/2)) \end{aligned} \quad (4.7)$$

Taking the Laplace transform of the (4.7),

$$\begin{aligned} \hat{W}_1(s) &= (sI - A + Le^{-s\frac{\phi_p}{2}})^{-1}(Be^{-s\frac{\phi_p}{2}}\tilde{A}_i + Le^{-s\phi_p}A_i) \\ \hat{A}_i(s) &= (sI - A + Le^{-s\frac{\phi_p}{2}})^{-1}(B\tilde{A}_i + L\hat{W}_1) \end{aligned} \quad (4.8)$$

Replacing  $M(s) = (sI - A + Le^{-s\frac{\phi_p}{2}})^{-1}$ , the following transfer functions are achieved.

$$\begin{aligned} \hat{A}_i(s) &= MB\tilde{A}_i + ML\hat{W}_1 \\ &= MB\tilde{A}_i + MLM(Be^{-s\frac{\phi_p}{2}}\tilde{A}_i + Le^{-s\phi_p}A_i) \\ &= (MB + MLMBe^{-s\frac{\phi_p}{2}})\tilde{A}_i + MLMLe^{-s\phi_p}A_i \\ &= \tilde{F}\tilde{A}_i + FA_i \end{aligned} \quad (4.9)$$

The characteristic equation of the prediction observer is  $M^{-1}(s)$ . Since the  $(A, C)$  pair of our virtual system is observable and  $L$  is a free design parameter, according to [38] it is always possible to locate the eigenvalues of  $A - LC$  in the left half plane, and the stability of  $A - LC$  will be satisfied for a small time delay. As stated, the parameter  $L$  should be determined. For the determination of the parameter  $L$  an iterative approach of trial and error, over the calculated transfer function and matrix  $A - LC$  in Equation (4.9) is conducted. Taking  $C = 1, A = -100 \cdot 2 \cdot \pi$  in our case, without including the delay, the observer gain is  $L < |A|$  for the eigenvalues to be on the left half plane. Our main purpose is predicting the future or delay-less

value of the predecessor acceleration and while doing that, put as a much as weight on communication received acceleration.

The second possible prediction observer topology stated in [24] is the full information prediction (FIP) observer. With a feedforward added to the 2-stage prediction observer, the block diagram of the 2-stage FIP observer is as follows.

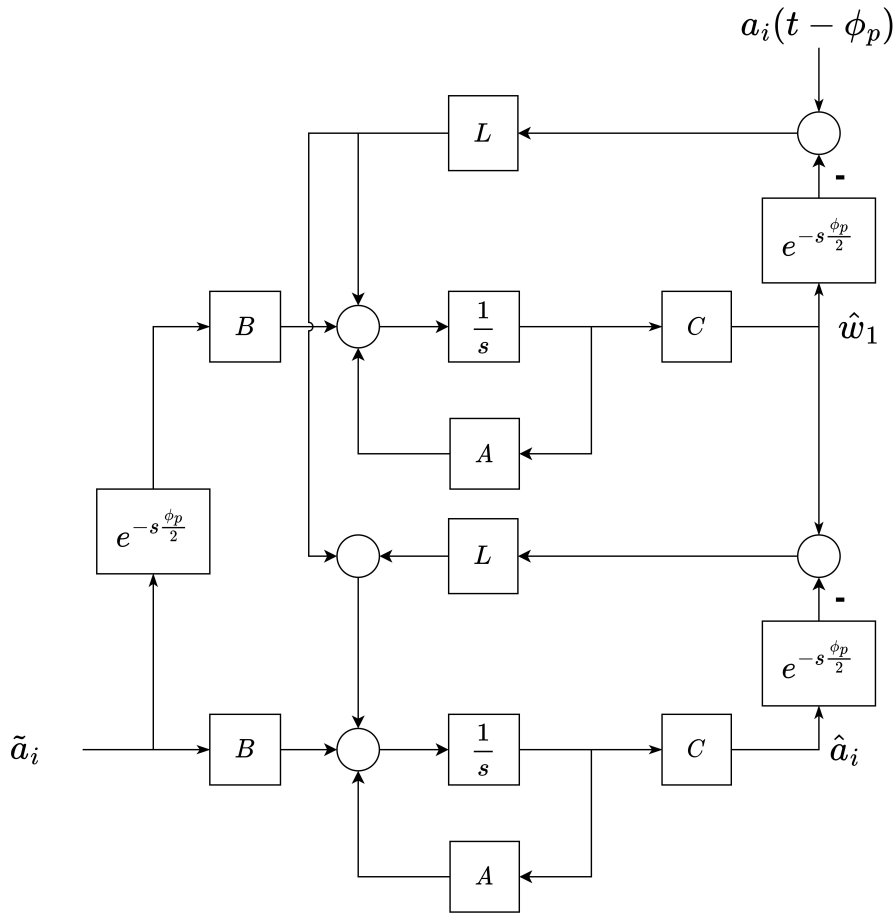


Figure 4.12: 2-stage FIP prediction observer block diagram.

With the added feedforward, the resulting transfer function between the estimated predecessor acceleration, communication received acceleration and predicted acceleration changes accordingly. For the same  $M(s) = (sI - A + Le^{-s\frac{\phi_p}{2}})^{-1}$  the related transfer functions are as follows.

$$\begin{aligned}
\hat{A}_i(s) &= (MB + ML(1 - e^{-s\frac{\phi_p}{2}})MB e^{-s\frac{\phi_p}{2}})\tilde{A}_i \\
&+ (ML + ML(1 - e^{-s\frac{\phi_p}{2}})ML)e^{-s\phi_p} A_i \\
&= \tilde{F}\tilde{A}_i + FA_i
\end{aligned} \tag{4.10}$$

The reason behind the comparison of these two topologies is the overall weight that can be distributed to the estimated and communicated accelerations. As can be seen, both have the same characteristic equations. Including the delay term as 0.1 s for simulation purposes, with trial and error, the observer gain is set as  $L = 360$  for both cases. The step responses of the transfer functions named as  $F(s)$  and  $\tilde{F}(s)$  are given in the following figure.

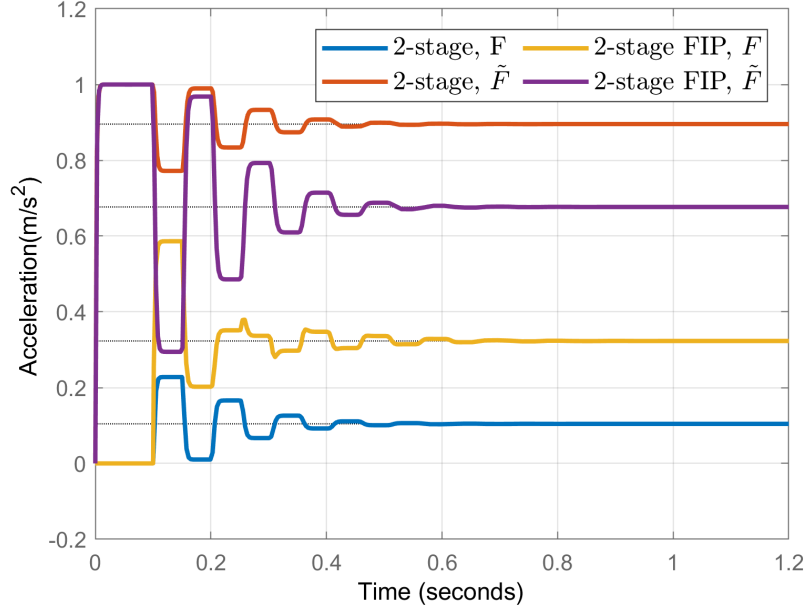


Figure 4.13: The prediction observer step responses.

As can be seen in the figure for the 2-stage FIP topology, at steady state the relation  $\hat{a}_i(t) = 0.636\tilde{a}_i(t) + 0.364a_i(t - \phi_p)$  is achieved whereas, for the 2-stage prediction observer  $\hat{a}_i(t) = 0.868\tilde{a}_i(t) + 0.133a_i(t - \phi_p)$  can be reached. The problem arisen from the direct usage of the estimated predecessor acceleration in the feedforward loop of MLPF topology, can be diminished by merging the  $\tilde{a}_i(t)$  and  $a_i(t - \phi_p)$  by similar steady state weights. Hence, the 2-stage FIP observer shows more promise for

the solution than the 2-stage prediction observer. For the selected weight, resulting Bode plots of the transfer functions  $F(s)$  and  $\tilde{F}(s)$  are calculated.

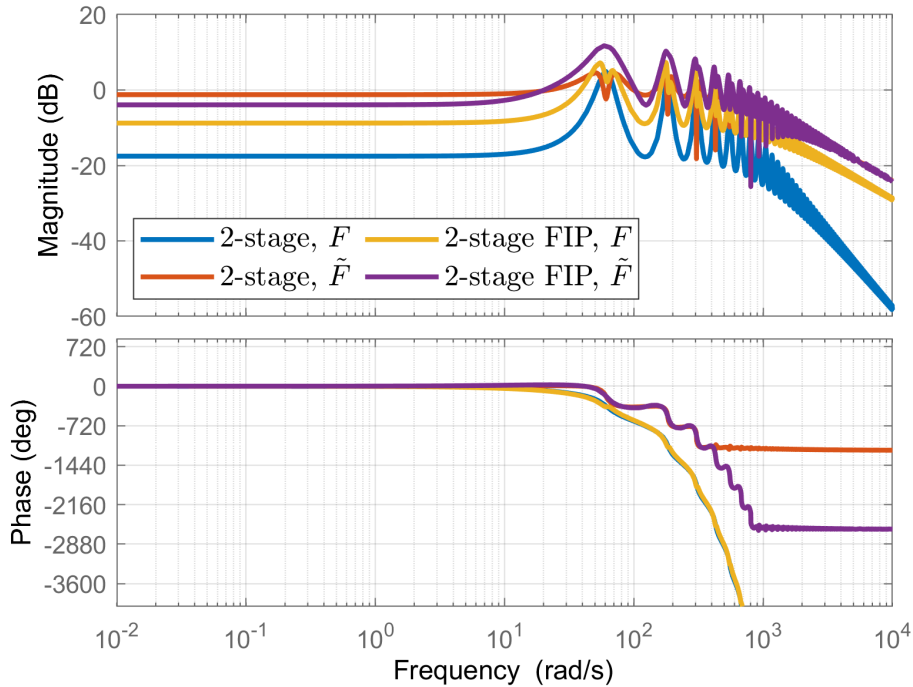


Figure 4.14: The bode plots of the  $F(s)$  and  $\tilde{F}(s)$  for  $L = 360$ .

As a result, the 2-stage FIP prediction observer is selected to use as predictor. A point worth mentioning is the reasoning behind the selection of number of stages for the prediction observer. As mentioned, the weight on communication received acceleration is wanted to be kept as large as possible. With the increasing number of stages in the prediction observer, the weight is given more to the estimated plant, thus deviating from our purpose. As a result the minimum number of stages is used. In the following section, the frequency domain effects of the prediction observer will be examined within the control architecture.

### 4.3.2 Modified Leader Predecessor Following with Prediction Observer

The block diagram of the MLPF with prediction observer, which will be called as MLPFO is given in the following figure. In this block diagram, the communicated

acceleration is shown as  $a_{i-1}^c = a_i(t - \phi_p)$  and the sensor information is shown as  $a_{i-1}^s$ , which actually corresponds to velocity and position measured from the sensor but with the integrator terms moved into the controller, named as acceleration as explained in Section 2.4.

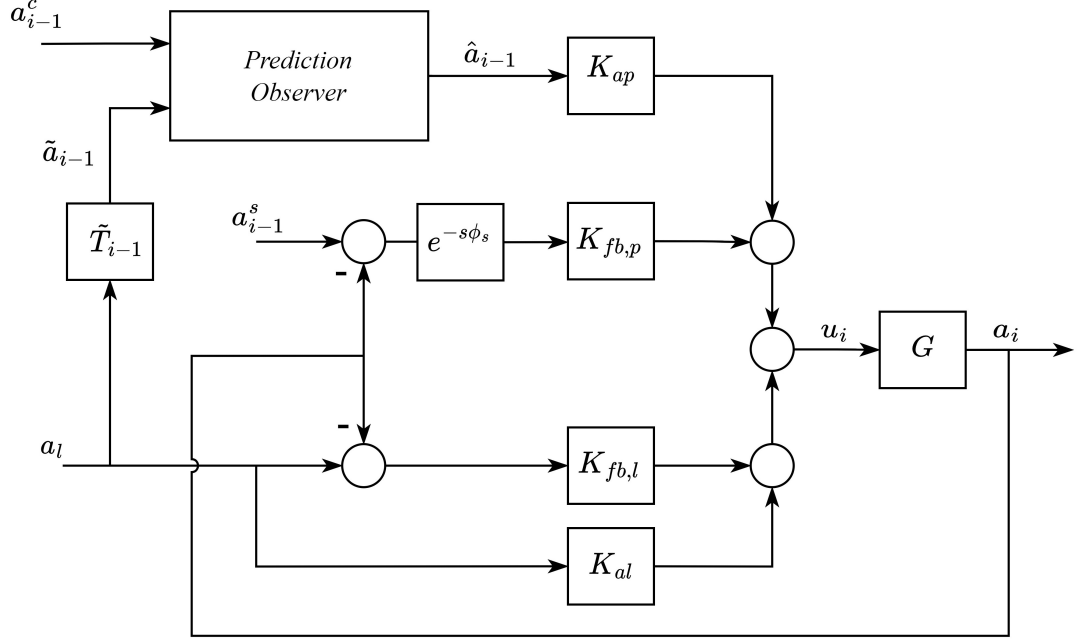


Figure 4.15: MLPFO block diagram.

After the inclusion of the prediction observer, the equations related to string stability must be recalculated. The frequency response of the prediction observer as can be seen in Figure 4.14 must be incorporated in the calculation. As done in previous sections, the equation set for the first two vehicles will be given. From the Equation (2.10) the following equation of  $T_p(s)$  is known. Since it will be required for the MLPFO case, the  $T_p(s)$  transfer function will be divided into two parts as follows. It must be noted that the delay terms are removed, as they are handled accordingly.

$$T_p(s) = \frac{GK_{ap}}{1 + GK_i} + \frac{GK_{fb,p}e^{-s\phi_s}}{1 + GK_i} = P_1(s) + P_2(s) \quad (4.11)$$

As with the MLPF case, with the predicted leader acceleration the first vehicle can receive the acceleration information of its predecessor without any delay, hence it is not required to use any type of prediction. So, for the first vehicle,

$$A_1(s) = T_p A_l + T_l A_l = T_1 A_l \quad (4.12)$$

For the second vehicle, using Equation (3.2),

$$\begin{aligned}
\tilde{A}_1(s) &= T_1 A_l = \tilde{T}_1 A_l = (T_p + T_l) A_l \\
\hat{A}_1(s) &= \tilde{F} \tilde{A}_1 + F A_1 \\
A_2(s) &= P_1 A_1 + P_2 \hat{A}_1 + T_l A_l = (P_1 + P_2 F) A_1 + P_2 F \tilde{A}_1 + T_l A_l \quad (4.13) \\
&= (P_1 + P_2 F) A_1 + (P_2 \tilde{F} \tilde{T}_1 + T_l) A_l \\
&= \bar{T}_p A_1 + T_{l,1} A_l = T_2 A_l
\end{aligned}$$

Then, the equation set can be generalized as follows for  $i \geq 1$ ,

$$\begin{aligned}
\tilde{A}_i(s) &= \tilde{T}_i A_l \\
\hat{A}_i(s) &= \tilde{F} \tilde{A}_i + F A_i \\
A_i(s) &= P_1 A_{i-1} + P_2 \hat{A}_{i-1} + T_l A_l \quad (4.14) \\
&= \bar{T}_p A_{i-1} + T_{l,i-1} A_l = T_i A_l \\
A_{i-1} - A_i &= (1 - \bar{T}_p) A_{i-1} - T_{l,i-1} A_l
\end{aligned}$$

where,

$$\begin{aligned}
\tilde{T}_i &= T_p \tilde{T}_{i-1} + T_l \\
T_{l,i} &= P_2 \tilde{F} \tilde{T}_i + T_l, T_{l,0} = T_l \\
T_i &= \bar{T}_p T_{i-1} + T_{l,i-1}, T_0 = 1 \\
S_i &= (1 - \bar{T}_p) T_{i-1} - T_{l,i-1}, \tilde{S}_i = S_i / s^2
\end{aligned} \quad (4.15)$$

As a result the transfer function between the errors can be found as the next equation with some algebraic manipulation.

$$\begin{aligned}
\Gamma_i(s) &= \frac{E_{i+1}(s)}{E_i(s)} = \frac{A_i - A_{i+1}}{A_{i-1} - A_i} \\
&= \begin{cases} \frac{(1 - \bar{T}_p) T_1 - T_{l,1}}{1 - T_1} & i = 1 \\ \bar{T}_p + \frac{T_{l,i-1} - T_{l,i}}{T_{i-1} - T_i} & i > 1 \end{cases} \quad (4.16)
\end{aligned}$$

Since for the first vehicle, we do not require the prediction, the equations are different for the transfer function between the first two distance errors. For the cases where  $i > 1$ , the equation can be written as

$$\Gamma_i(s) = \bar{T}_p(s) + \gamma_i(s). \quad (4.17)$$

The usage of the prediction observer changed the transfer function between the consecutive vehicle errors,  $\Gamma_i(s)$ , to an index dependent transfer function, whereby  $\bar{T}_p(s)$  is a fixed transfer function with  $\|\bar{T}_p(s)\|_\infty \leq 0.6108$ . For string stability, the characteristics of  $\gamma_i(s)$  must be examined and it must be shown that  $|\bar{T}_p(s) + \gamma_i(s)| \leq 1$  in order to have  $\|\Gamma_i(s)\|_\infty \leq 1$ . For the increasing index  $i$ ,  $\gamma_i(s)$  and  $\Gamma_i(s)$  are given in Figure 4.16 and 4.17 respectively for 23 vehicles. To observe the string stability characteristics better, a small range of frequencies are given for the magnitude bode plot of  $\gamma_i(s)$  and  $\Gamma_i(s)$ . For a 0.1 s PF communication and sensor delay, at  $i = 23$ , it is observed that the string stability of the vehicle platoon is compromised. Thus, with the proposed method, the string stability can be satisfied for a platoon with maximum 22 vehicles.

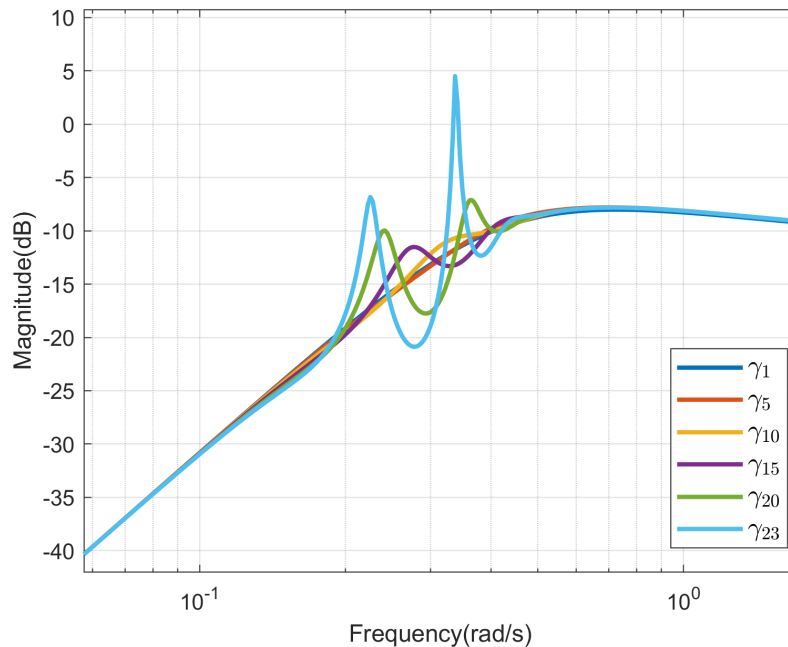


Figure 4.16: The magnitude bode plot of the  $\gamma_i(s)$ ,  $i > 1$ .

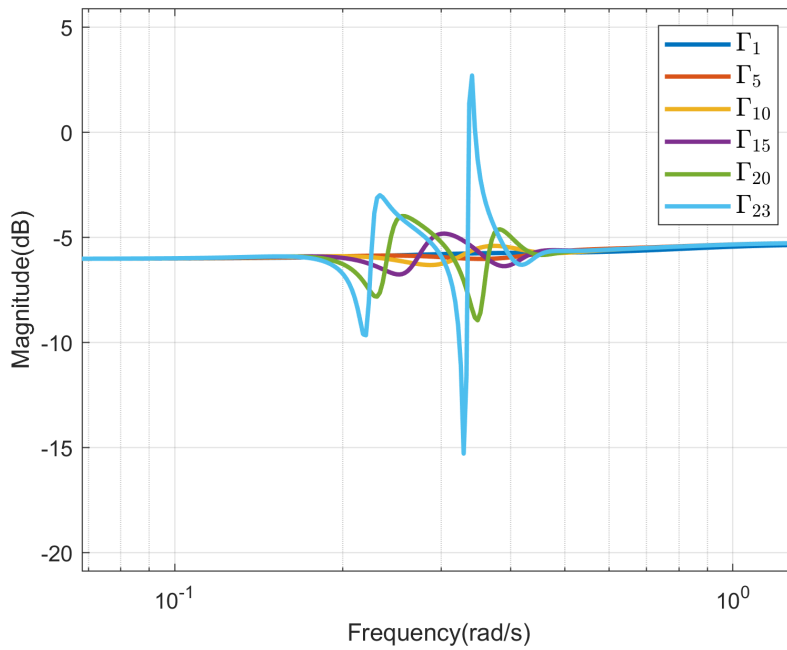


Figure 4.17: The magnitude bode plot of the  $\Gamma_i(s)$ .

To observe the evolution of the transfer function  $\gamma_i(s)$  and  $\Gamma_i(s)$ , all of the transfer functions up to  $i = 22$  is given in the Figure 4.18. The peak of the bode plot increases as the index  $i$  increases, which is shown by the arrows.

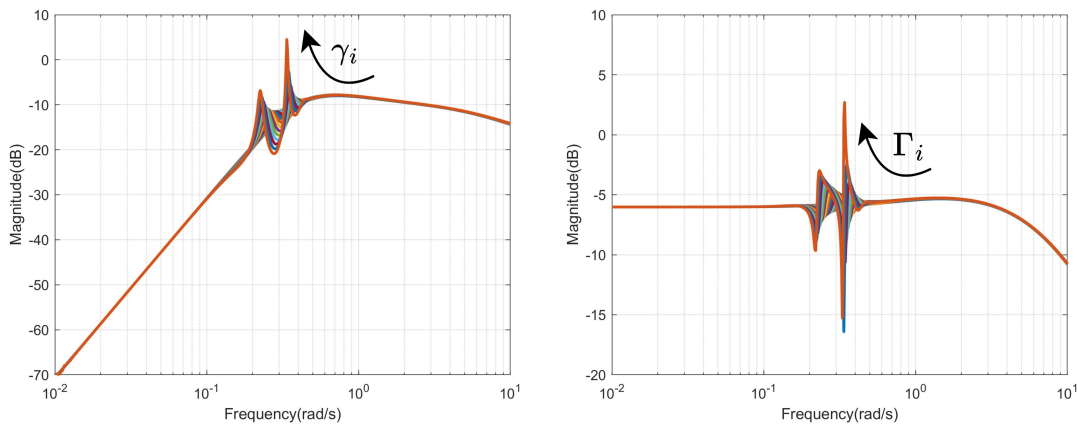


Figure 4.18: The magnitude plots of  $\Gamma_i(s)$  and  $\gamma_i(s)$ .

The string stability transfer function is calculated for the MLPFO case, taking the PF communication and sensor delay as 0.1 s. The number of vehicles for which the

string stability is satisfied, with respect to different PF sensor and communication delays can be seen in Figure 4.19. For the calculation of the string stable number of vehicles, the gain of the prediction observer is kept constant as  $L = 360$ . It can be observed that with increasing PF communication delay, the length of a string stable vehicle platoon is decreased. On the contrary, with increasing PF sensor delay, string stability is satisfied for a larger number of vehicles in the platoon.

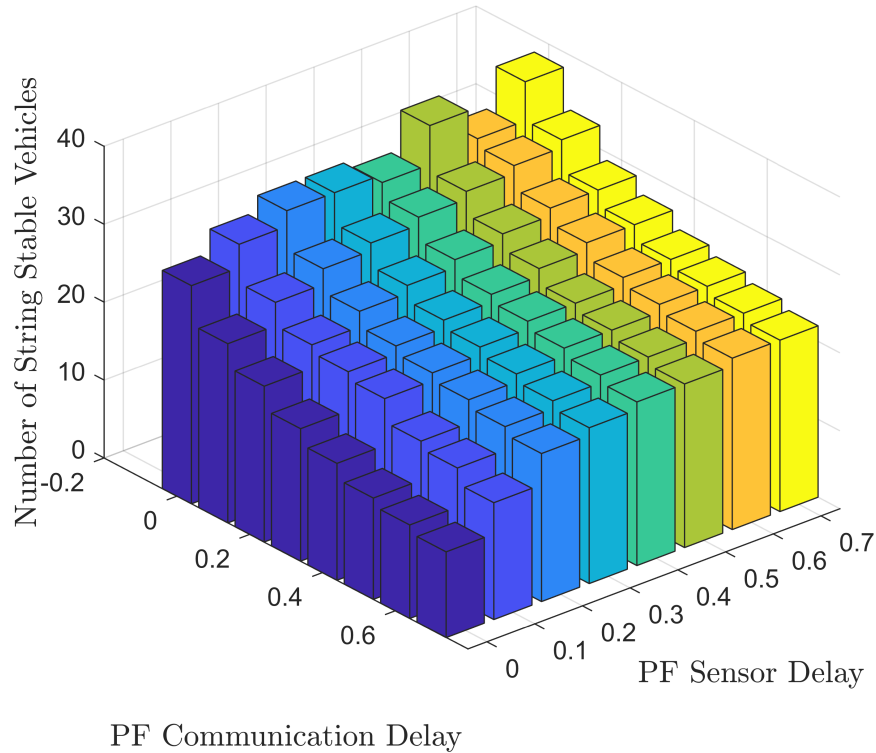


Figure 4.19: The string stable platoon length for different PF sensor and communication delays.

After showing the string stability characteristic of MLPFO, simulation results regarding standard cases will be shown. The results will be given comparatively to the MLPF topology, to observe the improvements. For the MLPF topology, only PF sensor delay exists in the loop, since the PF communication is removed. For the MLPFO topology, the PF communication and sensor delay are taken as 0.1 second. The distance errors and accelerations under step leader acceleration are given in Figures 4.20 and 4.21. An acceleration disturbance of the first vehicle is considered in Figure 4.22

and 4.23 and a velocity disturbance of the first vehicle is applied in Figure 4.24 and 4.25. Again for the simulation, a five vehicle platoon is simulated. The color red will be used for MLPF, whereas blue is for MLPFO.

As can be seen from Figure 4.20 and 4.21 the distance errors and accelerations are kept almost exactly the same, converging more to the ideal LPF case, resulting in the platooning performance of an ideal LPF vehicle platoon without any delays. Whilst, a minor maximum distance error improvement is observed under acceleration at Figure 4.22, the lag that can be seen on the accelerations of the vehicles in Figure 4.23 due to the estimated transfer function on MLPF, is improved with MLPFO with the introduction of the prediction observer. Furthermore, the maximum required acceleration is decreased. For the velocity disturbance, first two vehicles are skipped since their response is dominated by the velocity disturbance. From the Figure 4.22, a reduction at maximum distance can be seen, under first vehicle velocity disturbance. Similarly to acceleration disturbance case, the maximum acceleration and settling times are improved. A slight disadvantage of the introduced MLPFO topology is the limited number of vehicles in a platoon. For the string stability to be satisfied the boundary value of 22 vehicles should not be exceeded. However, platoons with more than 20 vehicles are not to be expected in practice.

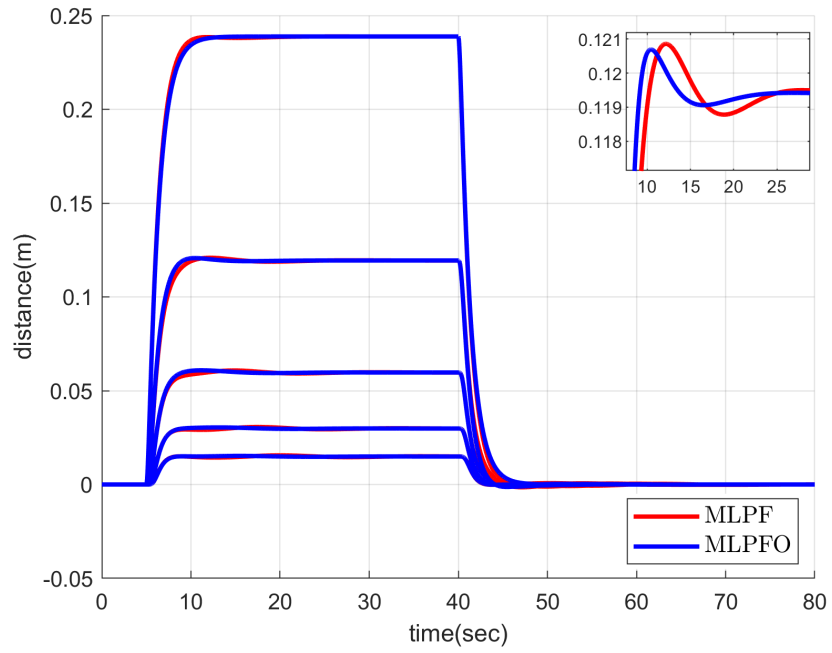


Figure 4.20: The distance errors of the vehicles for a step acceleration of the leader.

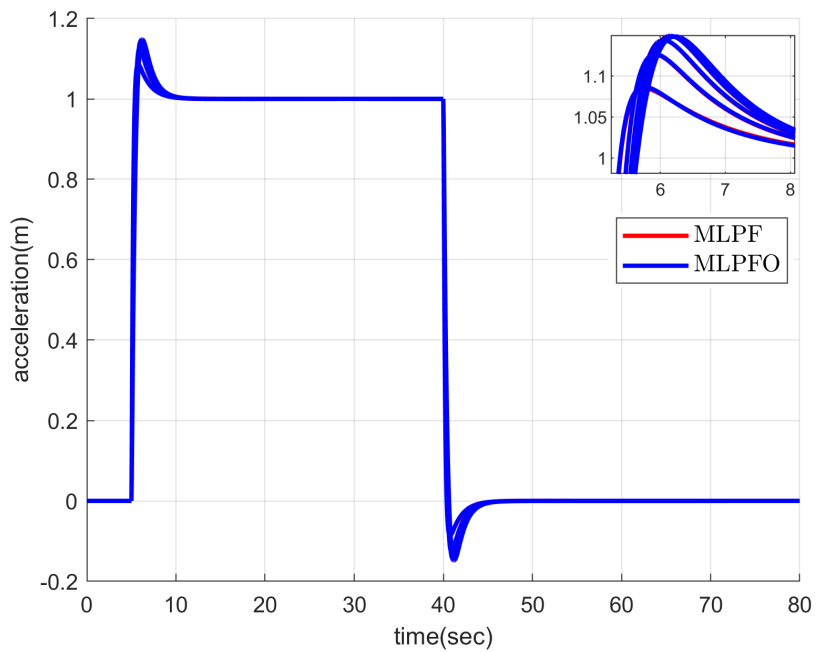


Figure 4.21: The accelerations of the vehicles for a step acceleration of the leader.

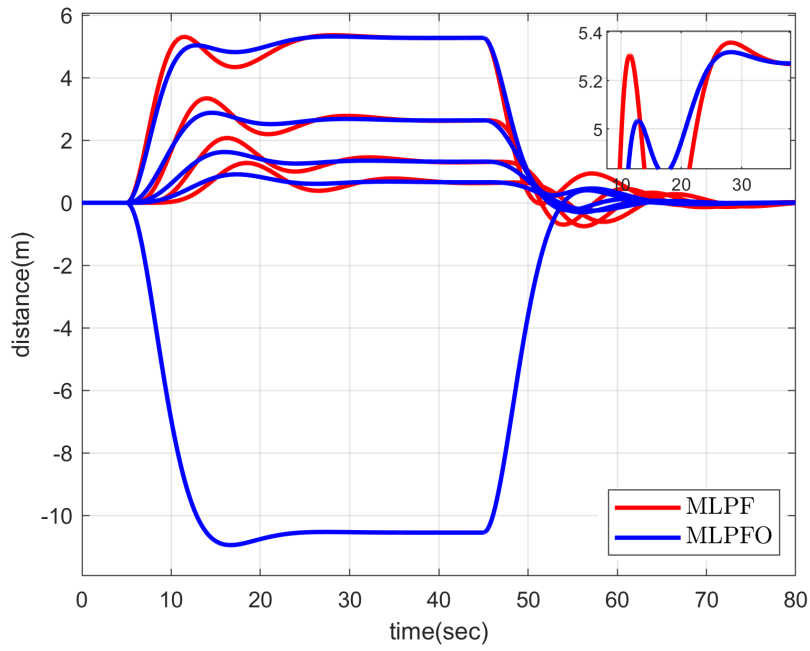


Figure 4.22: The distance errors of the vehicles for an acceleration disturbance at the first vehicle.

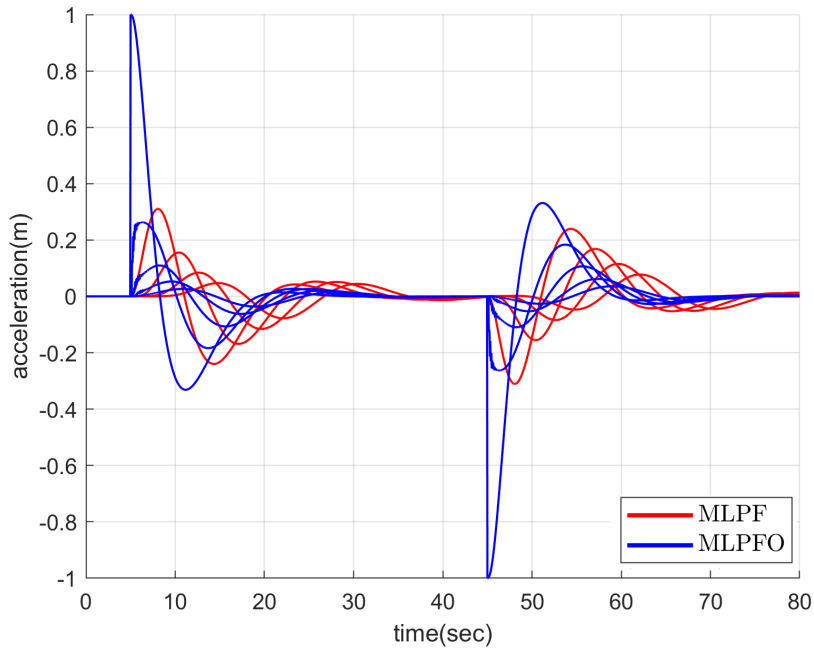


Figure 4.23: The accelerations of the vehicles for an acceleration disturbance at the first vehicle.

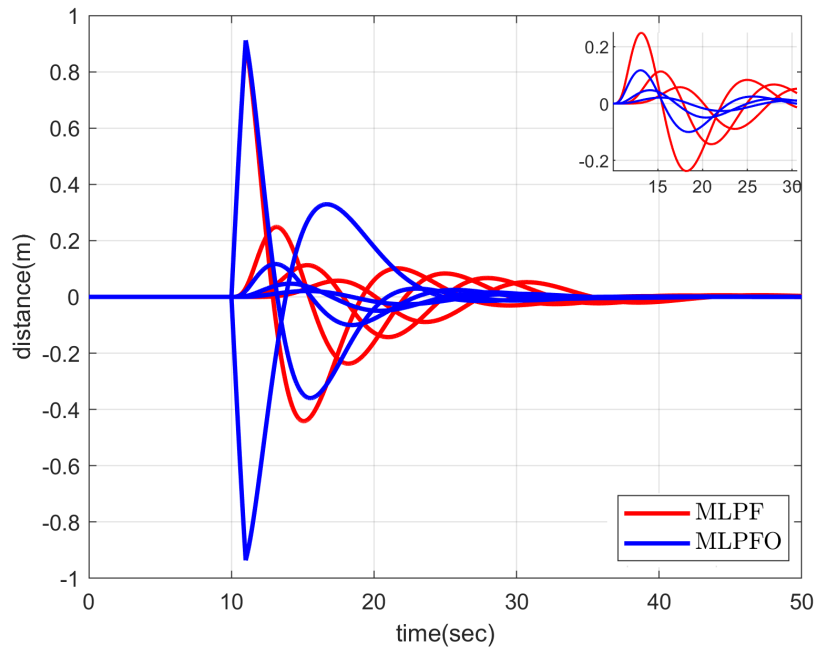


Figure 4.24: The distance errors of the vehicles for a velocity disturbance at the first vehicle.

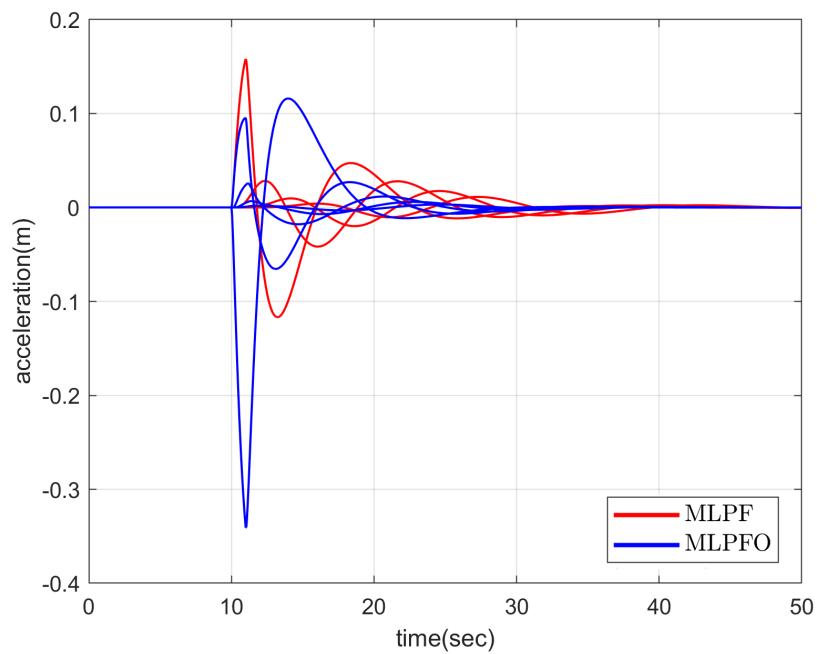


Figure 4.25: The accelerations of the vehicles for a velocity disturbance at the first vehicle.

#### 4.4 MLPFO with Smith Predictor

In this section a method to handle the remaining delay, which is the PF sensor delay will be given. The idea behind that method is as follows. The sensor delay is the smallest and deterministic one among the delays. The aim here is to handle the PF sensor delay with a Smith predictor, which exist only on the open loop path of the predecessor loop. In order to do that, the delay must be moved to a location where both the predecessor and leader loop is affected by it. As it is introduced, the LF communication delay is considered to be zero for this discussion. Knowing the timestamp of the received LF communication message, the attained information from leader can be buffered. The buffered information can be used with the same amount of PF sensor delay. By that way, it is possible to see the effect of the delay in both loops. Thus, the delay exist in both of the open loop paths. The block diagram of the defined control architecture, which will be named as MLPFOSP is given in Figure 4.26.

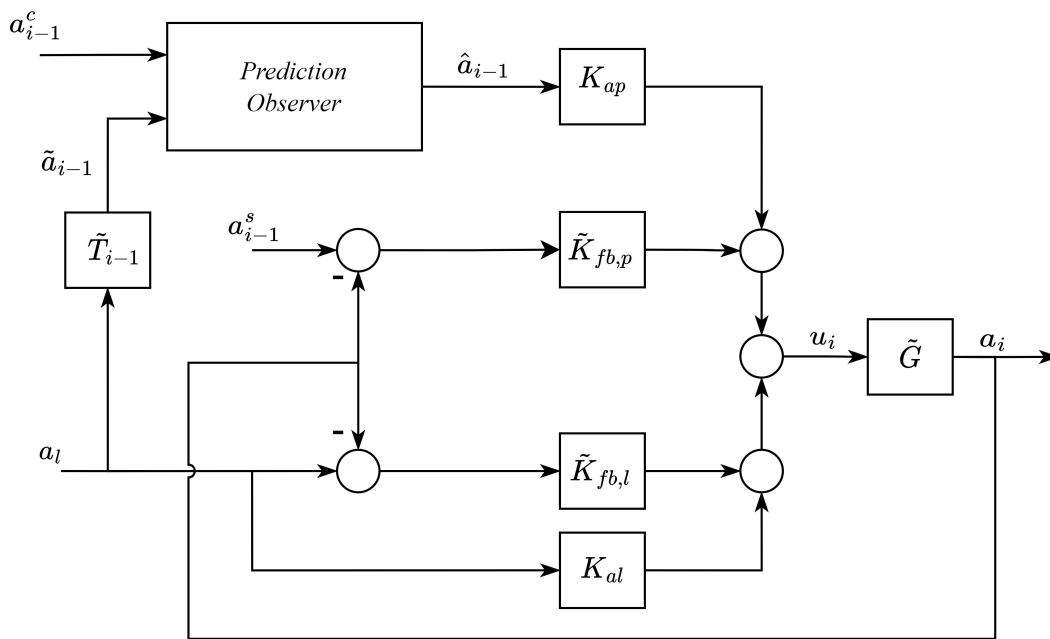


Figure 4.26: MLPFO with Smith predictor block diagram.

Since the delay is on both open loop paths now, it is combined with the plant  $\tilde{G}(s) = G(s)e^{-s\phi_s}$ . Furthermore, the feedback controllers of both loops are changed with their Smith predictor equivalents. In order to see this change better we can look at a

simple Smith predictor loop, where the delay compensation is implemented over the controller is given in Figure 4.27.

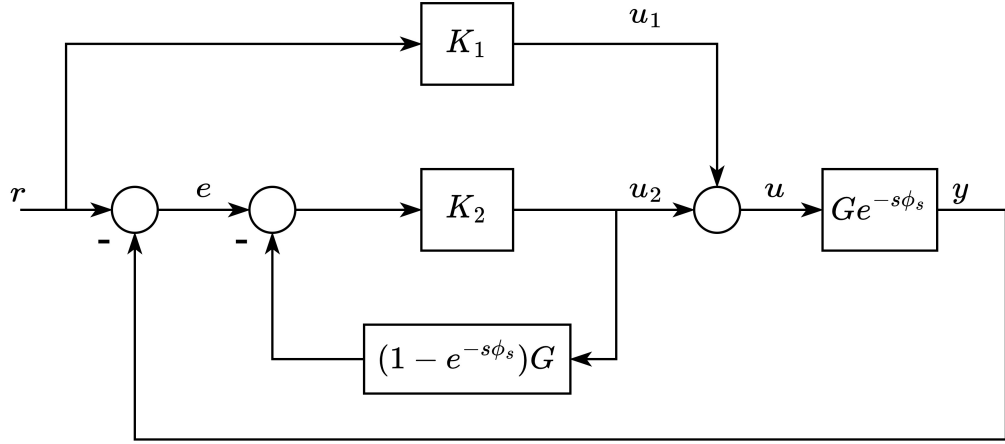


Figure 4.27: Smith predictor implemented loop block diagram.

When the equivalent transfer function from  $e$  to  $u_2$  is written, the new transfer functions of the controllers  $\tilde{K}_1$  and  $\tilde{K}_2$  can be found as

$$\begin{aligned}\tilde{K}_1 &= K_1 \\ \tilde{K}_2 &= \frac{K_2}{1 + (1 - e^{-s\phi_s})GK_2}\end{aligned}\quad (4.18)$$

Using the same approach on each of the feedback controllers of predecessor and leader loops, the controllers are changed as

$$\begin{aligned}\tilde{K}_{fb,p} &= \frac{K_{fb,p}}{1 + (1 - e^{-s\phi_s})G(K_{fb,p} + K_{fb,l})} \\ \tilde{K}_{fb,l} &= \frac{K_{fb,l}}{1 + (1 - e^{-s\phi_s})G(K_{fb,p} + K_{fb,l})}\end{aligned}\quad (4.19)$$

As can be seen from the block diagram in Figure 4.26, the prediction observer is still being used. The equations introduced in Section 4.3.1 are still valid. By replacing  $G(s)$ ,  $K_{fb,p}(s)$  and  $K_{fb,l}(s)$  with  $\tilde{G}(s)$ ,  $\tilde{K}_{fb,p}(s)$  and  $\tilde{K}_{fb,l}(s)$ , the same equation set can be used. With the Smith predictor introduction to the loop the string stability is again checked. With the same calculation done in the Section 4.3.1 it was found that for 25 vehicles the string stability can be satisfied. It can be seen that for vehicle 26 the  $\|\Gamma_i(s)\|_\infty > 1$ . The related magnitude bode plot of the  $\Gamma_i(s)$  can be seen in Figure 4.28.

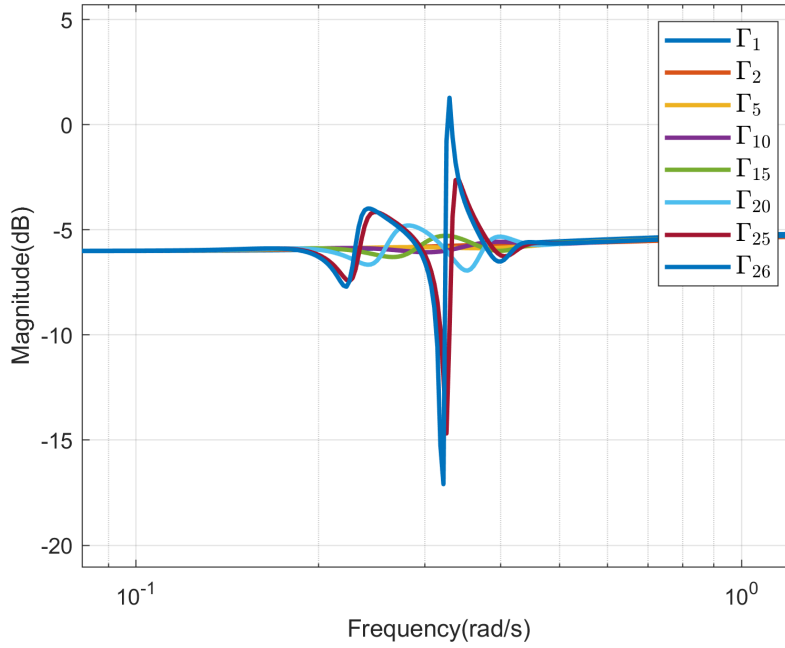


Figure 4.28: The magnitude bode plot of the  $\Gamma_i(s)$ .

After the validation of string stability for 25 vehicles, we can compare the MLPFO with Smith predictor topology, to MLPFO for the standard cases. For this comparison to be clear, the sensor delay is selected as a large value of  $0.5s$ . The PF communication delay is  $0.1s$  as before. The red color represents the MLPFO, while blue represents MLPFO with Smith predictor. The MLPFO with Smith predictor will be abbreviated as MLPFOSP. The comparison for the standard cases can be seen in Figure 4.29, 4.30, 4.31, 4.32, 4.33 and 4.34. The accelerations in 4.30 is given only for the first 10 seconds for a better observation.

As indicated in Section 3.3, the sensor delay is usually neglected since it is comparably small. It can be observed from the plots that the potential negative effects of the PF sensor delay is handled by the introduced control architecture. The response speed has increased, the overshoot and maximum acceleration are reduced, and a slight improvement to the maximum distance with respect to the MLPFO case is observed. The benefit would be smaller for a small PF sensor delay, nonetheless it is handled. Another benefit of using the given architecture is that the number of vehicles with a string stable distance error transfer function has increased.

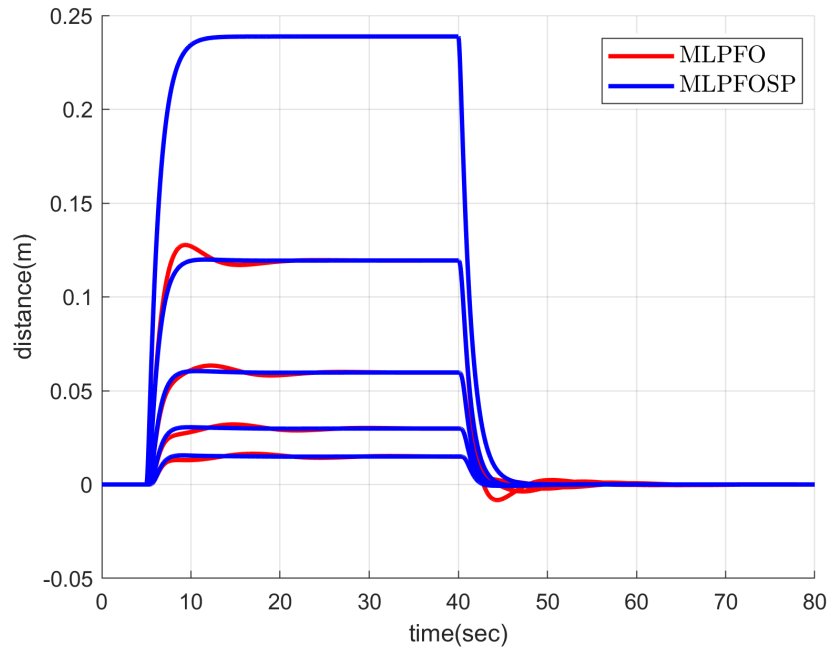


Figure 4.29: The distance errors of the vehicles for a step acceleration of the leader.

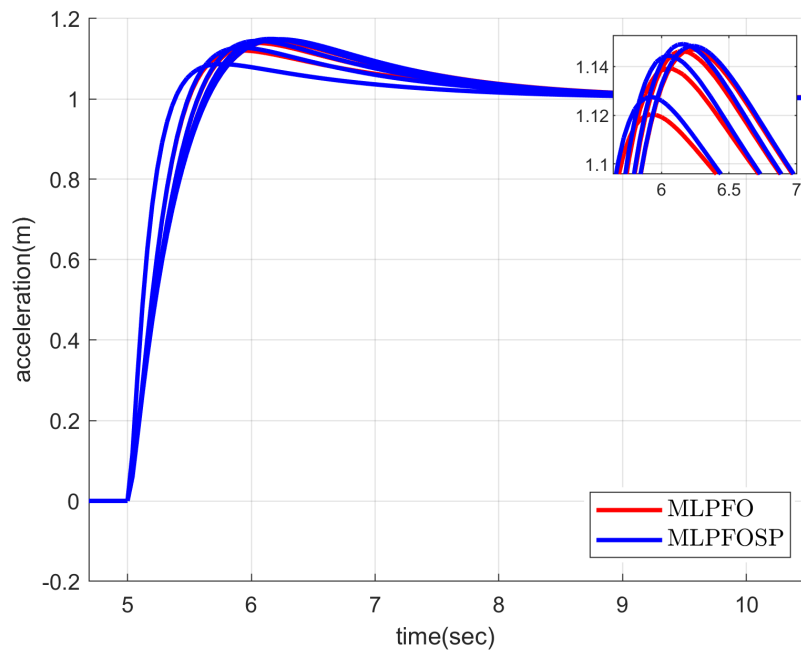


Figure 4.30: The accelerations of the vehicles for a step acceleration of the leader.

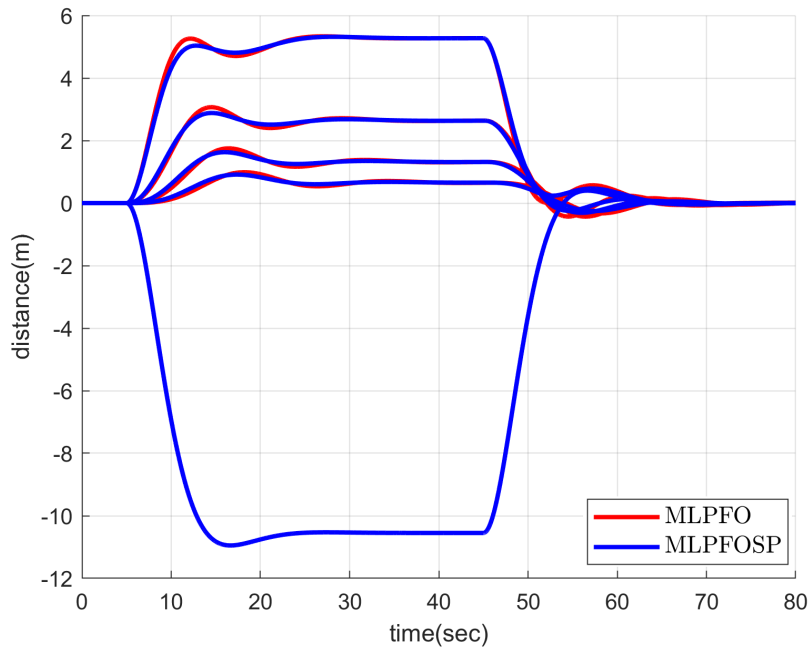


Figure 4.31: The distance errors of the vehicles for a acceleration disturbance at the first vehicle.

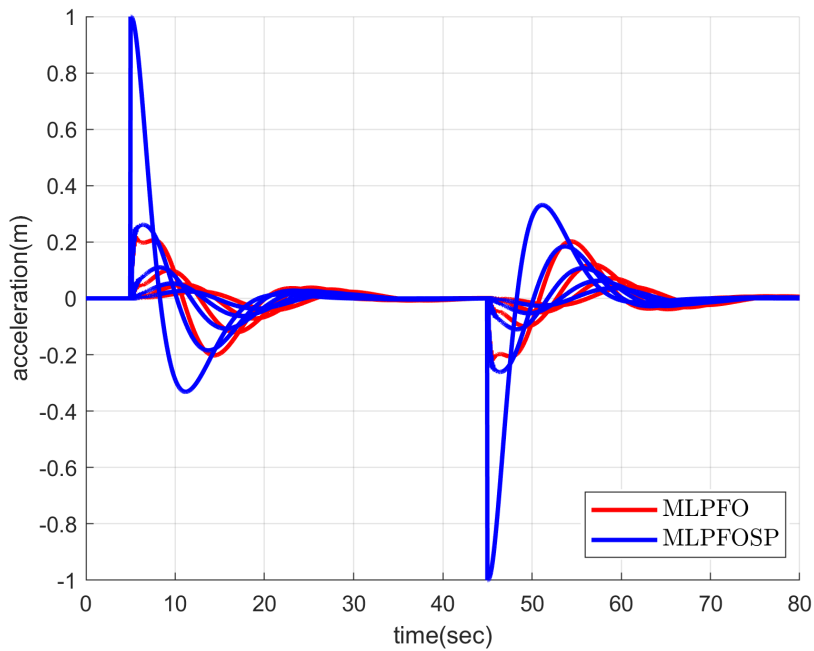


Figure 4.32: The accelerations of the vehicles for an acceleration disturbance at the first vehicle.

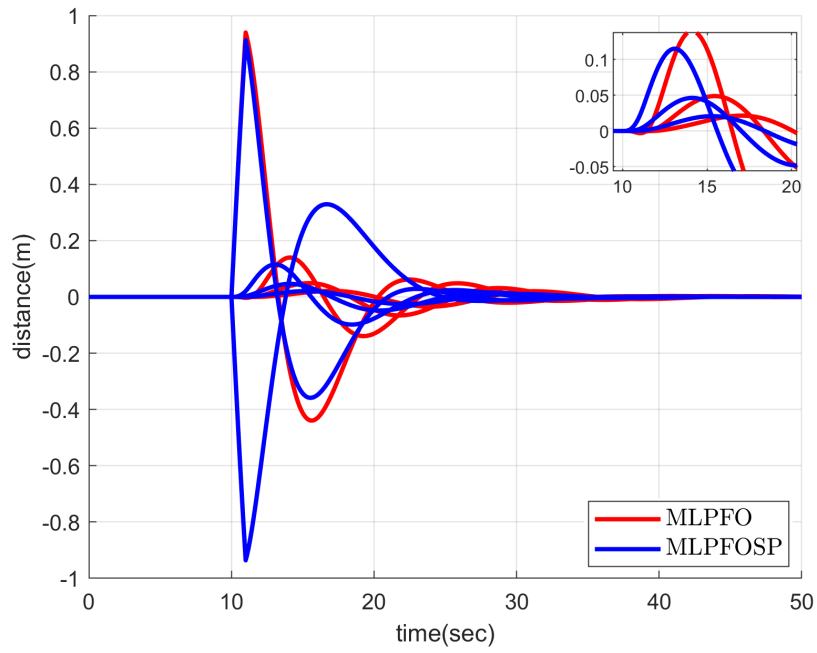


Figure 4.33: The distance errors of the vehicles for a velocity disturbance at the first vehicle.

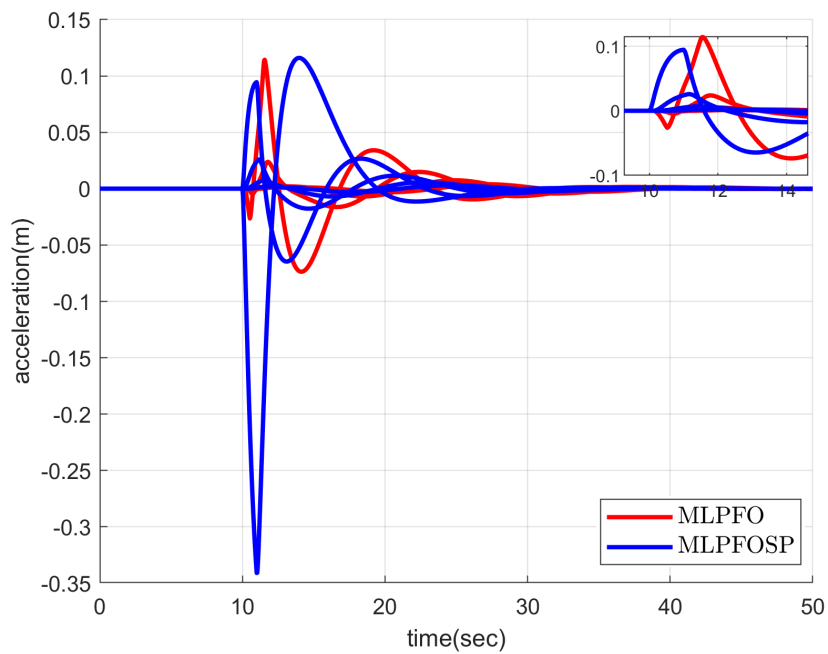


Figure 4.34: The accelerations of the vehicles for a velocity disturbance at the first vehicle.

In the Equation (2.2), the plant is introduced without any delay. With the architecture that was used to handle PF sensor delay, the plant actuation delay could also be handled. As can be seen in Figure 4.26, the delay is transferred into the open loop path and included in the same way as a plant delay would.

## 4.5 Comparison

In this section overall comparison of the introduced methods will be given for the standard defined cases. For the comparisons, the following topologies will be considered.

- Ideal LPF without any delay (red)
- LPF with all the delays included (blue)
- LPF with predicted leader acceleration (LPFPLA) (orange)
- MLPF (green)
- MLPFO (black)
- MLPFOSP (magenta)

For all these cases, all of the communication delays will be selected as  $0.1s$ . As defined ideal LPF is the delay free case, LPF with predicted leader acceleration is affected by PF sensor and communication delay, MLPF is only affected by PF sensor delay since the PF communication is removed, MLPFO is affected by the PF sensor delay, where the PF communication delay is compensated and at MLPFOSP both the PF sensor and communication delay is compensated. For MLPF, MLPFO and MLPFOSP the predicted leader acceleration has taken as a basis. Thus, none of them is affected by the LF communication delay. Again for the simulation a five vehicle platoon will be used. The comparison graphs for the standard cases can be seen in Figures 4.35, 4.36, 4.37, 4.38, 4.39 and 4.40.

From the given figures, it can be seen that, with iterative improvements, compensating and removing the effect of each delay at each step with a newly defined control

architecture, the response of the LPF control loop converged closely to the ideal case. From Figures 4.37 it can be observed that the distance error characteristic changed, while keeping the steady state distance error the same as the ideal case. For a clear view, the response of one the vehicles is given as a box figure. From Figures 4.38 and 4.40 it can be seen that with the removal of delays, the lagging characteristic of the acceleration is reduced. Moreover, the overall maximum acceleration is decreased. From the Figure 4.39, it can be interpreted that the responses under velocity disturbance is deviated the most from the ideal LPF case due to using the sensor read velocity and position indirectly. This demonstrates the performance trade off of the introduced control architecture.

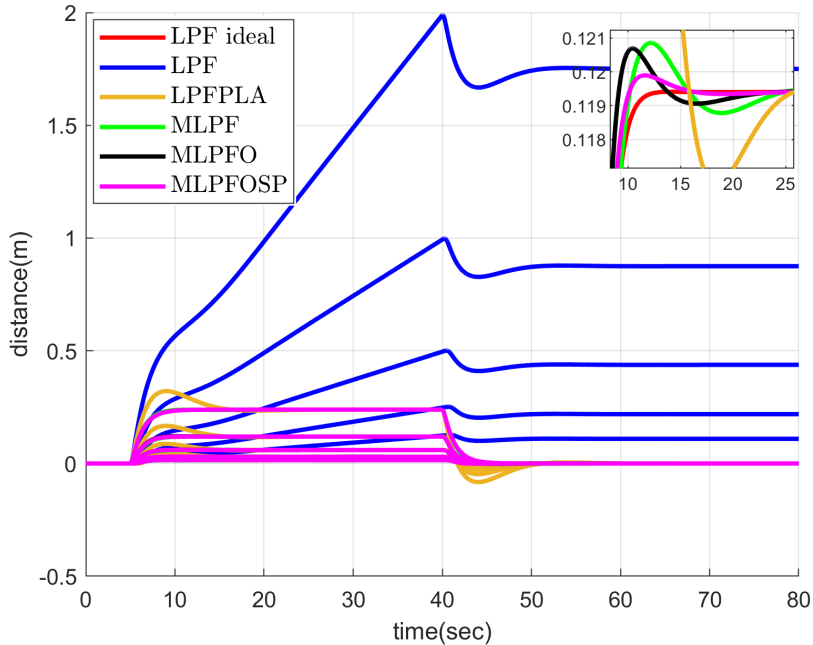


Figure 4.35: The distance errors of the vehicles for a step acceleration of the leader vehicle.

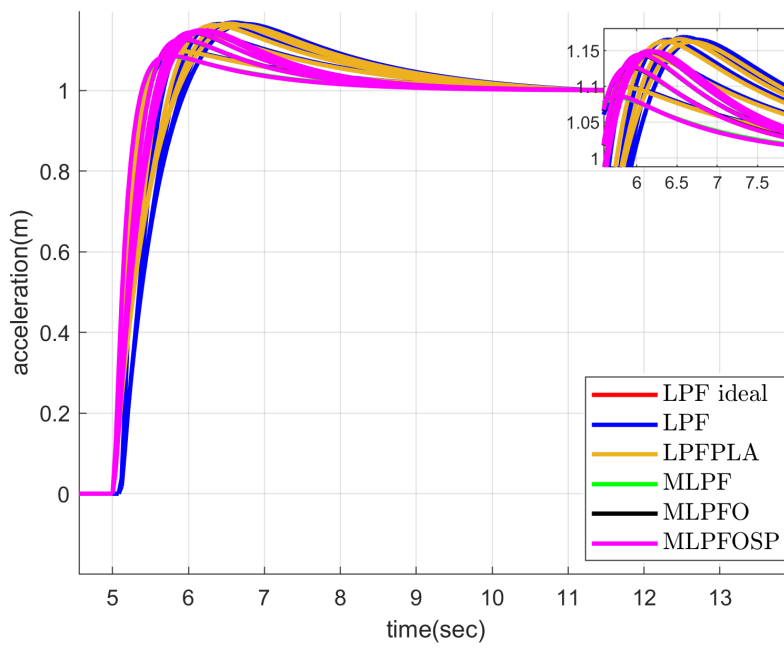


Figure 4.36: The accelerations of the vehicles for a step acceleration of the leader vehicle.

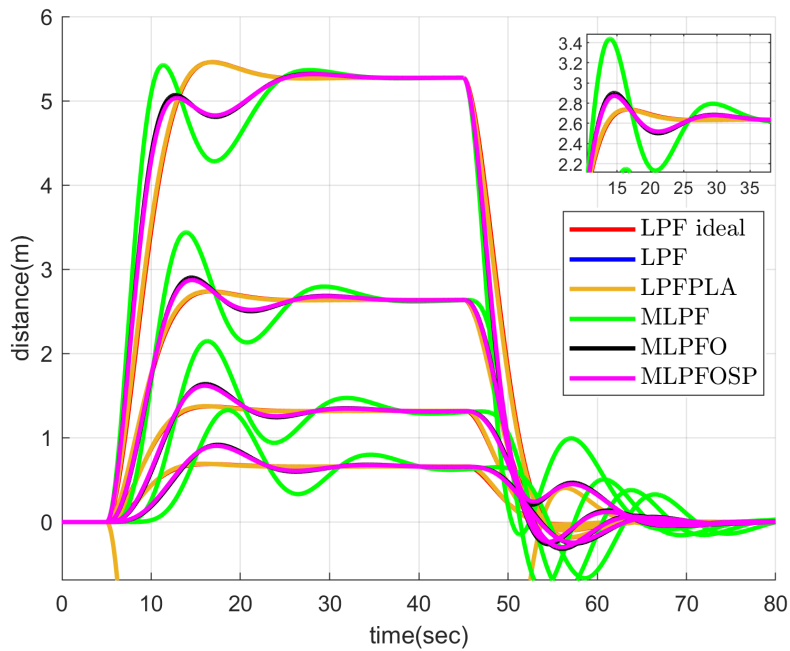


Figure 4.37: The distance errors of the vehicles for an acceleration disturbance at the first vehicle.

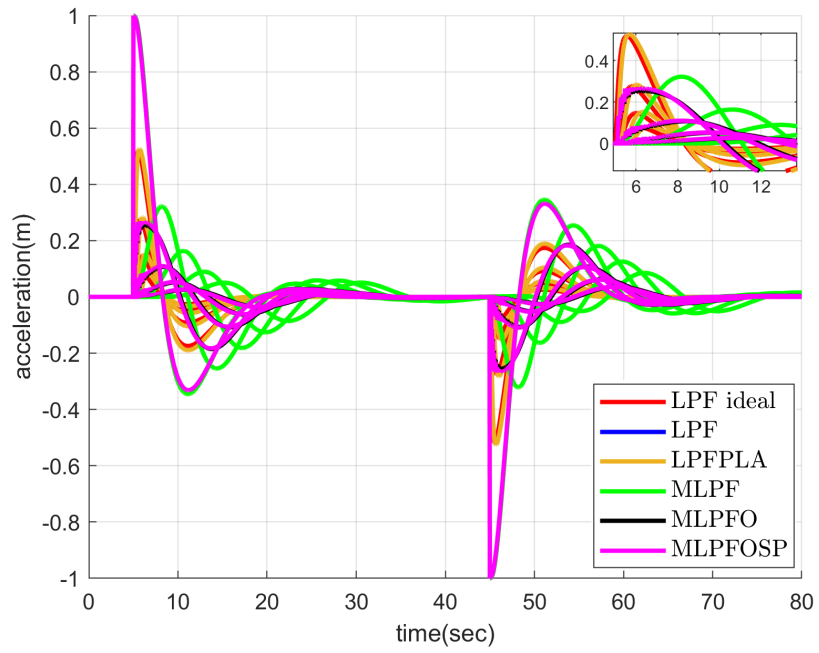


Figure 4.38: The accelerations of the vehicles for an acceleration disturbance at the first vehicle.

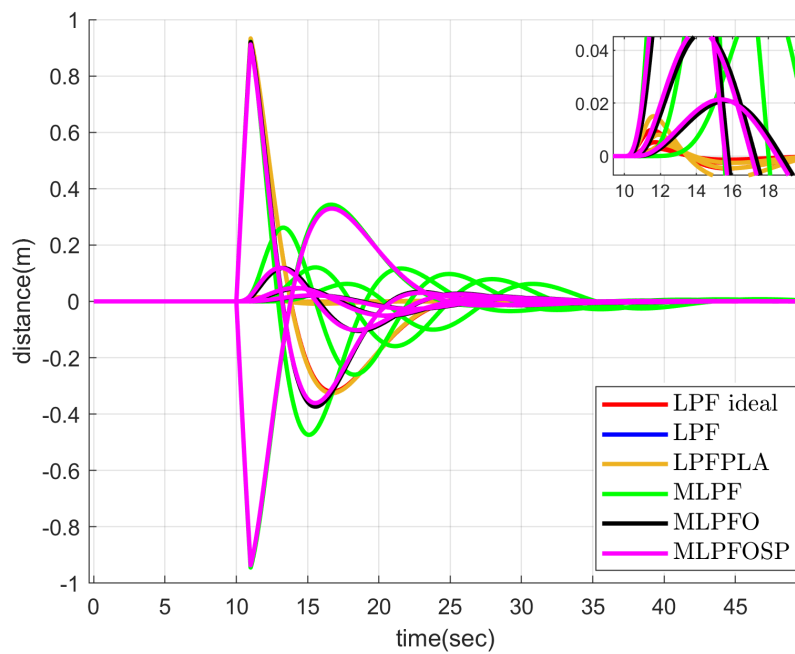


Figure 4.39: The distance errors of the vehicles for an velocity disturbance at the first vehicle.

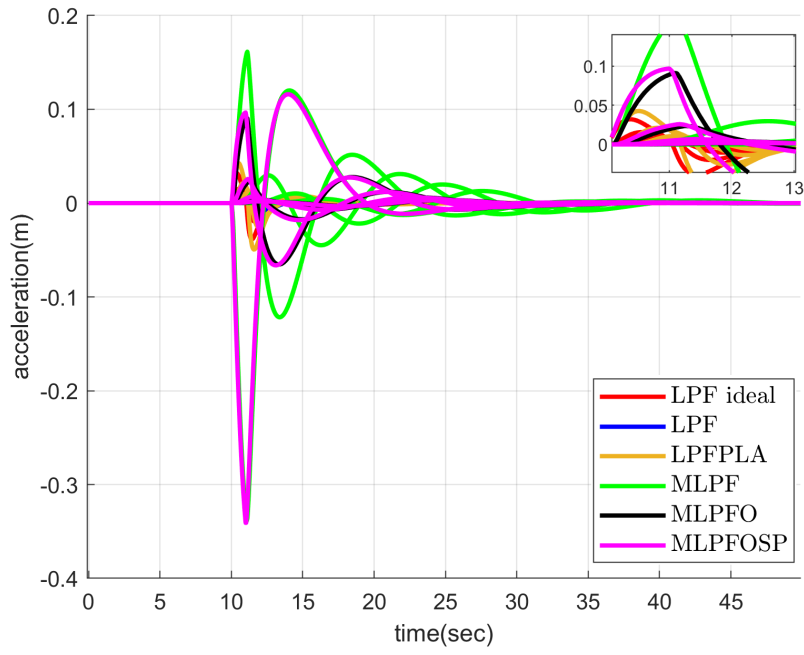


Figure 4.40: The accelerations of the vehicles for a velocity disturbance at the first vehicle.

## CHAPTER 5

### CONCLUSION

This thesis considers the leader predecessor following (LPF) topology for cooperative adaptive cruise control (CACC) in vehicle platoons under a constant spacing policy (CSP). Although the LPF topology with CSP is affected by various delays such as the leader follower (LF) and predecessor follower (PF) communication delay and the PF sensor delay, there is limited research on studying the effect of and finding remedies for these delays, which is particularly important when implementing CACC in practice.

Accordingly, the thesis first performs a comprehensive analysis of the delays in the LPF topology with CSP, whereby the condition of string stability and the performance of the CACC feedback loop are taken into account. For the solution to the described problems, the recurrent transfer function characteristic of the LPF topology with CSP is derived, analyzed and a  $H_\infty$  robust control synthesis procedure is introduced. Distinctly from the literature, the delays affecting the LPF topology with CSP are studied in frequency domain. The LF communication delay does not create any string stability problems but instead affects the applicability of the LPF topology with CSP by introducing large distance errors. The PF sensor and communication delay also do not lead to a violation of string stability for small enough values but they introduce overshoot in the system response in case of disturbances within a platoon.

In order to mitigate the negative effect of communication and sensor delays, several improvements of the standard LPF topology with CSP are proposed. Using the iterative transfer function, different control architectures are defined. First, a predicted leader acceleration method is introduced for removing the LF communication delay. Second, a new predecessor acceleration estimation topology is presented. To increase

the practicability of this topology, the utilization of a prediction observer is suggested. This prediction observer merges the estimated and communicated predecessor acceleration for handling the PF communication delay. Third, the overall control architecture is combined with a Smith predictor to eliminate the PF sensor communication delay. In the final topology, all the relevant delays are handled and the performance of the resulting LPF topology with CSP approaches the ideal form without communication delays, which is highly relevant for practical applications. At the end, an overall comprehensive comparison is presented. The given simulation results confirm that the ideal delay-free LPF topology with CSP is closely approximated.

It is possible that a mismatch occurs between the delay amount used for the design of the prediction observer and the instantaneous communication delay. As a potential future work, the properties of the modified leader predecessor following with prediction observer (MLPFO) can be further analyzed. For the modified leader predecessor (MLPF) topology, a study over the estimation transfer function can be done to further simplify it or even fix it for all the vehicles to achieve a simpler implementation. Finally, all the simulations can be carried out under fully simulated, non ideal wireless vehicle-to-vehicle communication with realistic scenarios.

## REFERENCES

- [1] Y. A. Harfouch, S. Yuan, and S. Baldi, “An adaptive switched control approach to heterogeneous platooning with intervehicle communication losses,” *IEEE Transactions on Control of Network Systems*, vol. 5, no. 3, pp. 1434–1444, 2018.
- [2] K. Lidström, K. Sjöberg, U. Holmberg, J. Andersson, F. Bergh, M. Bjäde, and S. Mak, “A modular cooperative adaptive cruise control system integration and design,” *IEEE Transactions on Intelligent Transportation Systems*, vol. 13, no. 3, pp. 1050–1061, 2012.
- [3] S. E. Shladover, C. Nowakowski, and X.-Y. Lu, “Using cooperative adaptive cruise control to form high-performance vehicle streams. definitions, literature review and operational concept alternatives,” 2018.
- [4] G. J. L. Naus, R. P. A. Vugts, J. Ploeg, M. J. G. van de Molengraft, and M. Steinbuch, “String-stable cooperative adaptive cruise control design and experimental validation: A frequency-domain approach,” *IEEE Transactions on Vehicular Technology*, vol. 59, no. 9, pp. 4268–4279, 2010.
- [5] S. Öncü, N. van de Wouw, W. P. M. H. Heemels, and H. Nijmeijer, “String stability of interconnected vehicles under communication constraints,” in *2012 IEEE 51st IEEE Conference on Decision and Control (CDC)*, pp. 2459–2464, 2012.
- [6] D. Swaroop and J. Hedrick, “String stability of interconnected systems,” *IEEE Transactions on Automatic Control*, vol. 41, no. 3, pp. 349–357, 1996.
- [7] Y. Qin and S. Li, “String stability analysis of mixed cacc vehicular flow with vehicle-to-vehicle communication,” *IEEE Access*, vol. 8, pp. 174132–174141, 2020.
- [8] J. C. Zegers, E. Semsar-Kazerooni, J. Ploeg, N. van de Wouw, and H. Nijmeijer,

- “Consensus-based bi-directional cacc for vehicular platooning,” in *2016 American Control Conference (ACC)*, pp. 2578–2584, 2016.
- [9] Z. Wang, G. Wu, and M. J. Barth, “A review on cooperative adaptive cruise control systems: Architectures, controls, and applications,” in *2018 21st International Conference on Intelligent Transportation Systems (ITSC)*, pp. 2884–2891, 2018.
- [10] S. Baldi, D. Liu, V. Jain, and W. Yu, “Establishing platoons of bidirectional cooperative vehicles with engine limits and uncertain dynamics,” *IEEE Transactions on Intelligent Transportation Systems*, vol. 22, no. 5, pp. 2679–2691, 2021.
- [11] Z. Wang, Y. Bian, S. E. Shladover, G. Wu, S. E. Li, and M. J. Barth, “A survey on cooperative longitudinal motion control of multiple connected and automated vehicles,” *IEEE Intelligent Transportation Systems Magazine*, vol. 12, no. 1, pp. 4–24, 2019.
- [12] C. Wu, Z. Xu, Y. Liu, C. Fu, K. Li, and M. Hu, “Spacing policies for adaptive cruise control: A survey,” *IEEE Access*, vol. 8, pp. 50149–50162, 2020.
- [13] B. Liu, F. Gao, Y. He, and C. Wang, “Robust control of heterogeneous vehicular platoon with non-ideal communication,” *Electronics*, vol. 8, no. 2, p. 207, 2019.
- [14] K. Massow, I. Radusch, and R. Shorten, “A numerical study on constant spacing policies for starting platoons at oversaturated intersections,” *IEEE Access*, vol. 10, pp. 43766–43786, 2022.
- [15] G. Rödönyi, “Leader and predecessor following robust controller synthesis for string stable heterogeneous vehicle platoons,” *IFAC-PAPERSONLINE*, vol. 48, no. 14, pp. 155–160, 2015.
- [16] G. Rödönyi and Z. Szabó, “Adaptation of spacing policy of autonomous vehicles based on an unknown input and state observer for a virtual predecessor vehicle,” in *2016 IEEE 55th Conference on Decision and Control (CDC)*, pp. 1715–1720, IEEE, 2016.

- [17] G. Rödönyi, “An adaptive spacing policy guaranteeing string stability in multi-brand ad hoc platoons,” *IEEE Transactions on Intelligent Transportation Systems*, vol. 19, no. 6, pp. 1902–1912, 2017.
- [18] F. Gao, S. E. Li, Y. Zheng, and D. Kum, “Robust control of heterogeneous vehicular platoon with uncertain dynamics and communication delay,” *IET Intelligent Transport Systems*, vol. 10, no. 7, pp. 503–513, 2016.
- [19] Y. Zhang, M. Wang, J. Hu, and N. Bekiaris-Liberis, “Semi-constant spacing policy for leader-predecessor-follower platoon control via delayed measurements synchronization,” *IFAC-PapersOnLine*, vol. 53, no. 2, pp. 15096–15103, 2020.
- [20] S. Darbha, S. Konduri, and P. R. Pagilla, “Vehicle platooning with constant spacing strategies and multiple vehicle look ahead information,” *IET Intelligent Transport Systems*, vol. 14, no. 6, pp. 589–600, 2020.
- [21] L.-y. Xiao and F. Gao, “Effect of information delay on string stability of platoon of automated vehicles under typical information frameworks,” *Journal of Central South University of Technology*, vol. 17, no. 6, pp. 1271–1278, 2010.
- [22] X. Liu, A. Goldsmith, S. S. Mahal, and J. K. Hedrick, “Effects of communication delay on string stability in vehicle platoons,” in *ITSC 2001. 2001 IEEE Intelligent Transportation Systems. Proceedings (Cat. No. 01TH8585)*, pp. 625–630, IEEE, 2001.
- [23] A. A. Peters, R. H. Middleton, and O. Mason, “Leader tracking in homogeneous vehicle platoons with broadcast delays,” *Automatica*, vol. 50, no. 1, pp. 64–74, 2014.
- [24] V. Fragoso-Rubio, M. Velasco-Villa, M. A. Hernández-Pérez, B. del Muro-Cuéllar, and J. F. Márquez-Rubio, “Prediction-observer scheme for linear systems with input-output time-delay,” *International Journal of Control, Automation and Systems*, vol. 17, no. 8, pp. 2012–2025, 2019.
- [25] L. Xiao, M. Wang, W. Schakel, and B. van Arem, “Unravelling effects of cooperative adaptive cruise control deactivation on traffic flow characteristics at merging bottlenecks,” *Transportation research part C: emerging technologies*, vol. 96, pp. 380–397, 2018.

- [26] K. C. Dey, L. Yan, X. Wang, Y. Wang, H. Shen, M. Chowdhury, L. Yu, C. Qiu, and V. Soundararaj, “A review of communication, driver characteristics, and controls aspects of cooperative adaptive cruise control (cacc),” *IEEE Transactions on Intelligent Transportation Systems*, vol. 17, no. 2, pp. 491–509, 2015.
- [27] P. Kavathekar and Y. Chen, “Vehicle platooning: A brief survey and categorization,” in *International Design Engineering Technical Conferences and Computers and Information in Engineering Conference*, vol. 54808, pp. 829–845, 2011.
- [28] A. A. Alam, A. Gattami, and K. H. Johansson, “An experimental study on the fuel reduction potential of heavy duty vehicle platooning,” in *13th International IEEE Conference on Intelligent Transportation Systems*, pp. 306–311, 2010.
- [29] R. A. Shet and F. Schewe, “Performance evaluation of cruise controls and their impact on passenger comfort in autonomous vehicle platoons,” in *2019 IEEE 89th Vehicular Technology Conference (VTC2019-Spring)*, pp. 1–7, 2019.
- [30] C. Nowakowski, J. O’Connell, S. E. Shladover, and D. Cody, “Cooperative adaptive cruise control: Driver acceptance of following gap settings less than one second,” in *Proceedings of the Human Factors and Ergonomics Society Annual Meeting*, vol. 54, pp. 2033–2037, SAGE Publications Sage CA: Los Angeles, CA, 2010.
- [31] S. Öncü, J. Ploeg, N. Van de Wouw, and H. Nijmeijer, “Cooperative adaptive cruise control: Network-aware analysis of string stability,” *IEEE Transactions on Intelligent Transportation Systems*, vol. 15, no. 4, pp. 1527–1537, 2014.
- [32] S. Darbha, S. Konduri, and P. R. Pagilla, “Benefits of vehicle-to-vehicle communication for autonomous and connected vehicles,” *IEEE Transactions on Intelligent Transportation Systems*, vol. 20, no. 5, pp. 1954–1963, 2018.
- [33] J. Ploeg, N. Van De Wouw, and H. Nijmeijer, “ $l_p$  string stability of cascaded systems: Application to vehicle platooning,” *IEEE Transactions on Control Systems Technology*, vol. 22, no. 2, pp. 786–793, 2013.
- [34] K. Zhou and J. C. Doyle, *Essentials of robust control*, vol. 104. Prentice hall Upper Saddle River, NJ, 1998.

- [35] E. Shaw and J. K. Hedrick, "String stability analysis for heterogeneous vehicle strings," in *2007 American Control Conference*, pp. 3118–3125, 2007.
- [36] A. M. H. Al-Jhayyish and K. W. Schmidt, "Feedforward strategies for cooperative adaptive cruise control in heterogeneous vehicle strings," *IEEE Transactions on Intelligent Transportation Systems*, vol. 19, no. 1, pp. 113–122, 2018.
- [37] M. Najafi, S. Hosseinnia, F. Sheikholeslam, and M. Karimadini, "Closed-loop control of dead time systems via sequential sub-predictors," *International Journal of Control*, vol. 86, no. 4, pp. 599–609, 2013.
- [38] W. Michiels, K. Engelborghs, P. Vansevenant, and D. Roose, "Continuous pole placement for delay equations," *Automatica*, vol. 38, no. 5, pp. 747–761, 2002.



## APPENDIX A

### CONTROLLERS

Table A.1: The controllers used in the thesis

Controller	Transfer Function
$K_{ap} = K_{al}$	$\frac{70.53s^3+205s^2+145.7s+0.001234}{s^4+40.38s^3+258.4s^2+298.1s+0.002468}$
$K_{vp} = K_{vl}$	$\frac{7.133s^2+15.25s+5.55}{s^4+40.38s^3+258.4s^2+298.1s+0.002468}$
$K_{pp} = K_{pl}$	$\frac{78.54s^2+148s+28.26}{s^5+40.38s^4+258.4s^3+298.1s^2+0.002468s}$